Fisheries and Oceans Canada | Pêches et Océans Canada
Ecosystems and Oceans Science | Sciences des écosystèmes et des océans

Canadian Science Advisory Secretariat (CSAS)

Research Document 2025/058

Quebec region

A Species Distribution Modeling Approach Based on Aerial Survey Observations from 2017 to 2022 to Predict North Atlantic Right Whale Habitats in the Estuary and Gulf of St. Lawrence

Arnaud Mosnier, Valérie Harvey, Stéphane Plourde,
Jean-François Gosselin, Caroline Lehoux

Fisheries and Oceans Canada,
Maurice-Lamontagne Institute,
850 Route de la Mer,
Mont-Joli, Quebec Canada G5H 3Z4

September 2025

Canada

Foreword

This series documents the scientific basis for the evaluation of aquatic resources and ecosystems in Canada. As such, it addresses the issues of the day in the time frames required and the documents it contains are not intended as definitive statements on the subjects addressed but rather as progress reports on ongoing investigations.

Published by:

Fisheries and Oceans Canada
Canadian Science Advisory Secretariat
200 Kent Street
Ottawa ON K1A 0E6

http://www.dfo-mpo.gc.ca/csas-sccs/
csas-sccs@dfo-mpo.gc.ca

ISSN 1919-5044
ISBN 978-0-660-78593-6 Cat. No. Fs70-5/2025-058E-PDF

Correct citation for this publication:

Mosnier, A., Harvey, V., Plourde, S., Gosselin, J.-F., and Lehoux, C. 2025. A Species Distribution Modeling Approach Based on Aerial Survey Observations from 2017 to 2022 to Predict North Atlantic Right Whale Habitats in the Estuary and Gulf of St. Lawrence. DFO Can. Sci. Advis. Sec. Res. Doc. 2025/058. iv + 83 p.

Aussi disponible en français :

Mosnier, A., Harvey, V., Plourde, S., Gosselin, J.-F., et Lehoux, C. 2025. Utilisation d'une approche de modélisation de la répartition des espèces basée sur des observations issues de relevés aériens réalisés de 2017 à 2022 pour prédire les habitats de la baleine noire de l'Atlantique Nord dans l'estuaire et le golfe du Saint-Laurent. Secr. can. des avis sci. du MPO. Doc. de rech. 2025/058. v + 88 p.

TABLE OF CONTENTS

ABSTRACT

The North Atlantic Right Whale (NARW) was historically abundant along the North Atlantic coasts, ranging from the Gulf of Mexico to Greenland and from northwestern Africa to Norway. Nowadays, the species is primarily found along the coastal regions of the eastern United States and Atlantic Canada, with an estimated population of only 356 individuals. Over the last decade, their distribution shifted significantly, with approximately 40% of the population moving from traditional summer feeding grounds to the Gulf of St. Lawrence (GSL). The high number of mortalities observed in 2017 and 2019 have led Fisheries and Oceans Canada to implement a monitoring program aimed at detecting whales, triggering protective management measures, and gathering information on their spatial and temporal distribution. Data from the surveys conducted between August 2017 and November 2022 were combined with environmental variables in Generalized Additive Mixed Models to identify factors influencing NARW distribution in the GSL and predict their likelihood of occurrence. Models were developed using data collected between 2017 and 2020, considering two-month periods, half-seasons and the entire season of NARW occurrence. Period-specific models were found to outperform the global model when tested over the training dataset (2017-2020 observations). However, the global model trained with data from the entire season of occurrence proved to be more accurate when tested against the independent observation dataset acquired in 2021-2022. The best model included depth, sea surface temperature, salinity and chlorophyll a as important factors influencing the probability of NARW occurrence. Additionally, it included mean sea level anomalies, thermal fronts, current speed, and bottom topography, likely due to their role in prey aggregation processes. The predicted probability maps generated by this study highlight the importance of several areas in the GSL, such as Shediac Valley, Bradelle Valleys, and West Anticosti, and provide insights into seasonal variations in distribution. These maps will inform the designation of conservation areas and guide management strategies to mitigate risks posed by shipping and fishing activities to this endangered population.

INTRODUCTION

The North Atlantic Right Whale (*Eubalaena glacialis, henceforth* NARW) used to be widespread throughout the North Atlantic Ocean in an area extending along the eastern coast of North America, from the Gulf of Mexico to Greenland, and along the western European coast, from Norway to the northwestern coasts of Africa (Figure 1, Schevill and Moore 1983, IWC 1986, Mead 1986, Mitchell et al. 1986, Reeves and Mitchell 1986, Monsarrat et al. 2015). Commercial harvesting over the past centuries drastically reduced their numbers (IWC 1986). It is assumed that right whales in the western North Atlantic might be the only functional unit remaining (IWC 2001, Frasier et al. 2022) but, with an abundance estimated to 356 individuals in 2022 (346–363; Linden 2023), this population is considered as one of the most endangered cetacean population in the world (Clapham et al. 1999).

Over the last decades, opportunistic sightings, passive acoustic monitoring, visual surveys, photo-identification and telemetry provided information about the seasonal distribution of NARWs within their current range (Mate et al. 1997, Baumgartner and Mate 2005, Brown et al. 2009, Davis et al. 2017, 2019, Simard et al. 2019). These studies suggested that NARWs occurred in only a small portion of their former range and were primarily observed in coastal areas along the eastern United States (US) and Atlantic Canada (Figure 1). Within that extent, at least part of the population migrates between the winter calving grounds located in the coastal waters of the southeastern United Stated (US) from Florida to North Carolina, and the summer feeding grounds located off New England and Canada (Winn et al. 1986). Major changes in NARW distribution occurred over the last decade. In the early 2010s, a reduction of NARWs sightings was observed in their traditional summer feeding grounds within the Gulf of Maine, Great South Channel, Bay of Fundy, and Scotian Shelf, while an increase was observed in Southern New England and in the GSL, an area not previously recognized as an important habitat for the population (Simard et al. 2019, Crowe et al. 2021, Meyer-Gutbrod et al. 2022). While NARWs were only occasionally observed in the GSL prior to 2015, a significant portion (40%) of this small population is now using it every year from early spring to late autumn, with high proportion of individuals showing a strong site fidelity (Simard et al. 2024, Crowe et al. 2021, St-Pierre et al. 2024a).

The recovery of NARW is limited by the low reproduction rate and important mortality rates associated with vessel strike and entanglement in fishing gear (Moore et al. 2004, Kraus et al. 2005, Brown et al. 2009, DFO 2014, Corkeron et al. 2018, Stewart et al. 2022). Information on habitat use by NARW has led to the legal designation of conservation areas and to implementation of management measures to minimize collision and entanglement risks on calving grounds and in traditional foraging areas along the US coast, the Grand Manan area and Roseway Basin (Figure 1; Vanderlann and Taggart 2009, Knowlton et al. 2012, Laist et al. 2014, Knowlton et al. 2016). Management measures have also been put in place since 2018 in the GSL where NARW is also vulnerable to vessel strikes and entanglement in fishing gears (Daoust et al. 2017, Bourque et al. 2020).

The efficiency of conservation measures would be reduced if NARW change their distribution so that their occurrence is no longer synchronized with the application of mitigation measures or if protected areas are no longer frequented. In order to focus monitoring efforts, enhance the effectiveness of mitigation measures and insure adequate protection of NARWs, there is a need to identify important habitats and understand the seasonal pattern of NARW habitat use within the GSL. The shift in NARW distribution from their historical feeding grounds to the GSL has been attributed to a decline in their main prey, *Calanus finmarchicus,* in their original habitats (Record et al. 2019, Meyer-Gutbrod et al. 2022), while several areas in the GSL may provide adequate prey abundance (Plourde et al. 2019, Sorochan et al. 2019, Gavrilchuk et al. 2021,

Sorochan et al. 2021, 2023, Plourde et al. 2024). Prey availability is definitively an important element to take into account to explain NARW distribution, but information on other environmental variables describing oceanographic conditions and bottom profile can also provide insight in the different cues that NARW may consider when searching for prey or locations where the latter are more easily accessible (Murison and Gaskin 1989, Baumgartner and Mate 2003, Baumgartner et al. 2003, Pendleton et al. 2012).

In this study, we integrated observations of NARW from systematic visual aerial line-transect surveys conducted by Fisheries and Oceans Canada (DFO) from August 2017 to November 2022, with environmental variables using a Species Distribution Model. The latter uses Logistic Generalized Additive Models to identify factors affecting the distribution of NARW in the GSL, and predict their relative probability of occurrence in this area. Annual and seasonal models from April to November were tested to identify the most efficient models and reveal potential seasonal changes in distribution. These models were then applied to predict the spatial and temporal distribution of NARW important habitats within the GSL.

MATERIALS AND METHODS

OBSERVATION DATABASE

The observation database included results from systematic line-transect visual aerial surveys conducted in the St. Lawrence Estuary (SLE) and GSL between 2017 and 2022. Most of the data was collected from the DFO science aerial surveillance program implemented in 2017 (see St-Pierre et al. 2024a). Surveys were first conducted from late August to mid-November 2017 over several potential foraging areas previously targeted (see St-Pierre et al. 2024a). Starting in 2018, the survey period was extended from April to November, and aerial coverage followed a more systematic and continuous design that included the SLE and GSL. Survey effort dedicated to the different parts of the GSL and SLE varied among years (Figure 2). Each year, a large proportion of the surveys was dedicated to the southern GSL (Figure 3, 5 to 11 surveys per years). The northern GSL was surveyed at least once a year (1 to 5 surveys per year), while other areas were surveyed less regularly, SLE (0 to 1 survey by year), Cabot Strait (0 to 4 per year), northeast GSL (0 to 2 surveys per year), Chaleur Bay (0 to 2 surveys per year), Northumberland Strait (0 to 2 surveys per year). A detailed description of the methodology and survey coverage is provided in St-Pierre et al. (2024a).

Data included in the database also come from another 15 systematic aerial surveys conducted from early May to mid-September between 2018 and 2022 (5 in 2018, 4 in 2019, 1 in 2020, 1 in 2021, 1 in 2022) to assess abundance and seasonal distribution of SLE beluga (Harvey et al. in prep[1], St-Pierre et al. 2024a). All of these surveys covered the SLE from Rimouski to Battures aux Loups Marins, 12 of them extended east of Rimouski to cover the lower portion of the SLE, with three surveys extending further east to cover the northwest GSL, the Gaspé peninsula and Chaleur Bay (Figure 3).

While this dataset encompasses surveys conducted with different objectives, the same protocol was applied consistently. Recorded information included the time when observers began and stopped actively searching for marine mammal (on and off effort), weather conditions (sea state, glare intensity, cloud cover), and for each marine mammal sighting, the species, group size and its location based on the inclination angle from horizon, angle from the platform heading and

[1] Harvey, V., Mosnier, A., St-Pierre, A.P., Lesage, V. and Gosselin, J.-F. In preparation. Seasonal Variation in Distribution and Habitat Use of St. Lawrence Estuary Beluga (Delphinapterus leucas) from Systematic Visual Line-transect Aerial Surveys. DFO Can. Sci. Advis. Sec. Res. Doc.

platform altitude and location obtained from a GPS device. When a NARW or a possible NARW was detected, the plane circled over the detection area for at least 20 minutes to confirm species identification, estimate group size and get a more accurate position of each individual (see St-Pierre et al. 2024a for details).

All NARWs detected while observers were actively searching for marine mammals were included in the analyses. In cases where the same individual was detected multiple times (i.e., by two observers seated on same side during passing mode, or within closing mode), the more accurate location, typically the position when the plane overpassed the individual during the closing procedure, was retained.

ACTUAL SURVEY COVERAGE

The area considered as actually surveyed was represented by the field of view of the observers when they were “on effort”. The field of view was considered as a buffer around the platform track with a width (3000 m) equal to the 95th percentile of the perpendicular distances between the platform track and the NARW observations. Potential differences between the periods “on effort” on the left or right side of the platform were considered with independent right and left side buffers. The effort maps were based on a grid of 1000 x 1000 m cells covering the SLE and GSL. Cell values were calculated as the sum of the surveyed areas covering each cell. Data processing was conducted in QGIS 3.34 (QGIS.org 2023).

MODELLING OCCURRENCE OF THE NARW

Extracting environmental conditions

The selection of the environmental covariates (Table 1) was based on their association with the occurrence of mysticeti species such as NARW or their preys (*Calanus* spp.), or with oceanographic processes associated with zooplankton prey aggregation. Ten different covariates (Table 1) were tested in the models, including bottom depth, bottom slope, seabed topography, water temperature, thermal fronts, chlorophyll a concentration, mean sea level anomalies, salinity, current speed and an index of foraging conditions for the NARW. To account for fine-scale habitat selection by NARWs, environmental covariates were extracted for each observation location and date, with the highest spatial resolution available and generally considering daily values, except for *Calanus* spp. modeling data (see below) which were limited to monthly predictions. This extraction was performed in R (R core Team 2023) using libraries “sf” (Pebesma 2018, Pebesma and Bivand 2023) and “terra” (Hijman 2023).

Static environmental data

Marine mammals behaviour and distribution, in particular those feeding on plankton, are known to be influenced by bio-physical oceanographic processes often associated with the seabed topography (Hui 1985, Murison and Gaskin 1989, Torres et al. 2013, Cox et al. 2018, Wyles et al. 2022). Basic characteristics of the seabed such as depth and slope were thus acquired at each sighting location. Depth was obtained from a 20 m resolution raster map created by interpolating data from the Canadian Hydrographic Service. Bottom slope was derived from the depth map by calculating the maximum rate of depth change (in degrees) over the distance between neighboring cells. Another index of the seabed morphology, the topographic position index (TPI; Weiss 2001), was also derived from the depth map using the “spatialEco” package (Evans and Murphy 2023) and used to classify the seabed according to 6 different classes: flat slope, valley, lower slope, middle slope, upper slope and ridge.

Dynamic environmental data

Oceanographic processes, occurring at both global and local scales, lead to the formation of distinct water masses, whose characteristics may serve as cues for marine mammals seeking prey in a dynamic ecosystem (Kenney et al. 2001, Pendleton et al. 2009, Abrahms et al. 2019, Milanesi et al. 2020, El-Gabbas et al. 2021). The Sea-Surface Temperature (SST) was obtained from daily gap-free maps generated by the Group for High Resolution Sea Surface Temperature (GHRSST) by combining complementary satellite and in situ observations within Optimal Interpolation systems. The SST value was extracted for the date of each observation. The mean at this location over the previous 15 days and the SST value 15 days prior were also calculated to examine potential delayed responses to thermal conditions. The water temperature and salinity in the 0-50 m depth layer, along with the temperature near the seabed were identified as drivers for *Calanus* spp. distribution in the GSL (Albouy-Boyer et al. 2016). Daily average values of water temperature in the 0-50 m depth layer, near the seabed, as well as throughout the entire water column were obtained from the Coastal Ice-Ocean Prediction System for the East Coast of Canada (CIOPS-E) (Paquin et al. 2024). The daily predictions of this oceanographic model were also used to extract the mean salinity in the 0-50 m depth layer.

Other characteristics such as current speed and the presence of thermal fronts are sometimes associated with areas of higher productivity, providing more predictable foraging conditions potentially aggregating preys and affecting whale distribution in foraging grounds (Baumgartner et al. 2003, Cotté et al. 2011, Harvey et al. 2017, Cox et al. 2018). We thus extracted the mean current velocity in the first 10 m of the water column, and also from the surface to a maximum of 150 m. The 10 – 150 m depth range encompassed the main range of diving depths recorded from NARW (Watwood and Buonantony 2012, Baumgartner and Mate 2003, Murison and Gaskin 1989) and the maximum bottom depth (100 m) where almost all the NARWs in the GSL were detected. Thermal fronts were identified on daily SST maps with an edge detection algorithm (Cayula and Cornillon 1995) available into the Marine Geospatial Ecology Tools (MGET) toolbox developed for ArcGIS 10 (Roberts et al. 2010). Distance to the closest front was calculated as well as the frequency of occurrence of thermal fronts in an area of 5 km around each observation. We also extracted Mean Sea Level Anomalies (MSLA), a measure of the altimetry of the sea surface, known to fluctuate with the dynamics and circulation patterns of the ocean. This variable enabled the identification of oceanic features such as eddies, upwelling, and downwelling zones (Nerem et al. 1990, Fu and Cheney 1995). Several studies have found a link between sea surface altimetry and whale occurrence patterns, foraging activities (Abrahams et al. 2018, Becker et al. 2016, Pardo et al. 2015, Warwick-Evans et al. 2022, Tao et al. 2023) and zooplankton abundance (Plourde et al. 2016). This information was extracted from daily maps of MSLA provided by the CMEMS (see data link above, Table 1).

Lastly, two indices linked to the productivity and accessibility of NARW preys were considered. In the southern GSL, where most NARW observations occurred, changes in the abundance of *Calanus* spp. are strongly influenced by ocean circulation associated with the Gaspé Current (Le Corre et al. 2023; Johnson et al. 2024). This water mass, along with several areas of strong tidal mixing and frontal zones, is characterized by relatively high chlorophyll a (Chla) concentration (Laliberté et Larouche 2023). Chla concentration, estimating phytoplankton biomass is considered as a proxy of local productivity. Daily gap-free maps provided by the Copernicus Marine Environment Monitoring Service (CMEMS; GlobColour products) and derived from data collected by multiple satellites, were used to obtain Chla concentration in our study area; each NARW sighting was associated with the average Chla value over the past 3 and 15 days. A monthly estimate of an index reflecting foraging conditions for NARWs was also extracted at each location. This index was based on the net energy (Enet) acquired during NARW foraging estimated with a bioenergetic foraging model coupled with a 3-D *Calanus* spp.

biomass (Plourde et al. 2024). As two different *Calanus* spp. models were available (referred as model 2 and model 3.3 in Plourde et al. 2024), Enet predictions were extracted from both. Enet mean values were also calculated over the entire season (Global: from April to November) as well as over two month periods from April to November (April-May, June-July, August-September, October-November), aligning with some of our modelling periods (see below) and corresponding to time frames that appeared to be relatively homogeneous in terms of *Calanus* predictions. Finally, to assess if NARW distribution could be influenced by a certain "knowledge" about the local prey availability acquired in previous years (Kenney 2001, Crowe et al. 2021), the average of the predictions of the *Calanus* models was calculated over the last 3 years, along with the associated variance. Both values were also associated with each sighting location.

Characterizing environment "not used" by whales

Due to availability and detection biases (Buckland et al. 2004), it is not possible to define with certainty the areas/environmental conditions where whales were absent. To reduce the likelihood of including environmental conditions where the possibility of whale occurrence was not negligible, we used two methods – one in the sampling strategy, described here, and the other during the modeling phase (see next section). Environmental conditions in which no NARW was detected were defined by generating random points within the surveyed area (e.g., a 3000 m buffer around the survey lines, see section above) at a density of 1 point/km² (Mosnier et al. 2022). However, no random points were allowed within a 250 m radius around each whale sighting to avoid considering a pseudo-absence in close proximity to a known whale location. This radius also accounted for potential errors in the recorded whale sighting coordinates. Each random point was given a time stamp corresponding to the date and time at which the distance from the survey platform was the shortest, and were given the local conditions prevailing during the survey at that date and time. Finally, the same variables describing the environment at each whale sighting location (i.e. Depth, Slope, TPI, Water temperature, Currents, Chla concentration, Thermal fronts, Salinity, MSLA and Enet of *Calanus* spp.) were also extracted for those random points.

Modelling Approach

Relationships between NARW occurrences and environmental covariates were assessed using logistic regressions fitted as Generalized Additive Mixed Models (GAMM) using the function "BAM" (special version of the "GAM" function for large dataset) from the R package "mgcv" (Wood et al. 2015, Wood et al. 2017). To constrain the model to compare environmental conditions within each survey (i.e., not mixing conditions between the various surveys), the date was considered as a random effect. Some dynamic variables (Water temperature, Current speed, Chla, Fronts, *Calanus* spp. model predictions) were available in various forms (e.g. daily values, means, lagged values). However, models only included one form of each of these variables at a time. Moreover, the Chla concentration and the variable representing the net energy gained (or lost) from exploiting local densities of *Calanus* spp. (Enet) were both used to represent the potential resources available to NARW and were not considered together in the same model. Finally, variables presenting a correlation coefficient greater than 0.5 (Appendix A) were not included simultaneously, resulting in a total of 44 927 models to be tested. No interactions were tested. Smoothed terms were represented using penalized regression splines with smoothing parameters selected by Maximum Likelihood. To keep the ecological interpretability of functional relationships, each spline was limited to five degrees of freedom.

Even if sampling of random points in the vicinity of the sightings was avoided, one could argue that random points representing pseudo-absences might still be located where an animal is present but not detected. To minimize this problem, we weighted the data included for each random point by an index of detectability based on detection curves (Appendix B) similar to

those used in distance sampling (Buckland et al. 1993). The “ddf” function from the R package “Distance” (Miller and Clark-Wolf 2023) was used to obtain detection curves accounting for perpendicular distance of the sightings, platform type (i.e. small size plane (Cessna 337 Skymaster, Partenavia (P68 Observer), medium size plane (DeHavilland DH-6 Twin Otter 300)) and local conditions during the survey (sea state, glare intensity). We tested multiple-covariate distance sampling (MCDS) formulations with hazard-rate and half normal key functions. The best model was selected based on its Akaike Information Criterion value. No additional correction was applied to account for the probability of a NARW to be at the surface when the plane surveyed an area (availability bias). Such a correction factor, generally based on telemetry data, was not available for this species in the GSL, and are believed to vary both spatially and seasonally (St Pierre et al. 2024a, Roberts et al. 2024). This weighting scheme allowed random points to be assigned an increasing importance with better observations conditions, thereby enhancing the probability of detecting a whale if present, and making these points a more accurate measure of true absence. As a complement, sightings were given a weight of 1 given they represented true presence.

Model training, model selection and performance testing

The models were trained with observational data obtained from surveys conducted between 2017 and 2020 to allow for the inclusion of *Calanus* model predictions, which were only available up to 2020. The observations from 2021 to 2022 were used as a testing dataset to evaluate model performances (see below). Moreover, to test for potential temporal changes in the NARW habitat selection over the main period where NARW occur in the GSL, models were successively fitted while considering data separated in two months periods (April-May, June-July, August-September, October-November), half-season periods (April-July, August-November), then finally data covering the entire season (April-November; hereafter referred to as the Global model).

The selection among GAMM models occurred through a two-step process. First, the shrinkage approach (Marra and Wood 2011) was applied during model fitting, allowing the exclusion of covariates that did not contribute significant information to the model by reducing the effective degree of freedom of their smooth terms to 0, or near 0. When such a situation occurred, the variable with the lowest degree of freedom was removed and the model refitted. Subsequently, for each time period (two months periods, half seasons, whole season), the list of final models were then ranked based on their AIC values, and models with a delta AIC <= 3 from the lowest value were retained as the best models.

Generally, Species Distribution Models performances are tested using cross-validation, i.e., by training the models on subsets of the available input data, and evaluating them on the complementary subset of the data. While this method is robust, the training and testing datasets obtained with this approach are not completely independent as they are sampled from the same dataset. However, here, we benefited from the fact we had access to a completely independent dataset obtained from different years of surveys. The models’ performance was evaluated for each time period, with different indices, successively considering the training (i.e., the data used to fit the models; 2017-2020 surveys), and the testing dataset (2021-2022 surveys) respectively. A receiver operating characteristic (ROC) curve (Fielding and Bell 1997) was constructed both for the training set (i.e. comparing predictions with the data used to fit the model – i.e. 2017-2020 survey data) and the testing set (this time comparing predictions with an independent dataset composed of survey data obtained in 2021 and 2022). The area under the ROC curve (AUC) was then used as a threshold-independent measure for model performance (Manel et al. 2001). The AUC ranges from 0.5 for models with no discriminatory power, to 1 for models with perfect discrimination. Intermediate values can be interpreted as follows: 0.5-0.6 = fail, 0.6-0.7 =

poor, 0.7-0.8 = fair, 0.8-0.9 = good, 0.9 to 1 = excellent. Since our dataset was heavily biased towards absence data, a threshold of 0.5 was inadequate for accurately classifying predictions as either presence or absence. To address this issue, the Youden index (Youden 1950) was used to define the optimal threshold and construct a confusion matrix allowing to obtain the proportion of correct classifications. The Symmetric Extremal Dependence Index (SEDI; Ferro and Stephenson 2011; Wunderlich et al. 2019) was also calculated based on the confusion matrix as another measure of model goodness-of-fit. It was preferred to the True Skill Statistic (Allouche et al. 2006) as it was found optimal for presence-absence/background Species Distribution Models (Wunderlich et al. 2019). This metric range from -1 to +1 with +1 indicating perfect agreement, and values of zero or less suggesting a performance no better than random.

Spatial representations of the predictions from the best models were produced and visually compared to observations. Daily maps were generated. Additionally, monthly mean and variance maps were produced to characterize the spatial and temporal variability of the predictions, and help identify regions consistently predicted as presenting conditions more conducive to the occurrence of NARW.

RESULTS

SPATIO-TEMPORAL VARIATION OF SURVEY EFFORT AND NARW DETECTION

Survey effort began in April, then rapidly increased to reach a maximum and relatively constant coverage from May to August, and then gradually decreased until November to a surveyed area similar to that of April (Figure 4). Most of the survey effort was conducted over the southern GSL (72% of the area covered) and the northwestern GSL (12%) (Figure 3 and Figure 4). The changes in the number of NARW observations may reflect these spatio-temporal variations in survey coverage, as the areas and periods with the highest number of observations corresponded to the areas and periods with the highest survey effort. In total, 1012 groups of NARWs comprising 1255 individuals were detected. The number of observations increased from April to June, remained relatively stable until August, and then decreased (Figure 4). Most NARWs (74%) were observed between June and August (Figure 4). Nearly all (96%) of the NARWs were detected in the southern GSL; 4% of the observations were in the northwestern GSL, with no NARWs sighted in others areas (Figure 5). The spatial distribution of the NARW detections varied seasonally. In April and May, NARWs were detected along the southern slope of the Laurentian Channel, in Eastern and Western Bradelle valleys, north of Prince Edward Island (PEI; mostly in 2022), as well as in the vicinity of Shediac Valley (Figure 5). NARWs mainly aggregated in these areas throughout the summer but were also detected in others valleys located in the southern GSL (Figure 5). Starting in August, however, NARWs sightings became more dispersed within both the southern and the northern GSL, with the majority of detections occurring at the western tip of Anticosti Island. No whales were observed in the vicinity of Shediac Valley in October and November. During that period, NARWs were primarily observed west of the Magdalen Islands and north of PEI.

NARW SPECIES DISTRIBUTION MODEL

Important variables

All best models identified in the different periods considered (April-July, April-May, June-July, August-Sept, August-November, and the global period covering April to November) included bottom depth as an explanatory variable, and most of them (all but April-May models) also incorporated salinity between 0 and 50 m (Table 2 and 3). Most models included one of the

covariates describing the SST, with models developed for periods after August also incorporating bottom temperature (not correlated with the SST, see Appendix A). Bottom temperature was also retained in the models describing the Global (April-November) period, but only when associated with *Calanus* predictions; however these models were not considered the best for this period. The classification of the seabed morphology based on the TPI appeared in the best models for the Global period, and for April-July and August-November. One of the two current speed covariates (0-10 m or 0-150 m) were retained in the Global and April-July models, but appeared only in the June-July and August-November models when associated with *Calanus spp.* predictions. Models including different Chla covariates (in particular Chla_15d), were typically assessed as the best ones. The only exception was observed for the April-May period, where no Chla nor Enet were present in the covariate list of the best models. While a model featuring a Enet covariate (EnetMod2_MeanLast3Y) was deemed equivalent (delta AIC = 0.8) to another model with Chla_15d for the June-July period, models incorporating Enet covariates generally had a higher AIC (lower is better).

Model performances

Overall, the proportion of the deviance explained by the best models (based on their AIC value) was relatively low (44.4 ± 6.0%; mean ± sd). However, the value of the AUC for these models suggested good performances when applied to the training dataset (Table 3 and 4; AUC = 0.89 ± 0.06; range 0.81–- 0.95). These models showed fair to good capabilities on the testing dataset composed of observations obtained during the 2021-2022 aerial surveys, with AUC ranging from 0.76 to 0.84 (mean 79.7 ± 0.03). The confusion matrix results showed a degradation of the models performances from 79.6 ± 15% (range: 53.6 – 95.2%) of correct classification of the presence on the training dataset to 74.3 ± 7.6% (range 66.1 – 87.9%) with the testing dataset. The proportion of correct classification of the absences also declined from 84.2 ± 5.4% with the training dataset to 74.4 ± 4.6% with the testing dataset. The symmetric extremal dependence index (SEDI) showed the same pattern, from a mean value of 0.75 ± 0.10 (range: 0.63 – 0.87) with the training dataset to 0.64 ± 0.06 (range 0.58 – 0.72) with the testing dataset. Note that the model assessment with the testing dataset was limited to models without *Calanus* prey layers (Enet) as the *Calanus* spp. modelling exercise did not extend beyond 2020.

The model fitted to the entire dataset (Global model) exhibited satisfactory performance (AUC = 0.864). It showed interesting results in classifying correctly 81.2% of the presences and 78.3% of the absences of the training dataset (Table 4). When its performance was assessed separately for each of the periods considered (Table 5), it generally showed poorer results than models developed specifically with the dataset of each period (Table 5 section training dataset VS Table 4 section training dataset). However, when the testing dataset was considered, the Global model performed better than the “period-specific” models (Table 5 section testing dataset VS Table 4 section testing dataset). For example, the Global model showed a mean correct classification of 82% and 84,1% for June-July and Aug-Sep, respectively (Table 5), while the corresponding “period-specific” models only had a mean correct classification of 77,9% and 77% for the same periods (Table 4).

Relationships with environmental variables

April-May

Models for this period of the year were based on an extremely low number of sightings (N = 21). The model with the lower AIC suggested a higher probability of NARW occurrence in deep waters (~ 150-450 m) and a probability increasing with the proximity of thermal fronts (Appendix C1). Interestingly, it also showed a negative relationship between the occurrence of NARW and the quantity of energy available (Enet) as predicted by *Calanus* model 3.3. An alternative model

(i.e. with a delta AIC < 3 from the best model), used another Enet covariate corresponding to the mean value during the last 3 years as predicted by *Calanus* model 3.3, the relationship with NARW occurrence remained however the same (Appendix C2). This model also included the SST observed with a 15 days lag as an additional explanatory variable. This model suggested a reduced likelihood of NARW occurrence in waters around 2.5°C whereas the probability increased for colder or warmer temperature.

June-July

Two alternative models were selected as best models for this period, one with an Enet covariate and the other with the Chla concentration as indexes of resource availability. The Enet covariate selected represented the mean value of the Enet over the last three years but this time as predicted by the other Calanus model (model 2, see Plourde et al. 2024). The relationship suggested a strong negative effect of the lowest Enet values (<- 0.9) on the probability of NARW occurrence (Figure A3.3). The latter then increased to Enet values around–- 0.8, stabilizing and then slowly decreasing to the highest values of Enet while retaining a significant positive effect. In the alternative model, the effect of the Chla, here as the mean Chla concentration observed over the last 15 days, was generally positive at concentrations lower than 6 mg/m³ with a maximum at around 2.5 mg/m³. Both models (Figure A3.3 and A3.4) showed a clear linear negative relationship between the salinity and the probability of NARW occurrence (i.e. decreased probability of occurrence in saltier waters). A clear positive relationship with the frequency of thermal fronts was also included in both models. Depth was retained into these two models but seemed to show a limited effect in the model involving the *Calanus* spp. predictions. In the other model (i.e. including Chla; Figure A3.4), results suggested that areas with depths less than 390 m had a higher probability of occurrence than deeper waters with the highest positive effect found around 110 m. The water temperature was also related to the probability of NARW occurrence in the two models but with two different covariates. In the model with *Calanus* spp predictions, a temperature around 5°C in the water column was considered to have a maximum positive impact on NARW potential occurrence. In the model with Chla, the water temperature is considered through one of the covariates of the SST linking the probability of NARW occurrence to the SST observed with a 15 days lag. The relationship showed an increasing trend from 0 to 7°C, followed by a decreasing trend up to 13°C, and then a renewed increase as the temperature continued to rise. NARW probability of occurrence also increased with decreasing current speed in the first 10 m of the water column. Finally, the Mean Sea Level Anomaly (MSLA) presented a dome shaped relationship with the probability of NARW occurrence, suggesting a maximum positive effect in areas with MSLA values around 0.9 cm.

August-September

Three highly similar models (Figure A3.5, A3.6 and A3.7) were selected as best models for this period. All included the Chla, the water depth, the salinity, the SST, bottom temperature, the thermal front frequency, the mean sea level anomalies (MSLA). One model included the morphology of the seabed (TPI) as an additional explanatory variable. The model with the lowest AIC included the Chla averaged over the last 15 days and showed a dome shaped relationship with a positive increasing effect from 0 to approximately 2.5 mg/m³ of Chla then decreasing to become a negative effect when Chla concentration was higher than 7 mg/m³. The other models suggested a linear negative relationship with Chla concentrations averaged over the last 3 days, and showing a positive effect that diminished until a Chla concentration of approximately 12 mg/m³, to become increasingly negative with larger values. The three models showed the same trend with bottom depth, with a slight but positive effect of water deeper than 150 m, but a negative effect for shallower waters. A linear effect was suggested with salinity, with a lower probability of NARW occurrence predicted as waters becomes saltier. The

relationship with 3-day lagged SST exhibited the same pattern as observed for the 15-day lagged SST in June-July, with an positive trend from 3 to 9°C, followed by a decreasing trend up to 16°C, and then back to a positive trend as the temperature continued to rise. The probability of NARW occurrence was also predicted by the three models to be linked to the frequency of thermal fronts in the area, with a dome shaped relationship suggesting a negative effect when the frequency of fronts was lower than 10%, and a maximum positive effect when this frequency was around 35%. The same decreasing curve was estimated with the MSLA, with a positive effect expected with values lower than 9 cm. The model including the TPI showed that the probability of NARW occurrence tended to be higher over the lower part of slopes but the effect was not very strong.

April-July

Models were also tested splitting the dataset into two “half-year” periods: April-July and August-November. In April-July, two very similar models (Figure A3.8 and A3.9) were selected as the best models. Both included Chla concentration, depth, salinity, SST, thermal front frequency in the area, MSLA in the explanatory variables. The only difference was the addition of the current speed in the first 10 m of the water column that was predicted to reduce the probability of NARW occurrence when the current speed increased. The relationships with the other variables were similar for the two models. The Chla concentration had a positive effect when lower than 7 mg/m³. The relationship was dome-shaped, with a maximum positive effect at around 2 mg/m³. Waters deeper than 400 m had a strong negative effect on the probability of NARW occurrence while shallower waters benefitted from a positive effect. The curve describing the relationship showed two bumps with maximums around 290 and 100 m, respectively. While not linear, the effect of the salinity on the probability of NARW occurrence was the same as previously described for the other seasons, with a reduced probability of NARW occurrence in saltier waters. SST temperatures between 9 and 16°C were predicted to have a negative effect, while higher temperatures were suggested to increase the likelihood of NARW presence. Their probability of occurrence also increased linearly with the frequency of thermal fronts in the area. A dome-shaped relationship with the MSLA suggested a maximum positive effect at 9 cm. Finally, a higher probability of NARW occurrence was expected in areas with a seabed classified as lower slopes and valleys.

August-November

For the second period of the year, the best model (Figure A3.10) showed again the same trend for the Chla, with a positive effect increasing from the lowest concentrations to 2.5 mg/m³, then declining until 7 mg/m³ and continuing as a negative effect with increasing Chla concentrations. The probability of NARW occurrence was highest at water depths between 50 and 275 m, and maximum at around 150 m. While selected in the model, the effect of salinity was more diffuse in this season. It kept the same trend with a lower probability of NARW occurrence in the saltiest waters, however, this probability also decreased as water became fresher than 25‰. The relationship with the SST, represented as the SST observed with a 3 days lag followed a pattern already described in June-July and August-September, i.e., an increasing probability of NARW occurrence with increasing temperatures from the lowest temperatures up to 9°C. A positive effect of the SST was expected between 6 and 13°C and became negative until the temperature increased to 19°C. The effect on the probability of NARW occurrence was then expected to keep increasing at higher temperatures. Temperature near the bottom was also selected in this model and showed a slight positive effect on predictions when values were between 1 and 7°C. A linear correlation indicated that NARW were more likely to occur with lower current speeds in the water column. The MSLA was predicted to have a positive impact on the predictions for anomalies lower than 8 cm. Finally, seabed structures categorized as lower slopes and valleys were linked to an increased probability of NARW presence.

Global period: April-November

The aim of the Global models was to find general relationships that would explain the occurrence of NARWs throughout their period of presence in the GSL. The best model (Appendix D1) incorporated the Chla concentration averaged over the last 15 days rather than the predictions from the *Calanus* spp. models. It also included information about bottom depth, salinity, SST, thermal fronts, currents, MSLA and seabed morphology. The relationship with the Chla was similar to what was described previously, with positive effects on the predictions until approximately 6 mg/m³ and a maximum around 2.3 mg/m³. The model suggested a slight positive effect of bottom depth on the probability NARW occurrence in waters 420-280 m deep then a larger positive effect from 40 to 280 m with a maximum at around 130 m. A higher salinity was predicted to lower the probability of NARW occurrence. The model also included an effect of the SST when considered with a 3 days lag. SST between 0 and 7°C and between 14 and 20°C were predicted to have a negative effect on the NARW occurrence, while it was positive between 7 and 14°C and for temperatures greater than 20°C. An inverse linear relationship described the effect of the current speed in the water column, leading to higher predictions of NARW presence in areas with lower current speed. As for the August-September and August-November models, a linear relationship suggested that lower values in MSLA was associated with a positive effect up to 7 cm, which then became negative beyond that value. Finally, areas with a seabed characterized by lower slopes or valleys were predicted to have a positive effect on the predicted probability of NARW occurrence than regions with other seabed characteristics.

Mapping predictions against observations

Visual inspection of the predictions maps produced from the different models confirmed that they generally provided results that were consistent with the observations. In particular, the best global model seemed to perform well in each of the period considered (Appendix E). Although the locations of whale sightings didn't consistently align with the higher probability of NARW occurrence predicted in the GSL, they were, in most cases, found in areas with at least moderate predictions.

Areas of higher probability of NARW occurrence

Overall, our models consistently predicted a higher probability of NARW occurrence in the northwest part of the southern GSL (Figure 6, Figure 7). This notably included, the basin between the American Bank and the Orphan Bank, the Shediac Valley, and the entrance of Chaleur Bay. Three valleys (Western and Eastern Bradelle valleys, and a small, nameless valley), located further east, perpendicular to the southern slope of the Laurentian channel, also appeared to be important during certain parts of the year. In addition, models frequently predicted higher probabilities of NARW occurrence north of Cape Breton and in Cabot Strait, between the Cape Breton coast and St. Paul Island. Finally, in the northern GSL, the Jacques-Cartier Strait and the area west of Anticosti Island were also sites of high predictions. It should be noted, however, that the area between the American Bank and the Orphan Bank, as well as the region around Cape Breton, showed a larger variance in the predicted values than the other locations enumerated above.

Across years, a recurrent pattern seemed to occur, with higher probabilities of NARW occurrences beginning to appear in May in the northwest of the southern GSL, along with some high predictions in the northern GSL around the western tip of Anticosti Island. By the end of June, higher predictions seemed to extend eastward (e.g. to the Bradelle valleys) and southward in the southern GSL with pulses of higher predictions moving through the southern GSL from north-west to south-east and exiting at the Cape Breton tip. Towards the end of

October, early November, the relative probability of NARW occurrence begins to diminish in the northern GSL, as well as in the southern GSL after mid-November, until the end of November (end of our model predictions).

Other areas were occasionally highlighted. At the beginning and at the end of the season (May-June and November respectively), portions of the Lower St. Lawrence Estuary briefly appeared with higher predictions that sometimes extended along the southern slope of the Laurentian channel up to the north east of the Gaspé peninsula. The Honguedo Strait along with the Laurentian Channel north of the Gaspé peninsula also showed occasionally a higher probability of NARW occurrence from June to early October. Lastly, the perimeter of the Anticosti gyre sometimes showed increased predictions along the north coast, which seemed to accumulate in some years at the entrance to the SLE.

DISCUSSION

Species distribution models have become an important tool in wildlife management and conservation. They allow the integration of observation data with various environmental information sources, with the aim to understand the relationships between the presence of a species of interest and its surrounding environmental conditions (Guisan and Zimmerman 2000). Furthermore, these models play a key role in identifying important habitat for conservation purposes, assisting in the prioritization of areas for the application of protection and management strategies (Guisan and Thuiller 2005, Elith and Leathwick 2009, Guisan et al. 2013).

Since 2015, an important increase in the occurrences of the endangered NARW in the GSL (Simard et al. 2019, Crowe et al. 2021) and, in particular, the high number of mortalities observed in 2017 (Daoust et al. 2017) and 2019 (Bourque et al. 2020) have led to the implementation of a NARW monitoring program. Objectives were multiple and included the implementation of management measures to protect them (Davies and Brillant 2019), acquisition of information on NARW spatial and temporal distribution to help predict suitable habitat over time and space.

The data acquired from the systematic aerial surveys conducted during this monitoring program currently constitute the gold standard, as information about survey effort and observation conditions are recorded along with the sightings of the species of interest (St-Pierre et al. 2024b In our models comparing NARW presence with pseudo-absence, we have used this information to define the area effectively observed during the survey, and to weight the data based on the probability of a whale being available to be detected by observers. We believe this approach has enhanced the quality of our models by prioritizing the most reliable information, thereby reducing biases associated with inaccurate representation of the species distribution (Philips et al. 2009).

The performances tests revealed that models developed for specific periods of the year (Two-months periods or half-season models) outperformed the model representing the overall relationship observed throughout the entire survey period (Global model - April to November) when applied to the dataset used for their training. This result was expected, as more time-specific models generally tend to better capture patterns that apply within the specified timeframe than when using a larger timeframe (Montero-Manso and Hyndman 2021). In the case of our NARW modelling exercise, they were considered to account for a potential change in behaviour across their period of presence in the GSL. However, when tested on the independent dataset from the 2021-2022 survey seasons, the Global model outperformed the “period-specific” models. This could be attributed to the fact that the Global model retained more general relationships while “period-specific” models may have been somewhat overfitted to the

relationships observed in 2017-2020. Another important point to consider is that “period-specific” models were trained with smaller datasets than the Global model, thus limiting their capabilities to learn from the data.

RELATIONSHIPS WITH ENVIRONMENTAL VARIABLES

The models tested in this study revealed links between NARW occurrences and several of the environmental variables considered. Here, we will discuss the relationships obtained with the Global model, but will extend our comments to the results of the other models when deemed appropriate.

Bottom depth was included in all of the best models, regardless of the time period considered. NARWs are known to have a relationship with water depth particularly in the context of foraging, with animal generally spending their time feeding at depth or near the surface (Baumgartner et al. 2003, Wright et al. 2024, Lesage et al. DFO. unpublished data). The Global model indicated a strong avoidance of the deepest waters of the GSL, which are located in the Laurentian Channel, although NARW occasionally occurred in this area where depths can reach 280-420 m. The highest positive effect of bottom depth on the probability of NARW occurrence was found at around 130 m. This value seemed high considering the actual distribution of the water depth at the sighting locations (Appendix F). However, when the model predictions were plotted against bottom depth (Appendix F), the distribution closely fitted the actual distribution, suggesting that other variables included in the model explained part of the NARW distribution in shallower waters. Further exploration of the data is needed to clarify these results, as bottom depth was not strongly correlated with any other covariates (Appendix A). Finally, the model also suggested a negative effect of bottom depth on NARW probability of occurrence at water depths less than 40 m, a relationship that could be linked to the quasi-absence of *Calanus* spp. at these depths (Blais et al. 2021).

The Sea Surface Temperature (SST) can be considered as a reliable predictor of right whale distribution. Peak sighting rates of NARWs in their calving range occurred at SST ranging from 12°C to 16°C (Keller et al. 2012, Gowan and Ortega-Ortiz 2014). In the spring, 95% of the NARW sighted in Cape Cod Bay were associated with dense *Calanus* densities and SST between 4 and 12°C, whereas during winter, when NARW are likely searching for alternative food sources such as *Pseudo-calanus,* 88% of the NARW sightings were associated with SST less than 4°C (Pendleton et al. 2012). In the GSL, our model suggested that SST between 7°C and 14°C positively influenced the probability of NARW occurrence, while temperatures between 0°C and 7°C and between 14°C and 20°C had a negative effect on their likelihood of presence.

The salinity was introduced as a covariate of NARW occurrence because it was retained in models explaining the occurrence and abundance of the main NARW prey, *Calanus* spp., in the GSL (Albouy-Boyer et al. 2016, Plourde et al. 2024). Additionally, it was also suggested that NARW could use salinity as a direct cue to detect different water masses during their migrations (Kenney 2001). In our models, the relationship between salinity and the probability of NARW occurrence was negative and linear. This aligned with the trend estimated between salinity and *Calanus hyperboreus* (stages IV and VI) and *Calanus finmarchicus* (stages V and VI) abundances in the area (Albouy-Boyer et al. 2016). Additionally, the low salinity water masses present in the GSL are a consequence of circulation patterns mostly driven by the Gaspé Current (Le Corre et al. 2023). This current is also linked to the transport of *Calanus* spp. into the southwestern GSL (Brennan et al. 2021; see below), where the majority of NARW have been observed.

An index of adequacy of *Calanus* spp. biomasses to fulfil NARW energetical needs (Enet), obtained from Plourde et al. (2024), was included in our models. However, this variable was not retained in any of the best models , and was instead generally replaced by Chla concentrations. This suggests that while the *Calanus* spp. model may accurately predict the spatial and temporal distribution of *Calanus* in the GSL, NARWs may not have used the resources proportionally to their availability or predicted benefit to NARW. However, the fact that we used monthly predictions of Enet while other variables such as Chla were available on a daily baisis, may have limited the capabilities of the models including Enet to fit as closely to the data as the other models. In any case, Chla concentration is recognized as an efficient proxy of food availability or related environmental conditions (Hlista et al. 2009, Torres et al. 2013, Carman et al. 2019). The relationship with the Chla concentration in the best models was generally described as having an increasing positive effect on NARW predicted presence up to approximately 2.5 mg/m³ beyond which effects were negative. Pulses of higher probability of NARW occurrence observed moving through the southern GSL were likely related to the ocean circulation and the advection of phytoplankton (represented by the Chla) in the system. This advection is also known to influence the spatial distribution and biomasses of *Calanus* spp. in the southern GSL, which are transported from the adjacent Laurentian channel via the Gaspé current (Brennan et al. 2019, 2021, Le Corre et al. 2023).

While SST, salinity and Chla concentration may represent markers of water masses associated to the transport of *Calanus* in areas used by NARW, four other variables included in the Global model can all be linked to conditions potentially inducing aggregation of NARW preys. Oceanographic structures such as gyres, eddies and frontal areas can be detected by satellite altimetry measures such as the MSLA (Robinson 2010), and have been considered in several studies to explain the distribution and movements of diverse marine mammal species (Correia et al. 2021, Cotté et al. 2011). Use of such an index in our models resulted in a significant relationship with the probability of NARW occurrence, generally decreasing toward positive sea level anomalies. Recognizing the importance of the Gaspé current as a key factor in the advection of zooplankton in the southern GSL, Tao et al. (2023) demonstrated that the gradient of the MSLA can be used to infer temporal variations in its intensity. In this study, higher MSLA were generally observed in the northern GSL area, although increasing values were noted along the Gaspé peninsula with intensification of the Gaspé current. In the current study, exploratory maps of the MSLA in the GSL during 2017-2020 (Appendix G) suggested that high MSLA values occurred in the Honguedo Strait in June-September, while lower values were observed in the Shediac Valley. However, the interpretation of the relationship between MSLA and the probability of NARW occurrence remains unclear.

As observed for rorqual species in the northern GSL (Doniol-Valcroze et al. 2007), our results also suggested that the probability of NARW occurrence increased with the frequency of thermal fronts in the area, particularly when approaching these fronts. Elevated concentrations of zooplankton are often observed near fronts (Olson et al. 1994, Beardsley et al. 1996) due to various potential mechanisms (Olson and Backus 1985, Franks 1992, Epstein and Beardsley 2001) and *Calanus* spp. are likely to be influenced in the same way in the GSL (Runge and Simard 1990). While the presence of thermal front areas suggested dynamic oceanographic processes, the models also found that the probability of NARW occurrence increased in area with low current speed in the water column. This could indicate that NARW did not use areas directly in the frontal area, but may have used areas along the edges of these fronts, boundaries between different water masses that may help concentrate zooplankton like *Calanus* spp..

The bottom topography can influence oceanic features such as currents, upwelling zones, and can contribute to the formation of eddies by directing the flow of water, creating obstacles that deflect currents, and may influence mixing of water masses (Owen 1981). We used the

topographic position index to classify the bottom morphology and found a significant positive effect of lower slopes and valleys on the probability of NARW occurrence, with middle slopes, upper slopes and ridges having instead a negative effect. This is consistent with the idea that the bottom of valleys on continental shelves may represent areas of concentration of *Calanus* spp. that are seeking deeper waters when going in diapause phase of their life cycle (LeCorre et al. 2023, Johnson et al. 2024, Plourde et al. 2024). These results appear consistent with the effect of the two previous variables (Front distance and Current speed) as valleys and bottom slopes could provide conditions slowing down the current and aggregating preys in basins, whereas the upper part of the slopes may show higher current speeds, potentially creating upwelling conditions.

IMPORTANT AREAS

These different relationships integrated in the Global model, allowed us to obtain prediction maps highlighting important areas for NARW in the GSL. The Shediac Valley already identified by the recurrent detections of NARW in the area (Simard et al. 2019, 2024, Crowe et al. 2021, St-Pierre et al. 2024a), also appeared in our predictions as important throughout most of the period of NARW presence in the GSL (predictions from April to November; Simard et al. 2019, Crowe et al. 2021). This area benefits from the advection of *Calanus*, mainly *Calanus hyperboreus*, by the Gaspé current, early in the season (Le Corre et al. 2023, Johnson et al. 2024). Later in the season, the model suggested an eastward and southward expansion of the area with conditions favorable to NARW occurrence in the southern GSL. To the east, three valleys located along the southern slope of the Laurentian channel (Western and Eastern Bradelle valleys and an unnamed trough) were highlighted, and to the south, valleys located west of the Bradelle Bank also appeared to become suitable starting at the end of July. The entrance to the Chaleur Bay also showed a periodic pattern of suitable conditions for NARW occurrence, mainly in early spring and autumn. Both the trough between the American and the Orphan Banks and an area encompassing the eastern part of Cape Breton showed high predictions of occurrence. However, these two areas also showed large temporal variabilities in the predictions, likely illustrating less predictability in food resource availability and explaining the limited number of observations at these sites (St-Pierre et al. 2024a). In the northern part of the GSL, higher probabilities of NARW occurrence were predicted in the Jacques-Cartier Strait and west of Anticosti Island early in the season and again in late August – September. Other areas, such as parts of the Honguedo Strait and the entrance of the St. Lawrence Estuary, were occasionally highlighted. There was however no clear pattern from our model predictions identifying specific areas within that region with a persistent high probability of NARW occurrence.

Most if not all the results of this modelling exercise concur with the different studies aiming to reveal the characteristics, and the spatial and temporal distribution of the NARW habitat in the GSL. The global model developed in this study using observations from the 2017-2020 surveys provided insights into potential processes explaining the occurrence of NARW in the GSL. Moreover, this model appeared to be relatively effective in predicting the independent dataset obtained from the 2021-2022 surveys, suggesting that the relationships found with the different variables considered are relatively robust.

Integrating the 2021-2022 information into the training dataset would enhance model predictions. However, due to the processing time required to run the various models, it was not feasible to apply an appropriate model selection methodology (e.g. cross-validation) with the merged dataset before the February 2024 National Marine Mammal Committee peer-review meeting.

SOURCES OF UNCERTAINTIES

Model errors are inherent in any predictive model and results from uncertainties in the model parameters. Maps of these errors are available for our predictions (Appendix H), and should be considered to interpret model results and assess the reliability of predictions. The largest variances in NARW probability of occurrence were observed mainly along the coast of the Chaleur Bay, in the Northumberland Strait, and for some models, in the St. Lawrence Estuary. They likely reflect the fact that NARW were rarely or not observed in these areas during DFO surveys, with only occasional reports from other sources, when they exist. Moreover, the covariates included in the models presented in this study, whether observed (depth, SST, Chla) or estimated via other models (CIOPS-E data, Calanus Enet), have their own uncertainties that are not incorporated into our predictions. Large freshwater discharge in the GSL carries colored dissolved organic matter which can bias the estimation of Chla from satellite imagery (Laliberté and Larouche 2023). Chla data included in our models were extracted from Globcolor products, provided by the Copernicus-Marine Environment Monitoring Service, which considers data from multiple satellites integrated with algorithms aiming to reduce this bias in coastal areas (Saulquin et al. 2018). However, these algorithms are optimized for global application, and additional regional corrections may be necessary to further reduce uncertainties for our study area (Laliberté and Larouche 2023). Our models also incorporated temperature data from two distinct sources: one derived from observation/estimation from satellite imagery (SST) and the others (temperature at various depth in the water column) from an oceanographic model (CIOPS-E). While CIOPS-E model is recalibrated daily based on a larger model that uses data assimilation (i.e. incorporation of observation data) to calibrate itself, discrepancies still persist between empirical measurements of temperatures and estimations used in our models (difference < 2°C; Paquin et al. 2024).

In our models, the data were weighted based on the conditions of observation, taking into account the probability of detection. However, this correction only addresses one of the two sources of bias associated with this type of observational data (i.e., aerial surveys). NARW observations are also limited by their availability (presence) at the surface when the plane flies over the area. In this study, we assumed that this bias was uniform across the entire study area and did not affect the results. Future steps could include using telemetry data to investigate whether the time NARW spend at the surface varies with environmental conditions (See Lesage et al. 2024 for an example on beluga), and incorporate spatial variations in availability bias into the habitat modeling approach.

Finally, because our models were mostly trained using daily environmental data, they can produce daily predictions. However, identifying important habitats should not rely on single day predictions but should consider a larger time frame allowing to take into account the variability of these predictions over months, seasons, years.

ACKNOWLEDGEMENTS

We thank SASAIR, Air Montmagny Service Inc and PAL Airlines and their pilots for flying aerial surveys. In addition to the many observers who participated in the aerial surveys, we thank Pascale Caissy, Pierre Goulet, Angélique Ollier, Anne Provencher St-Pierre and Caroline Sauvé for their help with the logistics and the validation of data collection. This research was financially supported by various program of Fisheries and Oceans Canada, particularly the Species at Risk program and the Oceans Protection Plan. Lastly, we dedicate this work to Stéphane Plourde, who sadly passed away in March 2025. Stéphane's dedication to research and his important contributions were invaluable, and his commitment will continue to inspire us.

REFERENCES CITED

Abrahms, B., Welch, H., Brodie, S., Jacox, M.G., Becker, E.A., Bograd, S.J., Irvine, L.M., Palacios, D.M., Mate, B.R., and Hazen, E.L. 2019. Dynamic Ensemble Models to Predict Distributions and Anthropogenic Risk Exposure for Highly Mobile Species. Divers. Distrib. 25:1182:1193.

Albouy-Boyer, S., Plourde, S., Pepin, P., Johnson, C.L., Lehoux, C., Galbraith, P.S., Hebert, D., Lazin, G., and Lafleur, C. 2016. Habitat modelling of key copepod species in the Northwest Atlantic Ocean based on the Atlantic Zone Monitoring Program. J. Plank. Res. 38(3), 589-603.

Allouche, O., Tsoar, A., and Kadmon, R. 2006. Assessing the accuracy of species distribution models: Prevalence, kappa and the true skill statistic (TSS). J. Applied. Ecol. 43:1223-1232.

Baumgartner, M.F., and Mate, B.R. 2003. Summertime foraging ecology of North Atlantic right whales. Mar. Ecol. Prog. Ser. 264:123–135.

Baumgartner, M.F., and Mate, B.R. 2005. Summer and fall habitat of North Atlantic right whales (*Eubalaena glacialis*) inferred from satellite telemetry. Can. J. Fish. Aquat. Sci. 62(3):527-543.

Baumgartner, M.F., Cole, T.V.N., Clapham, P.J., and Mate, B.R. 2003. North Atlantic right whale habitat in the lower Bay of Fundy and on the SW Scotian Shelf during 1999-2001. Mar. Ecol. Progr. Ser. 264:137-154.

Beardsley, R.C., Epstein, A.W., Chen, C., Wishner, K.F., Macaulay, M.C., and Kenney, R.D. 1996. Spatial variability in zooplankton abundance near feeding right whales in the Great South Channel. Deep-Sea Res. II: Top. Stud. Oceanogr. 43(7–8):1601-1625.

Becker, E., Forney, K., Fiedler, P., Barlow, J., Chivers, S., Edwards, C., Moore, A., and Redfern, J. 2016. Moving Towards Dynamic Ocean Management: How Well Do Modeled Ocean Products Predict Species Distributions? Remote Sens. 8(2):149.

Blais, M., Galbraith, P.S., Plourde, S., Devred, E., Clay, S., Lehoux, C., and Devine, L. 2021. Chemical and biological oceanographic conditions in the Estuary and Gulf of St. Lawrence during 2020. DFO Can. Sci. Advis. Sec. Res. Doc. 2021/060. iv + 67 p.

Bourque, L., Wimmer, T., Lair, S., Jones, M. and Daoust, P.-Y. 2020. Incident Report: North Atlantic Right Whale Mortality Event in Eastern Canada, 2019. Collaborative Report Produced by: Canadian Wildlife Health Cooperative and Marine Animal Response Society. 210 pp.

Brennan, C.E., Maps, F., Gentleman, W.C., Plourde, S., Lavoie, D., Chassé, J., Lehoux, C., Krumhansl, K.A. and Johnson, C.L. 2019. How transport shapes copepod distributions in relation to whale feeding habitat: Demonstration of a new modelling framework. Prog. Oceanogr. 171:1–21.

Brennan, C.E., Gentleman, W.C. and Lavoie, D. 2021. Ocean circulation changes drive shifts in *Calanus* abundance in North Atlantic right whale foraging habitat: A model comparison of cool and warm year scenarios. Prog. Oceanogr. 197:1–18.

Brown, M.W., Fenton, D., Smedbol, K., Merriman, C., Robichaud-Leblanc, K., et Conway, J.D. 2009. Recovery Strategy for the North Atlantic Right Whale (*Eubalaena glacialis*) inAtlantic Canadian Waters [Final]. Species at Risk Act Recovery Strategy Series. Fisheries and Oceans Canada. vi + 66 pp.

Buckland, S.T., Anderson, D.R., Burnham, K.P. and Laake, J.L. 1993. Distance Sampling: Estimating Abundance of Biological Populations. Chapman & Hall, London.

Buckland, S.T, Anderson, D.R., Burnham, K.P. and Laake, J.L., Borchers, D.L., and Thomas, L., 2004. *Advanced Distance Sampling.* Oxford University Press. Oxford.

Carman, V.G., Piola, A., O'Brien, T.D., Tormosov, D.D., and Acha, E.M. 2019. Circumpolar frontal systems as potential feeding grounds of Southern Right whales Prog. Oceanogr., 176. 102123.

Cayula J.F., and Cornillon P. 1995. Multi-image edge detection for SST images J. Atmos. Ocean. Technol., 12, pp. 821-829.

Clapham, P.J., Young, S.B. and Brownell, R.L., Jr. 1999. Baleen whales: conservation issues and the status of the most endangered populations. Mamm. Rev. 29:37-62.

Corkeron, P., Hamilton, P., Bannister, J., Best, P., Charlton, C., Groch, K.R., Findlay, K., Rowntree, V., Vermeulen, E., and Richard, P.M. 2018. The recovery of North Atlantic right whales, *Eubalaena glacialis*, has been constrained by human-caused mortality. R. Soc. Open Sci.5180892.

Correia, A.M., Sousa-Guedes, D., Gil, Á., Valente, R., Rosso, M., Sousa-Pinto, I., Sillero, N. and Pierce, G.J. 2021. Predicting cetacean distributions in the eastern North Atlantic to support marine management. Front. Mar. Sci. 8:643569.

Cotté, C., d' Ovidio, F., Chaigneau, A., Lèvy, M., Taupier-Letage, I., Mate, B., and Guinet, G. 2011. Scale-dependent interactions of Mediterranean whales with marine dynamics. Limnol. Oceanogr. 56:219–32.

Cox, S. L., Embling, C.B., Hosegood, P.J., Votier, S.C. and Ingram, S.N. 2018.Oceanographic Drivers of Marine Mammal and Seabird Habitat-Use Across Shelf-Seas: A Guide to Key Features and Recommendations for Future Research and Conservation Management. Estuar. Coast. Shelf. Sci. 212:294–310.

Crowe, L.M., Brown, M.W., Corkeron, P.J., Hamilton, P.K., Ramp, C., Ratelle, S., Vanderlaan, A.S. and Cole, T. V. 2021. In plane sight: A mark-recapture analysis of North Atlantic right whales in the Gulf of St. Lawrence. Endanger. Species Res. 46:227–251.

Daoust, P.Y., Couture, E.L., Wimmer, T. and Bourque, L. 2017. Incident report: North Atlantic right whale mortality event in the Gulf of St. Lawrence, 2017. Collaborative Report Produced by: Canadian Wildlife Health Cooperative, Marine Animal Response Society, and Fisheries and Oceans Canada. 256 pp.

Davies, K.T., and Brillant, S.W. 2019. Mass human-caused mortality spurs federal action to protect endangered North Atlantic right whales in Canada. Mar. Policy 104:157–162.

Davies, K.T., Brown, M.W., Hamilton, P.K., Knowlton, A.R. Taggart, C.T. and Vanderlaan, A.S. 2019. Variation in North Atlantic right whale *Eubalaena glacialis* occurrence in the Bay of Fundy, Canada, over three decades. Endanger. Species Res. 39:159–171.

Davis, G.E., Baumgartner, M.F., Bonnell, J.M., Bell,J., Berchok, C., Thornton, J.B., Brault, S., Charif, R.A., Cholewiak, D., Clark, C.W., Corkeron, P., Delarue, J., Dudzinski, K., Hatch, L., Hildebrand, J., Hodge, L., Klinck, H., Kraus, S., …Van Parijs, S.M. 2017. Long-term passive acoustic recordings track the changing distribution of North Atlantic right whales (*Eubalaena glacialis*) from 2004 to 2014. Sci. Rep. 7:13460.

DFO. 2014. Recovery Strategy for the North Atlantic Right Whale (*Eubalaena glacialis*) in Atlantic Canadian Waters [Final]. Species at Risk Act Recovery Strategy Series. Fisheries and Oceans Canada. vii + 68p.

Doniol-Valcroze,T., Berteaux, D., Larouche, P., and Sears, R. 2007. Influence of thermal fronts on habitat selection by four rorqual whale species in the Gulf of St. Lawrence Mar. Ecol. Prog. Ser. 335:207-216.

Elith, J., and Leathwick, J. R. 2009. Species distribution models: ecological explanation and prediction across space and time. Annu. Rev.Ecol. Evol. Syst. 40:677–697.

El-Gabbas, A., Van Opzeeland, I., Burkhardt, E., and Boebel, O. 2021. Dynamic Species Distribution Models in the Marine Realm: Predicting Year-Round Habitat Suitability of Baleen Whales in the Southern Ocean. Front. Mar. Sci. 8:802276.

Epstein, A.W. and Beardsley, R.C. 2001. Flow-induced aggregation of plankton at a front: a 2-D Eulerian model study. Deep Sea Res. *Part* II Top. Stud. Oceanogr. 48:395-418.

Evans, J.S. and Murphy, M.A. 2023. spatialEco. R package version 2.0-2.

Ferro, C.A.T., and Stephenson, D.B. 2011. Extremal dependence indices: Improved evaluation measures for deterministic forecasts of rare binary events. Weather Forecast 26(5): 699–713.

Fielding, A.H. and Bell, J.F. 1997. A Review of Methods for the Assessment of Prediction Errors in Conservation Presence/Absence Models. Env. Conserv. 24, 38-49.

Franks, P.J.S.1992. Sink or swim: accumulation of biomass at fronts. Mar. Ecol. Progr. Ser 82: 1-12.

Frasier, B. A., Springate, L., and Frasier, T. R. 2022. Genetic examination of historical North Atlantic right whale (*Eubalaena glacialis*) bone specimens from the eastern North Atlantic: Insights into species history, transoceanic population structure, and genetic diversity. Mar. Mamm. Sci.

Fu, L., and Cheney, R.E. 1995. Application of satellite altimetry to ocean circulation studies: 1987–1994. Rev. Geophys. 33: 213-223.

Gavrilchuk, K., Lesage, V., Fortune, S. M. E., Trites, A. W., and Plourde, S. 2021. Foraging habitat of North Atlantic right whales has declined in the Gulf of St. Lawrence, Canada, and may be insufficient for successful reproduction. Endanger. Species Res. 44:113-136.

Gowan, T.A. and Ortega-Ortiz, J.G. 2014. Wintering habitat model for the North Atlantic right whale (*Eubalaena glacialis*) in the southeastern United States. PLoS ONE 9:e95126.

Guisan, A. and Thuiller, W. 2005. Predicting species distribution: offering more than simple habitat models. Ecol. Lett. 8:993–1009.

Guisan, A., and Zimmermann, N. E. 2000. Predictive habitat distribution models in ecology. Ecol. Modell. 135:147–186.

Guisan, A., Tingley, R., Baumgartner, J.B., Naujokaitis-Lewis, I., Sutcliffe, P.R., Tulloch, A.I.T., Regan, T.J., Brotons, L., McDonald-Madden, E., Mantyka-Pringle, C., Martin, T.G, Rhodes, J.R., Maggini, R., Setterfield, S.A., Elith, J., Schwartz, M.W., Wintle, B.A., Broennimann, O., Austin, M., …Buckley, Y.M. 2013. Predicting species distributions for conservation decisions. Ecol. Lett. 16(12):1424-1435.

Harvey, G.K. A., Nelson, T. A., Fox, C. H. and Paquet, P. C. 2017. Quantifying marine mammal hotspots in British Columbia, Canada. Ecosphere 8(7):e01884. 10.1002/ecs2.1884.

Hijmans, R. 2023. terra: Spatial Data Analysis. R package version 1.7-37.

Hlista B.L., Sosik H.M., Martin Traykovski L.V., Kenney, R.D. et Moore M.J. 2009. Seasonal and interannual correlations between right whale distribution and calving success and chlorophyll concentrations in the Gulf of Maine,USA. Mar. Ecol. 394:289–302.

Hui, C.A. 1985. Undersea topography and the comparative distributions of two pelagic cetaceans. Fish. Bull. 83:472–475.

International Whaling Commission (IWC). 1986. Report of the workshop on the status of right whales. Report of the International Whaling Commission (Spec. Iss.10): 1–33.

International Whaling Commission (IWC). 2001. Report on the workshop on the comprehensive assessment of right whales: a worldwide comparison. J. Cetacean Res. Manage. (Spec. Iss.2) 2:1-60.

Johnson, C.L., Plourde, S., Brennan, C.E., Helenius, L.K., Le Corre, N. and Sorochan, K.A. 2024. The Southern Gulf of St. Lawrence as Foraging Habitat for the North Atlantic Right Whale. DFO Can. Sci. Advis. Sec. Res. Doc. 2024/077. iv + 43 p.

Keller, C.A., Garrison, L., Baumstark, R., Ward-Geiger, L.I. and Hines, E. 2012. Application of a habitat model to define calving habitat of the North Atlantic right whale in the southeastern United States. Endanger. Species Res. 18:73–87.

Kenney, R.D. 2001. Anomalous 1992 spring and summer right whale (*Eubalaena glacialis*) distribution in the Gulf of Maine. J. Cetac. Res. Manage. (Special Issue 2): 209-223.

Knowlton, A.R., Hamilton, P.K., Marx, M.K., Pettis, H.M. and Kraus, S.D. 2012. Monitoring North Atlantic right whale *Eubalaena glacialis* entanglement rates: A 30 year retrospective. Mar. Ecol. Prog. Ser. 466:293–302.

Knowlton, A.R., Robbins, J., Landry, S., McKenna, H., Kraus, S.D. and Werner, T.B. 2016. Effects of fishing gear strength on the severity of large whale entanglements. Conserv. Biol. 30:318–328.

Kraus, S.D., Brown, M.W., Caswell, H., Clark, C.W., Fujiwara, M., Hamilton, P.K., Kenney, R.D., Knowlton, A.R., Landry, S., Mayo, C.A., McLellan, W.A., Moore, M.J., Nowacek, D.P., Pabst, D.A., Read, A.J. and Rolland, R.M. 2005. North Atlantic Right Whales in Crisis. Science 309:561-562.

Laist, D.W., Knowlton, A.R., and Pendleton, D. 2014. Effectiveness of mandatory vessel speed limits for protecting North Atlantic right whales. Endanger. Species Res. 23(2):133–147.

Laliberté, J. and Larouche, P. 2023. Chlorophyll-a Concentration Climatology, Phenology, and Trends in the Optically Complex Waters of the St. Lawrence Estuary and Gulf. J. Mar. Syst. 238:103830.

Le Corre, N., Brennan, C.E., Chassé, J., Johnson, C.L., Lavoie, D., Paquin, J.-P., Soontiens, N. and Plourde, S. 2023. A biophysical model *of Calanus hyperboreus* in the Gulf of St. Lawrence: Interannual variability in phenology and circulation drive the timing and location of right whale foraging habitat in spring and early summer. Prog. Oceanogr. 219:1–20.

Lesage V., Wing S., Zuur A.F., Gosselin J.F., Tinker M.T., Mosnier A., St-Pierre A.P., Michaud R., and Berteaux D. 2024. Environmental, behavioral, and design-related factors affect accuracy and precision of beluga abundance estimates from aerial surveys. Front. Mar. Sci., 15. Volume 11.

Linden, D.W. 2023. Population size estimation of North Atlantic right whales from 1990-2022. US Dept. Commer. Northeast. Fish. Sci. Cent. Tech. Memo. 314. 14 p.

Manel, S., Williams, H.C. and Ormerod, S. 2001. Evaluating presence-absence models in ecology: the need to account for prevalence. J. Appl. Ecol. 38: 921-931.

Marine Mammal Commission. 2024. Marine Mammal Commission. An independent Agency of the U.S. Government. Accessed on 4 February 2024.

Marra, G., and Wood, S. N. 2011. Practical variable selection for generalized additive models. Comput. Stat.Data Anal. 55(7):2372-2387.

Mate, B.R., Nieukirk, S.L. and Kraus, S.D. 1997. Satellite-Monitored Movements of the Northern Right Whale. J. Wildl. Manage. 61(4):1393–1405.

Mead, J.G. 1986. Twentieth-century records of right whales (*Eubalaena glacialis*) in the northwestern North Atlantic. Rep. Int. Whal. Commn (Spec. Iss.10) 10:109-119.

Meyer-Gutbrod, E.L., Davies, K.T.A., Johnson, C.L., Plourde, S., Sorochan, K.A., Kenney, R.D., Ramp, C., Gosselin, J.-F., Lawson, J.W. and Greene, C.H. 2022. Redefining North Atlantic right whale habitat-use patterns under climate change. Limnol. Oceanogr. 68:S71- S86.

Milanesi, P., Della Rocca, F., and Robinson, R.A. 2020. Integrating dynamic environmental predictors and species occurrences: toward true dynamic species distribution models. Ecol. Evol. 10, 1087–1092.

Miller, D.L., and Clark-Wolf, T.J. 2023. Distance Sampling Detection Function and Abundance Estimation. R package version 1.0.9.

Mitchell, E., Kozicki, V.M. et Reeves, R.R. 1986. Sightings of right whales, *Eubalaena glacialis*, on the Scotian Shelf, 1966-1973. Rep.Iint. Whal. Commn (Spec. Iss.) 10:83101.

Moore, M.J., Knowlton, A.R., Krauss, S.D., McLellan, W.A. and Bonde, R.K. 2004. Morphometry, gross morphology and available histopathology in North Atlantic right whale (*Eubalaena glacialis*) mortalities (1970–2002). J. Cetacean Res. Manag. 6:199-214.

Mosnier, A., Gosselin, J.-F., and Lesage, V. 2022. Seasonal distribution and concentration of four baleen whale species in the St. Lawrence Estuary based on 22 years of DFO observation data. DFO Can. Sci. Advis. Sec. Res. Doc. 2020/053. iv + 119 p.

Monsarrat, S., Pennino, M.G., Smith, T.D., Reeves, R.R., Meynard, C.N., Kaplan, D.M., and Rodrigues, A.S.L. 2015. Historical summer distribution of the endangered North Atlantic right whale (*Eubalaena glacialis*): a hypothesis based on the environmental niche of a congeneric species. Divers. Distrib. 21: 925–937.

Montero-Manso P., and Hyndman R.J. 2021. Principles and algorithms for forecasting groups of time series: Locality and globality. Int. J. Forecast. 37 (4), 1632-1653.

Murison, L.D., and Gaskin, D.E. 1989. The distribution of right whales and zooplankton in the Bay of Fundy, Canada. Can. J. Zool. 67:1411-1420.

Nerem, R.S., Tapley, B.D., and Shum, C.K. 1990. Determination of the ocean circulation using Geosat altimetry. J. Geophys. Res. 95(C3):3163–3179.

Olson, D.B. and Backus, R.H. 1985. The concentrating of organisms at fronts: a cold-water fish and a warm-core ring. J. Mar. Res. 43:113-137.

Olson, D.B., Hitchcock, G.L., Mariano, A.J., Ashjian, C.J., Peng, G., Nero, R.W. and G.P. Podestá. 1994. Life on the edge: Marine life and fronts. Oceanography 7(2):52–60.

Owen, R.W. 1981. Front and eddies in the sea: mechanisms, interactions and biological effects, in Analysis of marine ecosystems, A.R. Longhurst ed. Academic Press. London. 197-233.

Paquin, J.-P., Roy, F., Smith, G. C., MacDermid, S., Lei, J., Dupont, F., Lu, Y., Taylor, S., St-Onge-Drouin, S., Blanken, H., Dunphy, M., and Soontiens, N. 2024. A new high-resolution Coastal Ice-Ocean Prediction System for the East Coast of Canada. Ocean Dyn. 74, 799-826.

Pardo, M.A., Gerrodette, T., Beier, E., Gendron, D., Forney, K.A., Chivers, S.J., Barlow, J. and Palacios, D.M. 2015. Inferring Cetacean Population Densities from the Absolute Dynamic Topography of the Ocean in a Hierarchical Bayesian Framework. *PLOS One* 10: 1–23.

Pebesma, E. 2018. Simple Features for R: Standardized Support for Spatial Vector Data. The R Journal 10:439-446.

Pebesma, E., and Bivand, R. 2023. Spatial Data Science: With Applications in R (1st ed.). Chapman and Hall/CRC.

Pendleton, D., Pershing, A., Brown, M., Mayo, C., Kenney, R., Record, N., and Cole, T. 2009. Regional-scale mean copepod concentration indicates relative abundance of North Atlantic right whales. Mar. Ecol. Prog. Ser. 378, 211–225.

Pendleton, D.E., Sullivan, P.J., Brown, M.W., Cole, T.V.N., Good, C.P., Mayo, C.A., Monger, B.C., Phillips, S., Record, N.R. and Pershing, A.J. 2012. Weekly predictions of North Atlantic right whale *Eubalaena glacialis* habitat reveal influence of prey abundance and seasonality of habitat preferences. Endanger. Species Res. 18(2):147–161.

Phillips, S.J., Dudík, M., Elith, J., Graham, C.H., Lehmann, A., Leathwick, J., and Ferrier, S. 2009. Sample selection bias and presence-only distribution models: implications for background and pseudo-absence data. Ecol. Appl., 19 (1) pp. 181-197.

Plourde, S., Lehoux, C., McQuinn, I.H., and Lesage, V. 2016. Describing krill distribution in the western North Atlantic using statistical habitat models. DFO Can. Sci. Advis. Sec. Res. Doc. 2016/111. v + 34 p.

Plourde, S, Lehoux, C., Johnson, C.L., Perrin, G., and Lesage, V. 2019. North Atlantic right whale (*Eubalaena glacialis*) and its food: (I) a spatial climatology of *Calanus* biomass and potential foraging habitats in Canadian waters. J. Plankton Res. 41(5): 667–685.

Plourde, S., Lehoux, C., Roberts, J.J., Johnson, C.L., Record, N., Pepin, P., Orphanides, C., Schick, R.S., Walsh, H.J., and Ross, C.H. 2024. Describing the Seasonal and Spatial Distribution of Calanus Prey and North Atlantic Right Whale Potential Foraging Habitats in Canadian Waters Using Species Distribution Models. DFO Can. Sci. Advis. Sec. Res. Doc. 2024/039. v + 71 p.

QGIS.org 2023. QGIS Geographic Information System. Open Source Geospatial Foundation Project.

R Core Team. 2023. R: A Language and Environment for Statistical Computing. R Foundation for Statistical Computing, Vienna, Austria.

Record, N.R., J.A. Runge, D.E. Pendleton, W.M. Balch, K.T.A. Davies, A.J. Pershing, C.L. Johnson, K. Stamieszkin, R. Ji, Z. Feng, S.D. Kraus, R.D. Kenney, C.A. Hudak, C.A. Mayo, C. Chen, J.E. Salisbury, and C.R.S. Thompson. 2019. Rapid Climate-driven circulation changes threaten conservation of endangered North Atlantic Right Whales. Oceanography 32(2): 162-169.

Reeves, R.R. and Mitchell, E. 1986. American pelagic whaling for right whales in the North Atlantic. Rep. Int. Whal. Commn (Spec. Iss.10) 10:221-254.

Roberts, J.J., Best, B.D., Dunn, D.C., Treml, E.A. and Halpin, P.N. 2010 Marine Geospatial Ecology Tools: An integrated framework for ecological geoprocessing with ArcGIS, Python, R, MATLAB, and C++. Environ. Model. Softw. 25:1197-1207.

Roberts JJ, Yack TM, Fujioka E, Halpin PN, Baumgartner MF, Boisseau O, Chavez-Rosales S, Cole TVN, Cotter MP, Davis GE, DiGiovanni RA, Ganley LC, Garrison LP, Good CP, Gowan TA, Jackson KA, Kenney RD, Khan CB, Knowlton AR, Kraus SD, Lockhart GG, Lomac-MacNair KS, Mayo CA, McKenna BE, McLellan WA, Nowacek DP, O'Brien O, Pabst DA, Palka DL, Patterson EM, Pendleton DE, Quintana-Rizzo E, Record NR, Redfern JV, Rickard ME, White M, Whitt AD, and Zoidis AM. 2024. North Atlantic right whale density surface model for the US Atlantic evaluated with passive acoustic monitoring. Mar. Ecol. Prog. Ser. 732:167–192.

Robinson, I. S. 2010. Discovering the Oceans from Space. The Unique Applications of Satellite Oceanography. Berlin: Springer.

Runge, J.A. and Simard, Y. 1990. Zooplankton of the St. Lawrence Estuary. *In* Oceanography of a Large-Scale Estuarine System (eds M.I. El-Sabh and N. Silverberg).

Saulquin, B., Gohin, F., and Fanton d'Andon, O. 2018. Interpolated fields of satellite-derived multi[1]algorithm chlorophyll-a estimates at global and European scales in the framework of the European Copernicus-Marine Environment Monitoring Service. J. Oper. Oceanogr., 12, 47–57.

Schevill, W.E. and Moore, K.E. 1983. Townsend's unmapped North Atlantic right whales (*Eubalaena glacialis*). Breviora 476:1-8.

Simard, Y., N. Roy, S. Giard, and F. Aulanier. 2019. North Atlantic right whale shift to the Gulf of St. Lawrence in 2015, revealed by long-term passive acoustics. Endanger. Species Res. 40:271–284. doi:10.3354/esr01005.

Simard, Y., Giard, S., Roy, N., Royer, P., Chartrand-Lemieux, M.-E., and Perreault, E. 2024. Time-Space Distribution of North Atlantic Right Whale in Gulf of St-Lawrence from Acoustic Monitoring between 2010 and 2022. DFO Can. Sci. Advis. Sec. Res. Doc. 2024/046. vi + 26 p.

Sorochan, K.A., Plourde, S., Morse, R., Pepin, P., Runge, J., Thompson, C., and Johnson, C.L. 2019. North Atlantic right whale (*Eubalaena glacialis*) and its food: (II) interannual variations in biomass of *Calanus* spp. on western North Atlantic shelves. J. Plankton Res. 41(5): 687–708. doi:10.1093/plankt/fbz044.

Sorochan, K.A., Plourde, S., Morse, R., Pepin, P., Runge, J., Thompson, C., and Johnson, C.L. 2019. North Atlantic right whale (*Eubalaena glacialis*) and its food: (II) interannual variations in biomass of *Calanus* spp. on western North Atlantic shelves. J. Plankton Res. 41(5): 687–708. doi:10.1093/plankt/fbz044.

Sorochan, K.A., Plourde, S., Baumgartner, M.F., and Johnson, C.L. 2021. Availability, supply, and aggregation of prey (*Calanus* spp.) in foraging areas of the North Atlantic right whale (*Eubalaena glacialis*). ICES J. Mar. Sci. 78(10):3498–3520.

Sorochan, K.A., Plourde, S. and Johnson, C.L. 2023. Near-bottom aggregations of *Calanus* spp. Copepods in the southern Gulf of St. Lawrence in summer: significance for North Atlantic right whale foraging. ICES J. Mar. Sci. 80:787-802.

Stewart, J. D., Durban, J. W., Fearnbach, H., Hamilton, P. K., Knowlton, A. R., Lynn, M. S., Miller, C. A. et al. 2022. Larger females have more calves: influence of maternal body length on fecundity in North Atlantic right whales. Mar. Ecol. Prog. Ser. 689: 179–189.

St-Pierre, A.P., Koll-Egyed, T., Harvey, V., Lawson, J.W., Sauvé, C., Ollier, A., Goulet, P.J., Hammill, M.O., and Gosselin, JF. 2024a. Distribution of North Atlantic Right Whales, *Eubalaena glacialis*, in Eastern Canada from Line-Transect Surveys from 2017 to 2022. DFO Can. Sci. Advis. Sec. Res. Doc. 2024/059. iv + 68 p.

St-Pierre, A.P., Lesage, V, Mosnier, A., Tinker, M.T. and Gosselin, J.-F. 2024b. Summer abundance estimates for St. Lawrence Estuary beluga (*Delphinapterus leucas*) from 52 visual line transect surveys and 11 photographic surveys conducted from 1990 to 2022. DFO Can. Sci. Advis. Sec. Res. Doc. 2023/048. v + 82 p.

Tao, J., Shen, H., Danielson, R.E., and Perrie, W. 2023. Characterizing the Variability of a Physical Driver of North Atlantic Right Whale Foraging Habitat Using Altimetric Indices. J. Mar. Sci. Eng, 11, 1760.

Torres, L.G., Smith, T.D., Sutton, P., MacDiarmid, A., Bannister, J., Miyashita, T., and Franklin, J. 2013. From exploitation to conservation: habitat models using whaling data predict distribution patterns and threat exposure of an endangered whale. Divers. Distrib., 19 (2013), pp. 1138-1152

Vanderlaan, A.S. and Taggart, C.T. 2009. Efficacy of a voluntary area to be avoided to reduce risk of lethal vessel strikes to endangered whales. Conserv. Biol. 23(6):1467–1474.

Warwick-Evans, V., Kelly, N., Dalla Rosa, L., Friedlaender, A., Hinke, J.T., Kim, J.H., Kokubun, N., Santora, J.-A., Secchi, E.R., Seyboth, E. and Trathan, P.N. 2022. Using seabird and whale distribution models to estimate spatial consumption of Antarctic krill to inform fishery management. Ecosphere 13:e4083. 10.1002/ecs2.4083.

Watwood, S.L. and Buonantony, D.M. 2012. Dive Distribution and Group Size Parameters for Marine Species Occurring in Navy Training and Testing Areas in the North Atlantic and North Pacific Oceans. NUWC-NPT Tech. Doc. 12.085, Naval Undersea Warfare Center Division, Newport, RI.

Weiss, A. 2001. Topographic position and landforms analysis. In: Poster presentation, ESRI user conference, San Diego, CA.

Winn, H.E., Price, C.A., and Sorensen, P.W. 1986. The distributional ecology of the right whale *Eubalaena glacialis* in the western North Atlantic. Rep. Inter. Whal. Comm. (Special Issue 10):129–138.

Wood, S.N., Goude, Y., and Shaw, S. 2015. Generalized additive models for large datasets. J. R. Statist. Soc., Series C 64(1):139-155.

Wood, S.N., Li, Z., Shaddick, G., and Augustin N.H. 2017. Generalized additive models for gigadata: modelling the UK black smoke network daily data. J. Amer. Statist. Ass. 112:519, 1199-1210.

Wunderlich, R.F., Lin, Y.-P., Anthony, J., and Petway, J.R. 2019. Two alternative evaluation metrics to replace the true skill statistic in the assessment of species distribution models. Nature Conserv. 35:97-116.

Wright, A.J., Gabaldon, J., Zhang, D., and Hamilton, P. 2024. Bimodal vertical distribution of right whales *Eubalaena glacialis* in the Gulf of St. Lawrence. Endanger. Species Res. 54:155-166.

Wyles, H.M.E., Boehme, L., Russell, D.J. and Carter, M.I. 2022. A novel approach to using seabed geomorphology as a predictor of habitat use in highly mobile marine predators: implications for ecology and conservation. Front. Mar. Sci. 9.

Youden, W.J. 1950. Index for rating diagnostic tests. Cancer 3:32–5.

TABLES

Table 1. Environmental and biological variables used to predict the spatial distribution of North Atlantic right whales, Eubaleana glacialis, in the Gulf and the Estuary of St. Lawrence between April and November from 2017 and 2022.

Predictors	Description	Unit	Spatial resolution	Temporal resolution	Source	Reference
Depth	Maximum depth of the water column	m	20 m	static variable	Canadian Hydrographic Service	-
Slope	Maximum rate of depth change	Degree	20 m	static variable	Based on depth map (see Materiel and Method)	-
Topographic position index (TPI)	Identify the topographic features of the seabed: flat slope, valley, lower slope, middle slope, upper slope and ridge	-	20 m	static variable	Based on depth map (see Materiel and Method)	-
SST	Sea-surface temperature (SST) at the observation date	ºC	1/100º	Daily	Group for High resolution Sea Surface Temperature (GHRSST)	JPL-L4_GHRSST-SSTfnd-MUR-GLOB-v02.0-fv04.11
SST_15d	Mean SST values over 15 days prior to the observation date	ºC	1/100º	Daily	GHRSST	JPL-L4_GHRSST-SSTfnd-MUR-GLOB-v02.0-fv04.11
SST_lag3d	SST value 3 days prior to the observation date	ºC	1/100º	Daily	GHRSST	JPL-L4_GHRSST-SSTfnd-MUR-GLOB-v02.0-fv04.11
SST_lag15d	SST value 15 days prior to the observation date	ºC	1/100º	Daily	GHRSST	JPL-L4_GHRSST-SSTfnd-MUR-GLOB-v02.0-fv04.11
T0_50	Mean temperature from 0 to 50 m	ºC	1/36º	Daily	CIOPS-E	Paquin et al. (2024)
Tmod_NB	Mean temperature near the seabed (near bottom)	ºC	1/36º	Daily	CIOPS-E	Paquin et al. (2024)
Tmod_mean	Mean temperature throughout the water column	ºC	1/36º	Daily	CIOPS-E	Paquin et al. (2024)
CurMean010	Mean value of current speed from 0 to 10 m	m/s	1/36º	Daily	CIOPS-E	Paquin et al. (2024)

Predictors	Description	Unit	Spatial resolution	Temporal resolution	Source	Reference
CurQ50_0150	Median value of current speed from 0 to a maximum of 150 m	m/s	1/36°	Daily	CIOPS-E	Paquin et al. (2024)
S0_50	Salinity from 0 to 50 m	‰	1/36°	Daily	CIOPS-E	Paquin et al. (2024)
Front_dist	Distance to the closest front	m	1/100°	Daily	Based on daily SST maps (see Materiel and Method)	-
FrontFreq_5km	Frequency of fronts within 5 km	-	1/100°	Daily	Based on daily SST maps (see Materiel and Method)	-
MSLA	Mean sea level anomaly	m	1/4°	Daily	Copernicus Marine Environment Monitoring Service (CMEMS)	SEALEVEL_GLO_PHY_L4_MY_008_047
Chla_3d	Concentration of chlorophyll a (Chla) 3 days prior to the observation date	mg/m^3	1/4°	Daily	CMEMS-Globcolor Product	OCEANCOLOUR_GLO_BGC_L4_MY_009_104
Chla_15d	Mean Chla 15 days prior to the observation date	mg/m^3	1/4°	Daily	CMEMS-Globcolor Product	OCEANCOLOUR_GLO_BGC_L4_MY_009_104
EnetMod1_month	*Calanus* spp. energy available to NARW (Enet)	$kJ\ g^{-1}$	1/12°	Monthly	*Calanus* spp model 3.3	Plourde et al. (2024)
EnetMod2_month	Enet	$kJ\ g^{-1}$	1/12°	Monthly	*Calanus* spp model 2	Plourde et al (2024)
EnetMod1_2monthsMean	Mean Enet value over 2 months	$kJ\ g^{-1}$	1/12°	Bi-monthly average	*Calanus* spp model 3.3	Plourde et al (2024)
EnetMod2_2monthsMean	Mean Enet value over 2 months	$kJ\ g^{-1}$	1/12°	Bi-monthly average	*Calanus* spp model 2	Plourde et al (2024)
EnetMod1_MeanLast3Y	Mean Enet value over the last 3 seasons	$kJ\ g^{-1}$	1/12°	Monthly	*Calanus* spp model 3.3	Plourde et al (2024)
EnetMod2_MeanLast3Y	mean Enet value over the last 3 seasons	$kJ\ g^{-1}$	1/12°	Monthly	*Calanus* spp model 2	Plourde et al (2024)

Table 2. Covariates included in the best models predicting the probability of North Atlantic right whale occurrence in the Estuary and Gulf of the St. Lawrence over two-months, or half-season periods or globally from April to November. Results are shown for models including or not Calanus spp. as a covariate. Covariates included in all, some or none of the models are indicated as dark grey, light grey and white, respectively.

	Apr.-May	June-July	Aug.-Sept.	Oct.-Nov.	Apr.-July	Aug.-Nov.	Global Apr.-Nov.
	Without Calanus Predictions included as a covariate						
Depth							
TPI							
S0_50							
FrontFreq_5km							
Front_dist							
SST_15d							
SST_lag15d							
SST_lag3d							
Tmod_mean							
Tmod_NB							
CurMean010							
CurQ50_0150							
MSLA							
Chla_15d							
Chla_3d							
	With Calanus Predictions included as a covariate						
Depth							
TPI							
S0_50							
FrontFreq_5km							
Front_dist							
SST_15d							
SST_lag15d							
SST_lag3d							
Tmod_mean							
Tmod_NB							
CurMean010							
CurQ50_0150							
MSLA							
EnetMod2_month							
EnetMod1_2monthsMean							
EnetMod2_2monthsMean							
EnetMod1_MeanLast3Y							
EnetMod2_MeanLast3Y							

Table 3. Covariates included in the best models selected to predict the probability of North Atlantic right whale occurrence in the Estuary and Gulf of the St. Lawrence over two months, half seasons (four month periods) or globally (April to November). The number of presences and pseudo-absences considered in each period is shown in brackets. Models including Calanus spp. predictions as a covariate are highlighted in grey. Akaike Information Criterion (AIC) values obtained for each model are provided, allowing comparisons within the same period. The Area Under the Receiver Operating Criterion Curve (AUC) values measuring model performance are provided for their application on the training dataset (AUC_{train}) and the testing dataset (AUC_{test}).

		Model formulation	AIC	AUC_{train}	AUC_{test}
Two - Months Periods	**April-May** (21/54580)	~ Depth + Front_dist + EnetMod1_2montMean	191.3	0.94	NA*
		~ Depth + SST_lag15d + Front_dist + EnetMod1_MeanLast3Y	192.5	0.95	NA*
		~ Depth + SST_15d + Front_dist	199.4	0.78	0.38
	June-July (288/123709)	~ Depth + Tmod_mean + S0_50 + FrontFreq_5km + CurMean010 + EnetMod2_MeanLast3Y	2244.2	0.93	NA*
		~ Depth + MSLA + SST_lag15d + S0_50 + FrontFreq_5km + ChloA_15d	2245.0	0.93	0.82
	Aug-Sept (211/137275)	~ Depth + slope + MSLA + SST_lag3d + S0_50 + FrontFreq_5km + EnetMod2_month	1808.9	0.82	NA*
		~ Depth + MSLA + SST_lag3d + Tmod_NB + S0_50 + FrontFreq_5km + ChloA_15d	1771.2	0.83	0.84
		~ Depth + TPI + MSLA + SST_lag3d + Tmod_NB + S0_50 + FrontFreq_5km + ChloA_3d	1772.3	0.82	0.78
		~ Depth + MSLA + SST_lag3d + Tmod_NB + S0_50 + FrontFreq_5km + ChloA_3d	1772.9	0.81	0.76
	Oct-Nov (71/66635)	~ Depth + TPI + Tmod_mean + FrontFreq_5km + EnetMod2_MeanLast3Y	699.9	0.85	NA*
		~ Depth + MSLA + SST_lag3d + Tmod_NB + S0_50 + FrontFreq_5km + ChloA_15d	705.2	0.89	0.7
Half-season periods	**Apr-Jul** (309/178289)	~ Depth + TPI + SST_lag15d + S0_50 + FrontFreq_5km + CurQ50_0150 + EnetMod2_MeanLast3Y	2565.5	0.92	NA*
		~ Depth + TPI + MSLA + SST_lag15d + S0_50 + FrontFreq_5km + ChloA_15d + CurMean010	2459.2	0.94	0.77
		~ Depth + TPI + MSLA + SST_lag15d + S0_50 + FrontFreq_5km + ChloA_15d	2461.3	0.94	0.77
	Aug-Nov (282/203910)	~ Depth + TPI + MSLA + SST_lag3d + Tmod_NB + S0_50 + CurQ50_0150 + EnetMod1_2monthsMean	2612.7	0.79	NA*
		~ Depth + TPI + MSLA + SST_lag3d + Tmod_NB + S0_50 + ChloA_15d + CurQ50_0150	2583.5	0.83	0.80
Whole Season	**Global** (591/382199)	~ Depth + slope + TPI + SST_lag3d + Tmod_NB + S0_50 + FrontFreq_5km + CurMean010 + EnetMod2_2monthsMean	5422.3	0.84	NA*
		~ Depth + slope + TPI + MSLA + SST_lag3d + Tmod_NB + S0_50 + Front_dist + CurMean010 + EnetMod2_2monthsMean	5423.9	0.84	NA*
		~ Depth + TPI + MSLA + SST_lag3d + S0_50 + Front_dist + ChloA_15d + CurQ50_0150	5304.1	0.86	0.83

* Enet data not available in the testing dataset (2021-2022 surveys)

Table 4. Performance indicators for the best models predicting the occurrence of North Atlantic right whales (NARW), Eubaleana glacialis, in the Estuary and Gulf of St. Lawrence from April to November (Global model) and over two-month periods, and half seasons (four month periods). Performance indicators include: The Area Under the Curve (AUC), i.e. representing the probability that the model will rank conditions where NARW occurred higher than conditions where they were absent; the True Positive (TP) and the True Negative (TN), i.e.the proportion of instances where the model correctly predicted the presence and absence respectively; the Accuracy, i.e. the proportion of total predictions that were correct; and finally the Symmetric extremal dependence index (SEDI), a skill score providing meaningful results in the case of rare events (limited number of observations compared to a large proportion of zeros representing pseudo-absence in our dataset). Note: If alternative models existed for a specific period (i.e., with a delta AIC ≤ 3 from the lowest AIC), only the performance of the model with the lowest AIC was presented. Moreover, for the April-May and Oct-Nov periods, the best model included a variable derived from another model (the Calanus spp. model), for which predictions were not available in the testing dataset (2021-2022); therefore, performance values were not provided in these cases.

	Best models performances						
	Training dataset (2017-2020)						
Models	Global	Apr_May	June_July	Aug_Sept	Oct-Nov	Apr_July	Aug_Nov
AUC	0.864	0.944	0.931	0.829	0.846	0.940	0.829
TP	0.812	0.952	0.906	0.597	0.873	0.903	0.709
TN	0.783	0.857	0.816	0.934	0.646	0.828	0.800
Accuracy	0.797	0.905	0.861	0.765	0.760	0.865	0.755
SEDI	0.752	0.922	0.861	0.722	0.689	0.867	0.668
	Testing dataset (2021-2022)						
Models	Global	Apr_May	June_July	Aug_Sept	Oct-Nov	Apr_July	Aug_Nov
AUC	0.830	NA	0.824	0.840	NA	0.774	0.798
TP	0.740	NA	0.817	0.879	NA	0.675	0.777
TN	0.803	NA	0.741	0.660	NA	0.759	0.710
Accuracy	0.771	NA	0.779	0.770	NA	0.717	0.744
SEDI	0.701	NA	0.718	0.709	NA	0.584	0.643

Table 5. Performance indicators for the best Global model (i.e. the best model obtained by fitting the entire dataset from April to November; see Table 2) when applied to predict the occurrence of North Atlantic right whales (NARW), Eubaleana glacialis, in the Estuary and Gulf of St. Lawrence from April to November (Global model), over different periods of two-months each, and over half-seasons (four-month periods). Each column presents the performance of the best model trained with the entire dataset (Global model) when applied on each period considered. Performance indicators include: The Area Under the Curve (AUC), i.e. representing the probability that the model will rank conditions where NARW occurred higher than conditions where they were absent; the True Positive (TP) and True Negative (TN), i.e., the proportion of instances where the model correctly predicted the presence and absence, respectively; the Accuracy, i.e. the proportion of total predictions that were correct; and finally, the Symmetric extremal dependence index (SEDI), a skill score providing meaningful results in the case of rare events (limited number of observations compared to a large proportion of zeros representing pseudo-absence in our dataset).

	Best global model performances on the different periods						
	Training dataset (2017-2020)						
Period	Global	Apr_May	June_July	Aug_Sept	Oct_Nov	Apr_July	Aug_Nov
AUC	0.864	0.772	0.889	0.859	0.790	0.891	0.841
TP	0.812	0.952	0.872	0.782	0.747	0.829	0.787
TN	0.783	0.517	0.788	0.776	0.739	0.828	0.750
Accuracy	0.797	0.734	0.830	0.779	0.743	0.828	0.769
SEDI	0.752	0.683	0.811	0.716	0.640	0.807	0.696
	Testing dataset (2021-2022)						
Period	Global	Apr_May	June_July	Aug_Sept	Oct_Nov	Apr_July	Aug_Nov
AUC	0.830	0.648	0.866	0.897	0.628	0.824	0.846
TP	0.740	0.882	0.868	0.897	0.805	0.711	0.767
TN	0.803	0.471	0.771	0.785	0.406	0.813	0.825
Accuracy	0.771	0.676	0.820	0.841	0.606	0.762	0.796
SEDI	0.701	0.519	0.794	0.831	0.317	0.683	0.750

FIGURES

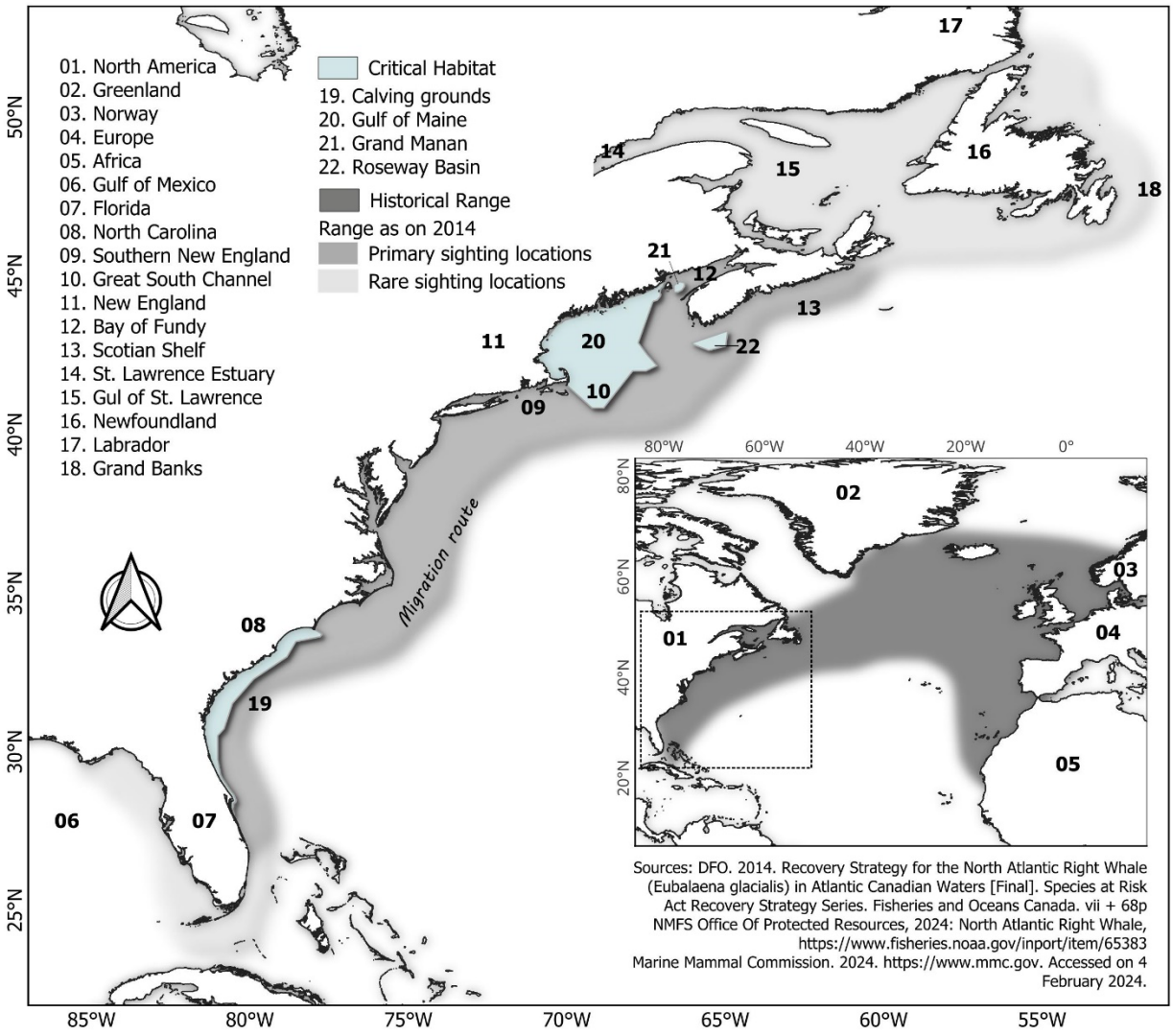

Figure 1. Historical distribution (reproduced from Marine Mammal Commission 2024) and range as of 2014 (reproduced from DFO 2014) of North Atlantic right whale, Eubaleana glacialis, as well as areas in United States and Canada legally designated as Critical Habitat for the population.

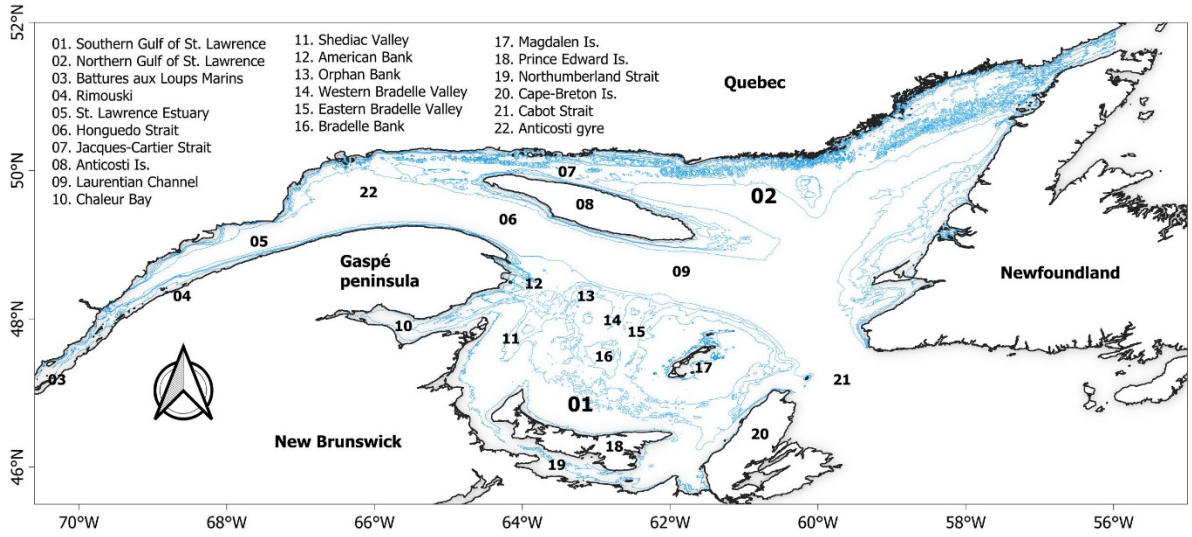

Figure 2. Estuary and Gulf of St. Lawrence and place names used in this document. The blue lines represented the 20 m, 60 m, 80 m, 100 m and 200 m isolines.

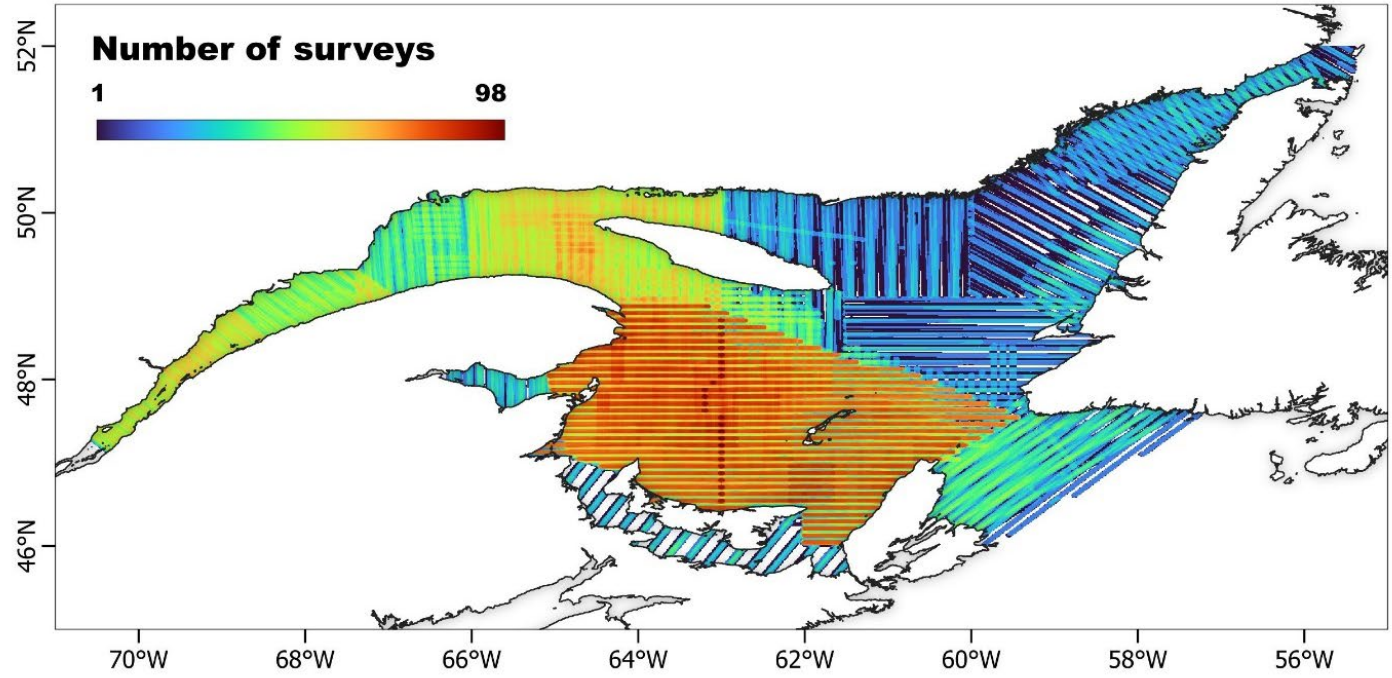

Figure 3. Effort in terms of number of systematic line-transect aerial visual surveys covering the Estuary and Gulf of St. Lawrence that were conducted by DFO from April 1st to November 30th between 2017 and 2022.

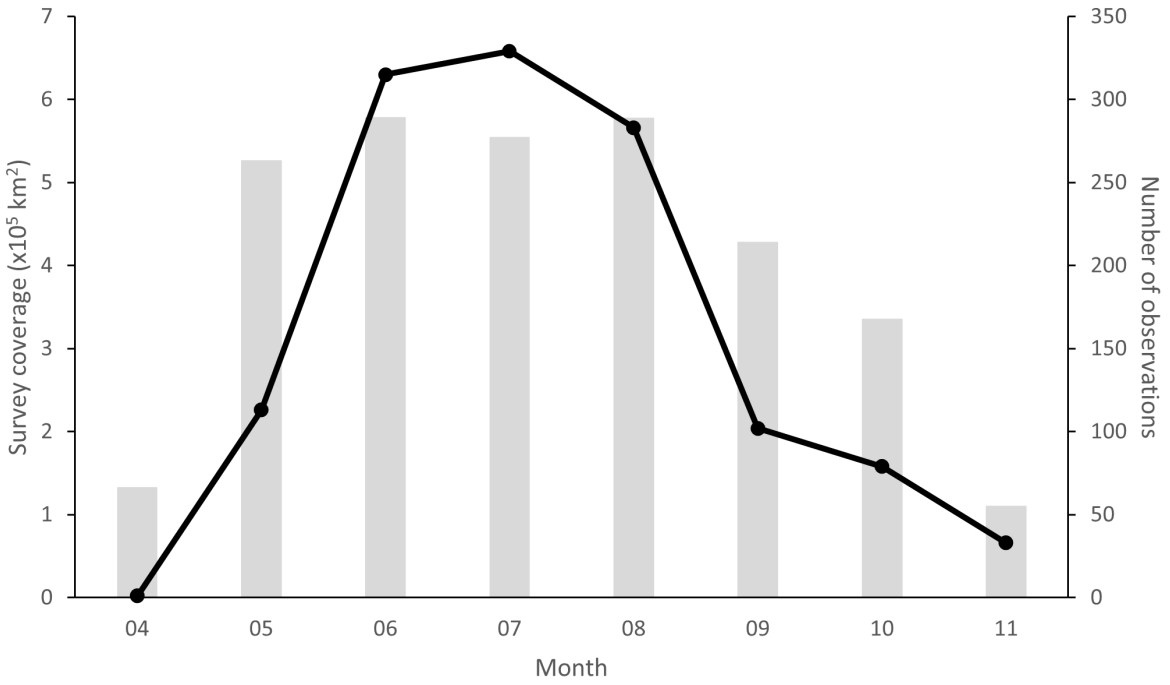

Figure 4. Monthly distribution of the area covered (grey bars) by the systematic line-transect visual aerial surveys conducted by DFO in the Estuary and Gulf of St Lawrence from April 1st to November 30th during 2017-2022, with the exception of 2017, when surveys began on August 29th. The black line represents the number of North Atlantic right whales (Eubaleana glacialis) detected during these surveys.

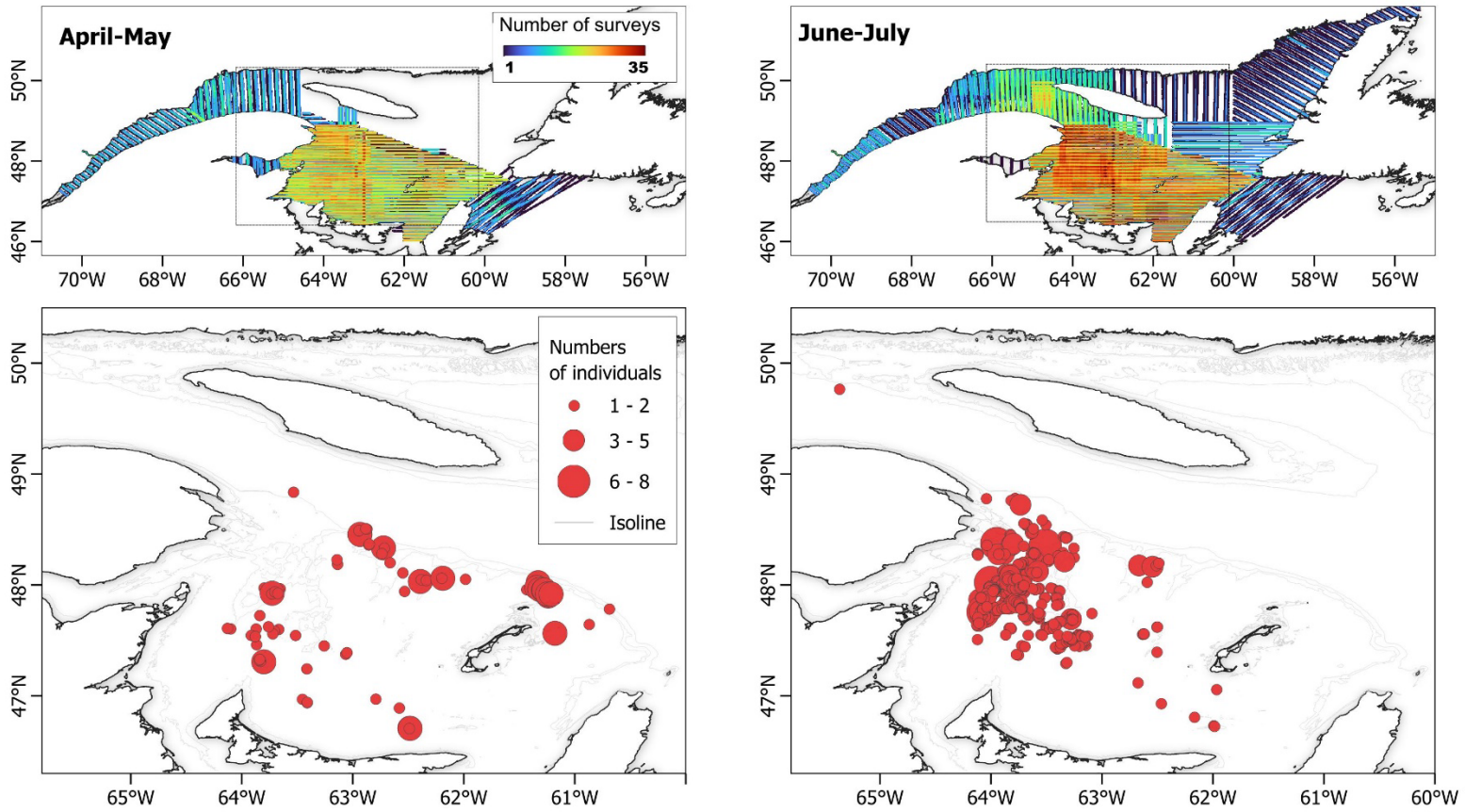

Figure 5. Survey effort (upper panels) and locations of North Atlantic right whale sightings (bottom panels, red dots), Eubalaena glacialis, detected during systematic line-transect aerial visual surveys conducted from 29 August 2017 to 6 November 2022 in the Estuary and Gulf of St. Lawrence. The data is presented for (a) April-May, (b) June-July, (c) August-September and (d) October-November, respectively.

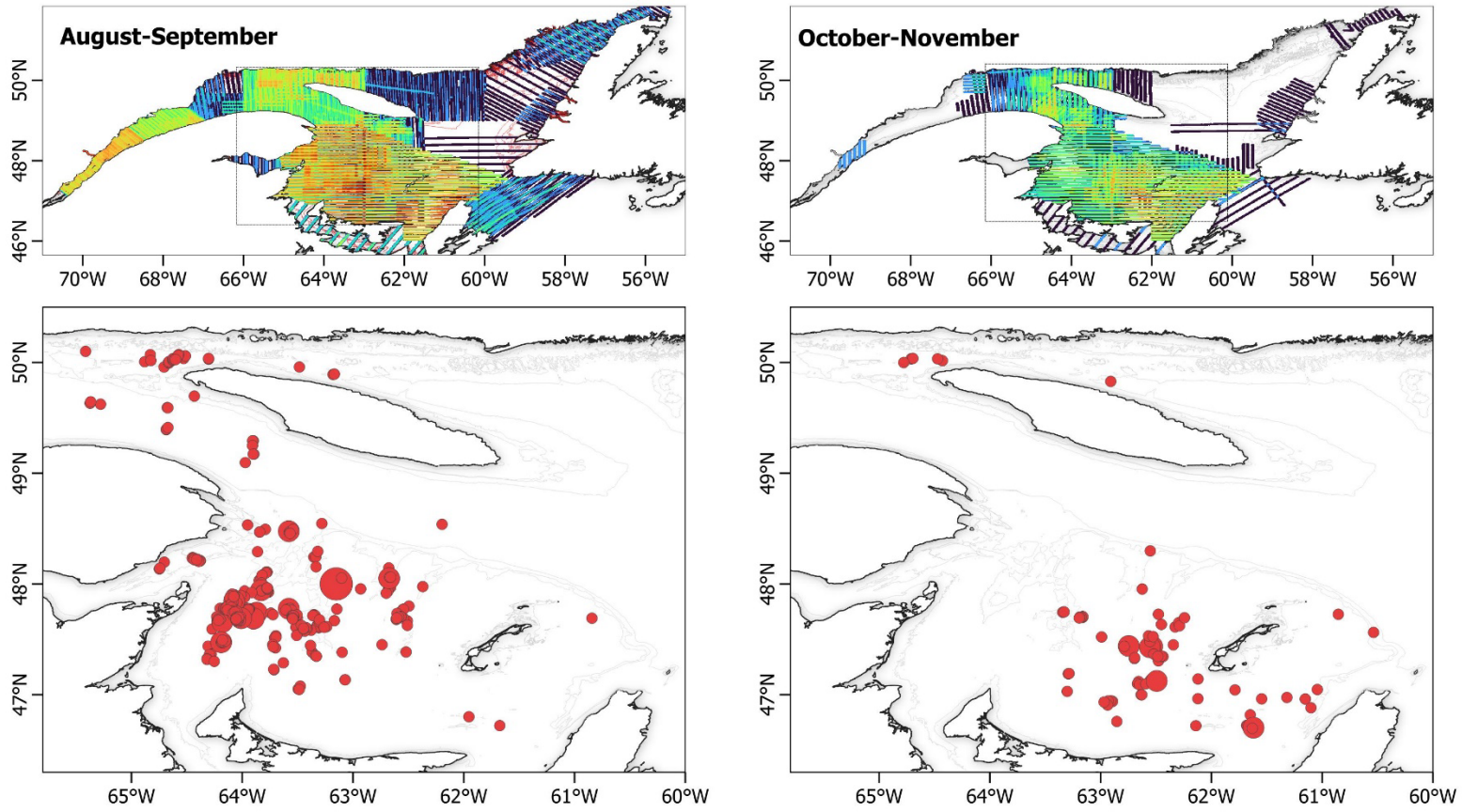

Figure 5 (continued). Survey effort (upper panels) and locations (bottom panels, red dots) of North Atlantic right whale sightings, Eubalaena glacialis, detected during systematic line-transect aerial visual surveys conducted from 29 August 2017 to 6 November 2022 in the Estuary and Gulf of St. Lawrence. The data is presented for (a) April-May, (b) June-July, (c) August-September and (d) October-November, respectively.

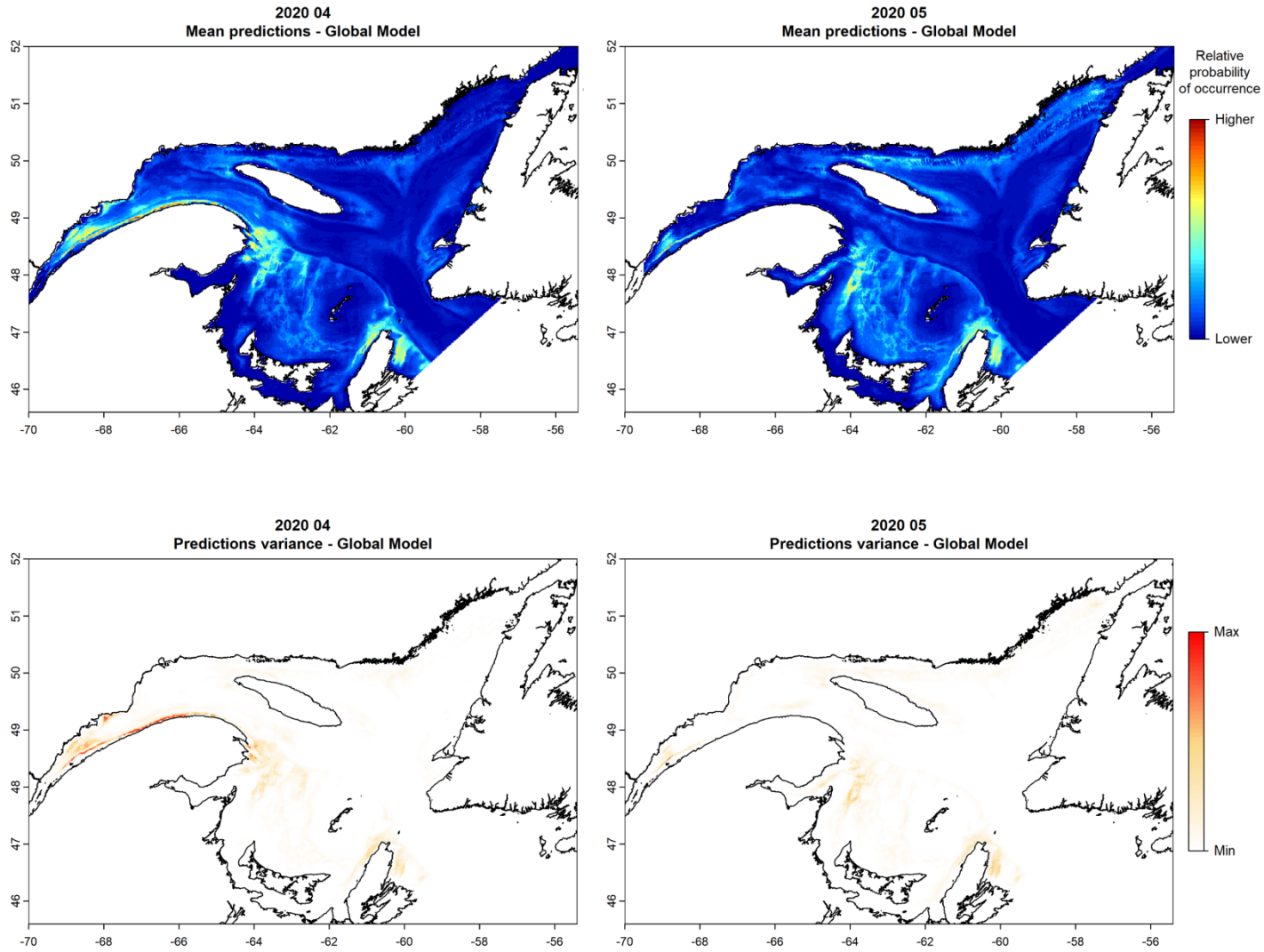

Figure 6. Monthly mean prediction maps from the Global model for year 2020 (upper panels) and the monthly variance of these predictions (lower panel). Note: all monthly mean prediction maps and variance maps use the same color scale so they can be compared directly.

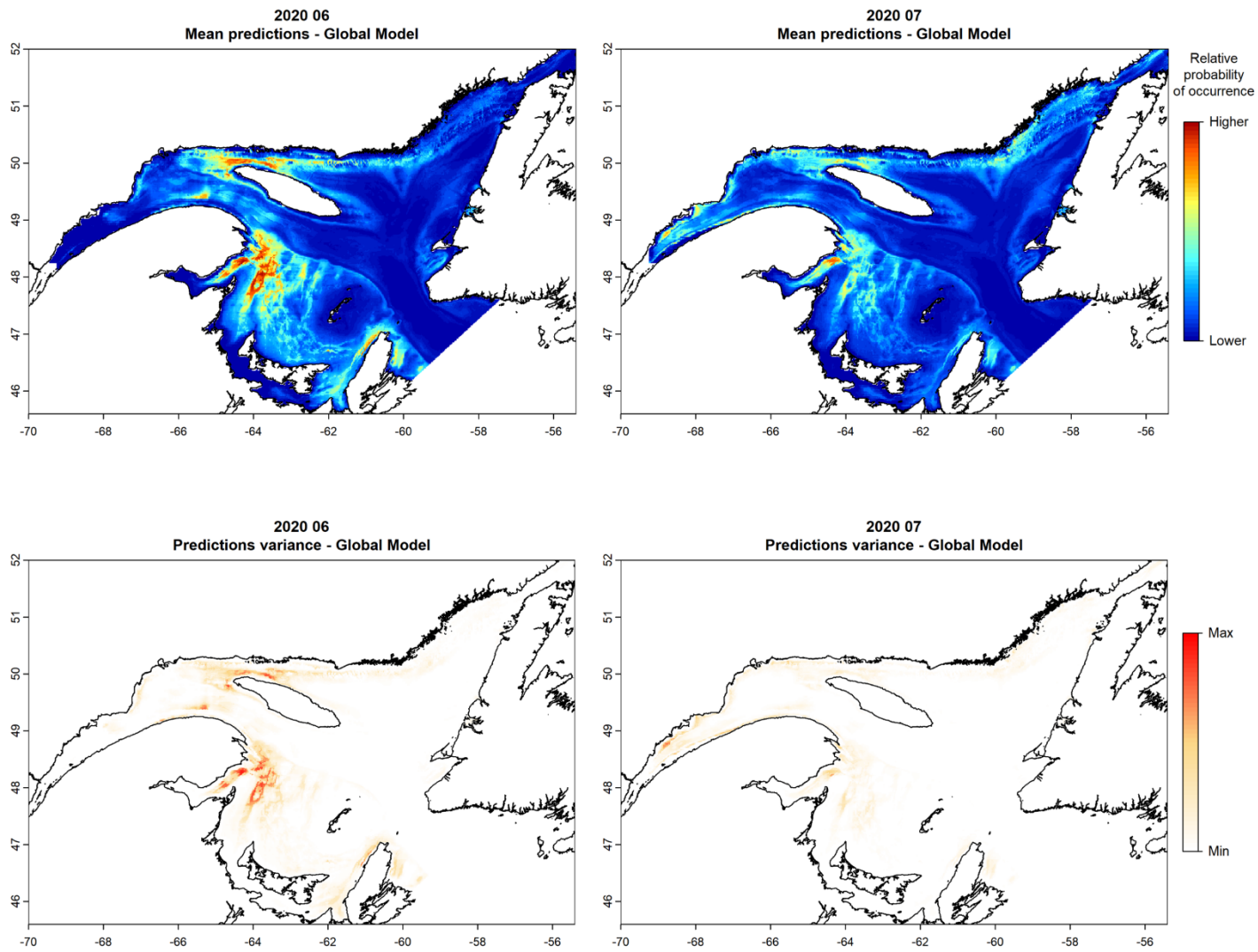

Figure 6. (continued) Monthly mean prediction maps from the Global model for year 2020 (upper panels) and the monthly variance of these predictions (lower panel). Note: all monthly mean prediction maps and variance maps use the same color scale so they can be compared directly.

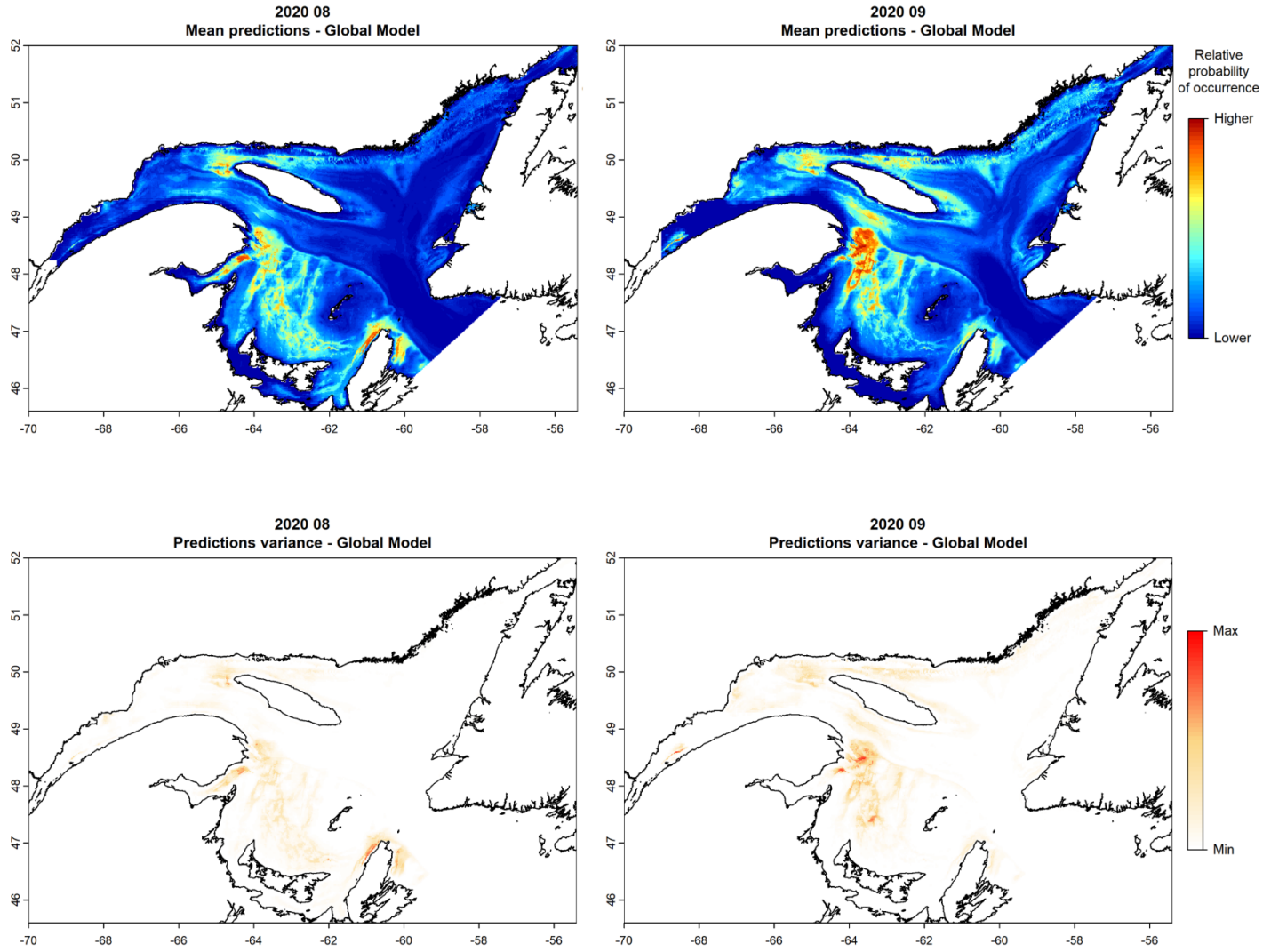

Figure 6 (continued). Monthly mean prediction maps from the Global model for year 2020 (upper panels) and the monthly variance of these predictions (lower panel). Note: all monthly mean prediction maps and variance maps use the same color scale so they can be compared directly.

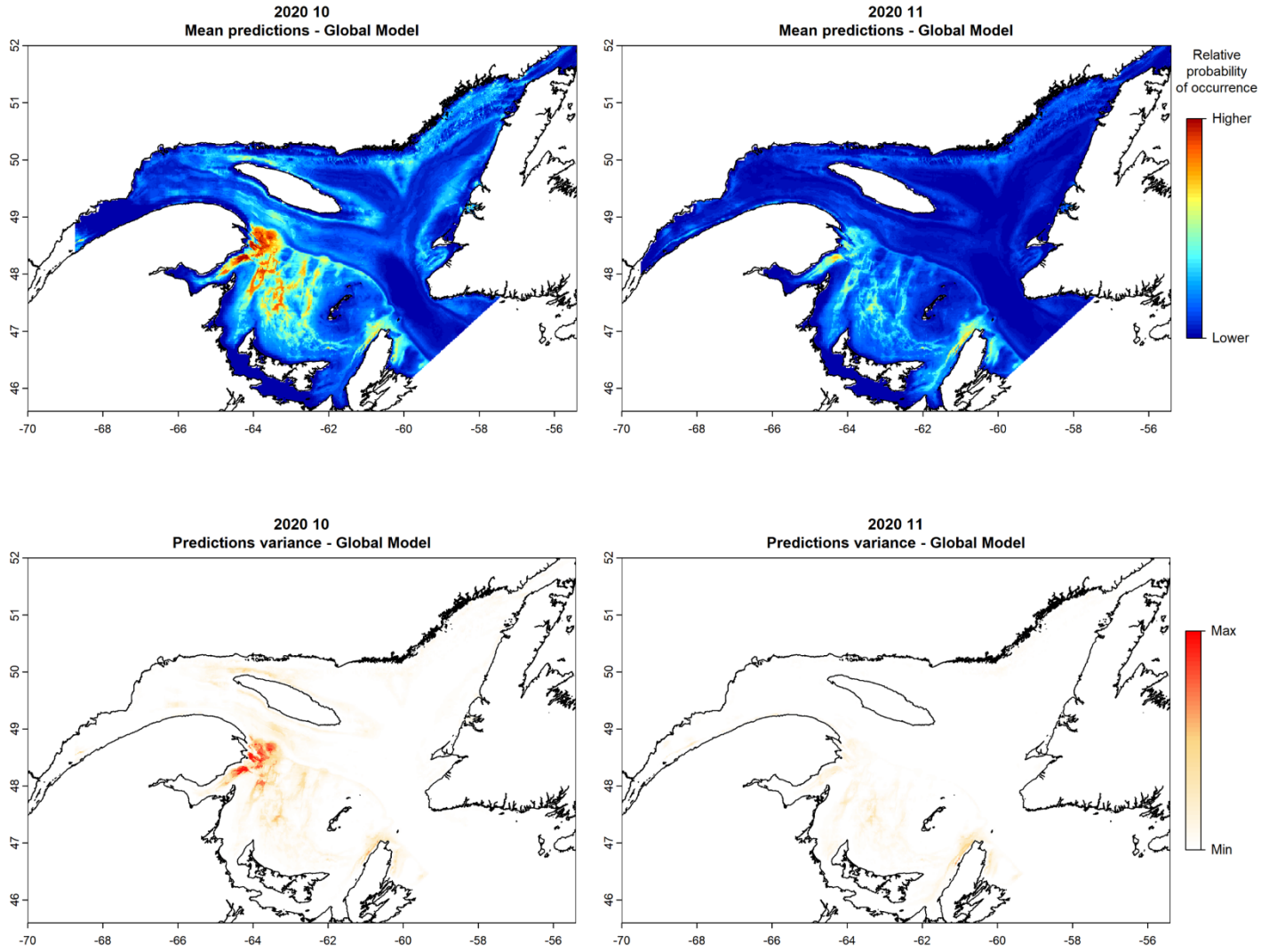

Figure 6 (continued). Monthly mean prediction maps from the Global model for year 2020 (upper panels) and the monthly variance of these predictions (lower panel). Note: all monthly mean prediction maps and variance maps use the same color scale so they can be compared directly.

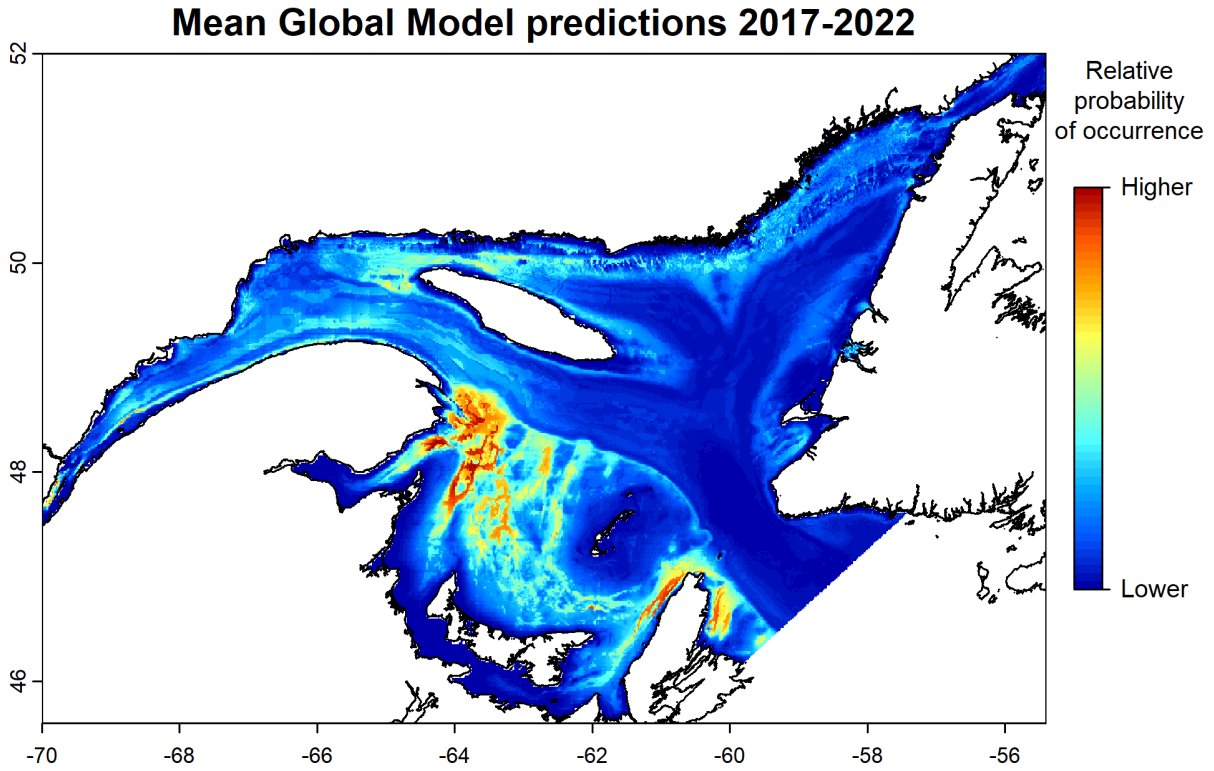

Figure 7. Mean predictions map from the Global model over the period 2017-2022 (i.e. considering daily predictions from April to November 2017-2022).

APPENDIX A. CORRELATION BETWEEN POTENTIALS PREDICTORS OF NORTH ATLANTIC RIGHT WHALES DISTRIBUTION

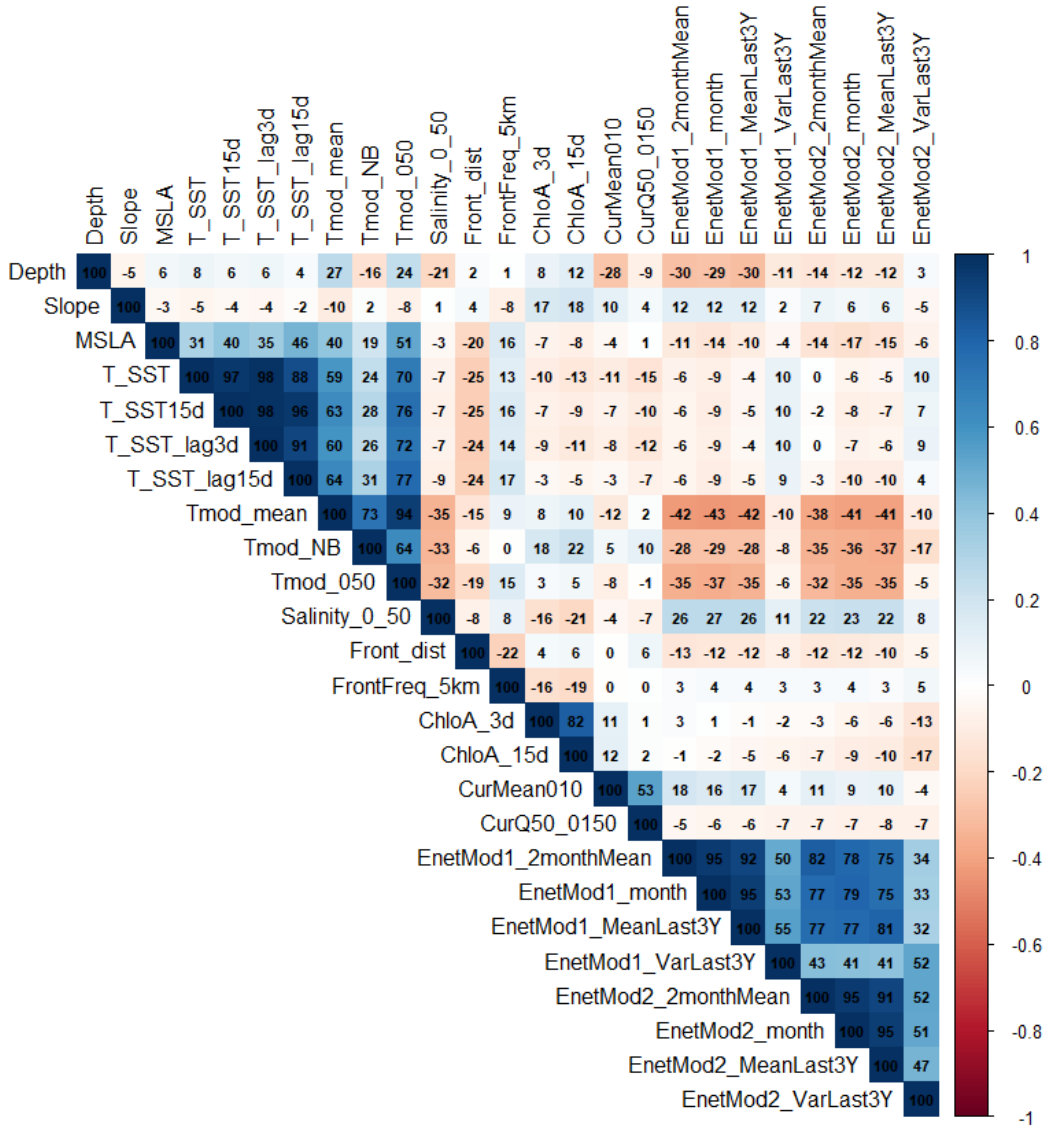

Figure A1. Correlations for all pairs of potential predictors used to predict the probability of occurrence of North Atlantic right whales, Eubalaena glacialis, in the Estuary and Gulf of St. Lawrence. Positive and negative correlations are displayed in blue and red, respectively. Darker colors indicate stronger correlation.

APPENDIX B. PROBABILITY OF DETECTION

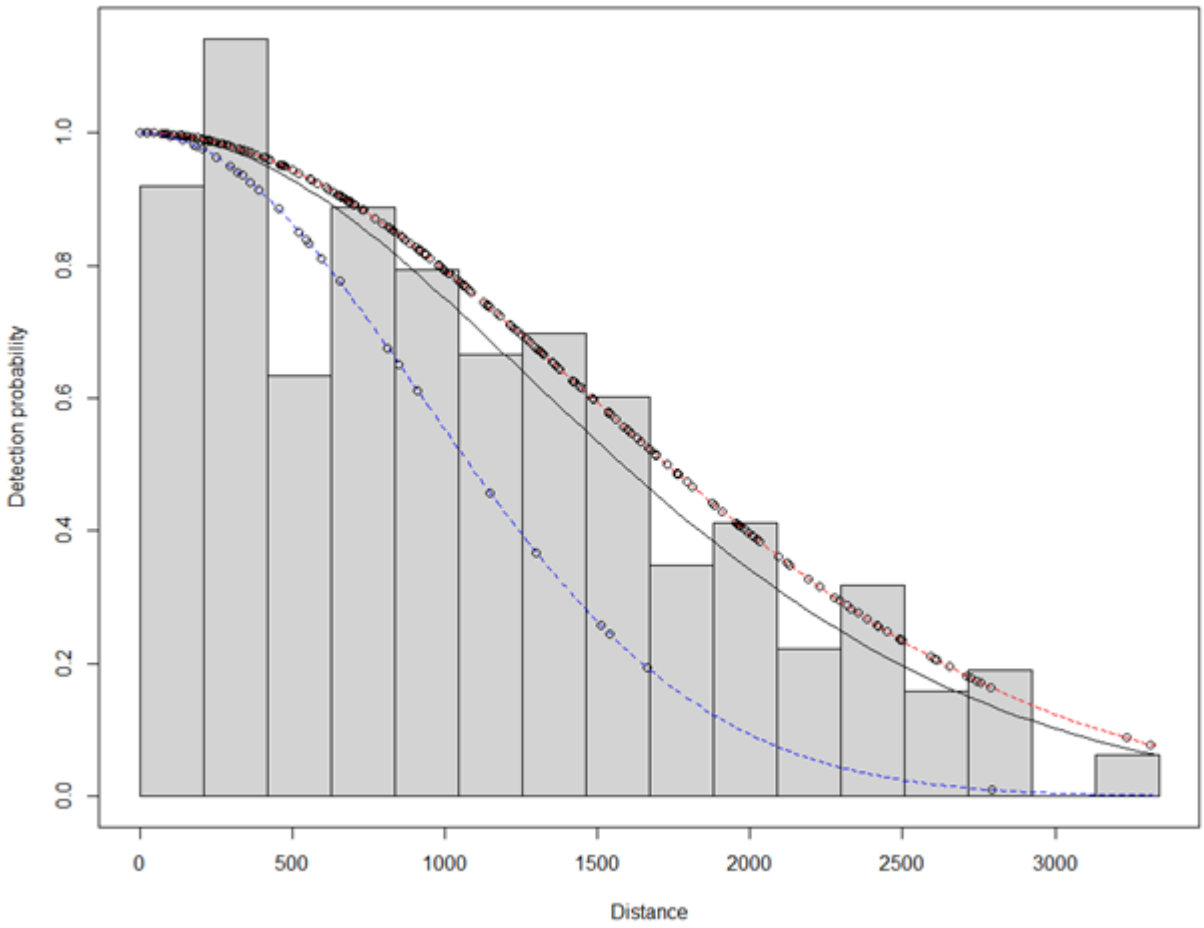

Figure B1. Distribution of perpendicular distances of 254 groups of North Atlantic right whales, Eubalaena glacialis, detected during systematic line-transects aerial visual surveys conducted by DFO in the Estuary and Gulf of St. Lawrence from 29 August 2017 to 06 November 2022. The detection curve was fitted using a half-normal key function, while including platform type as a covariate. The red and blue lines illustrate the detection curves fitted to detections from the small size planes (Cessa 337 Skymaster and Partenavia (P86 Observer)) and the medium size plane (DeHavilland DH-6 Twin Otter), respectively.

APPENDIX C. RELATIONSHIP BETWEEN NARW OCCURRENCE AND EXPLANATORY VARIABLES INCLUDED IN THE BEST SEASONAL MODELS

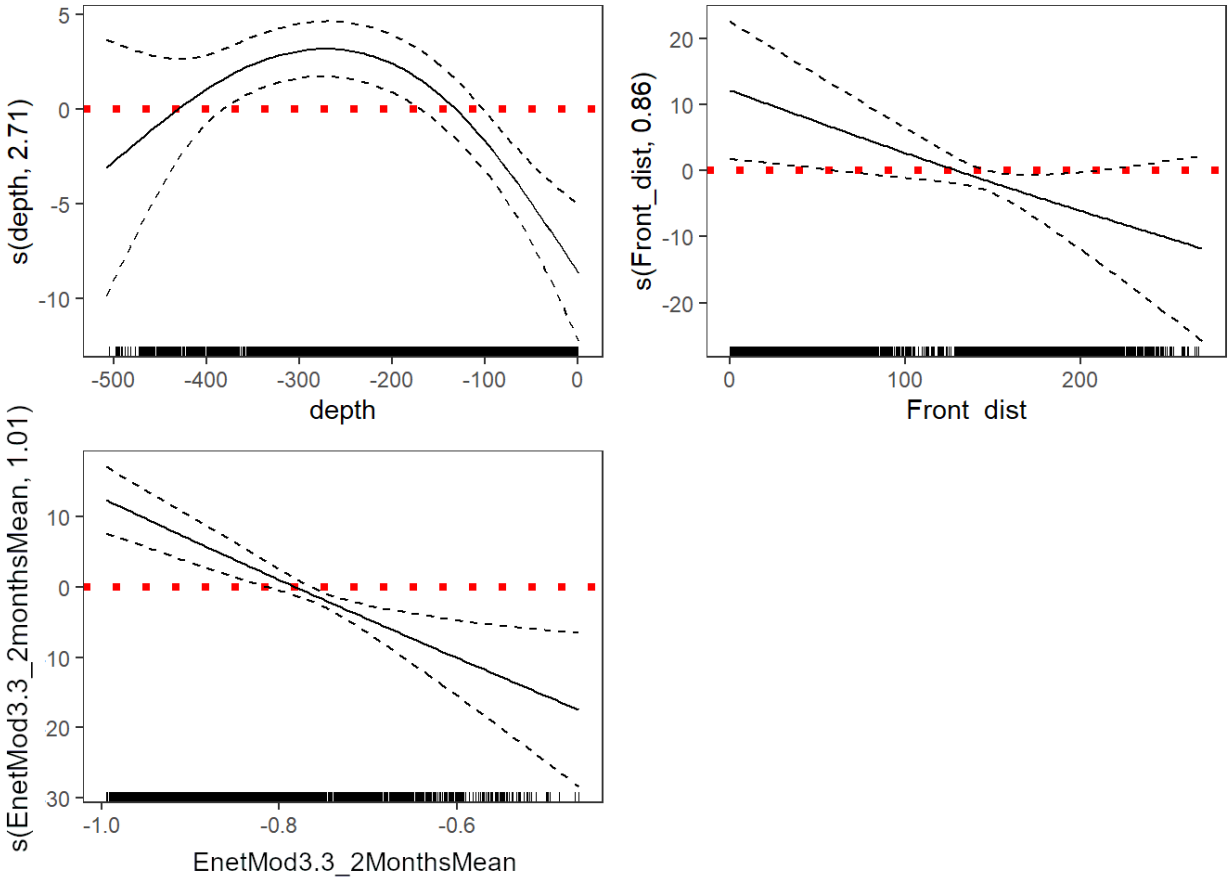

Figure C1. Estimated relationship between North Atlantic right whales, Eubalaena glacialis, occurrence in the Estuary and Gulf of St. Lawrence and explanatory variables considered in the first of two alternative best models (delta AIC <=3) for the April-May period.

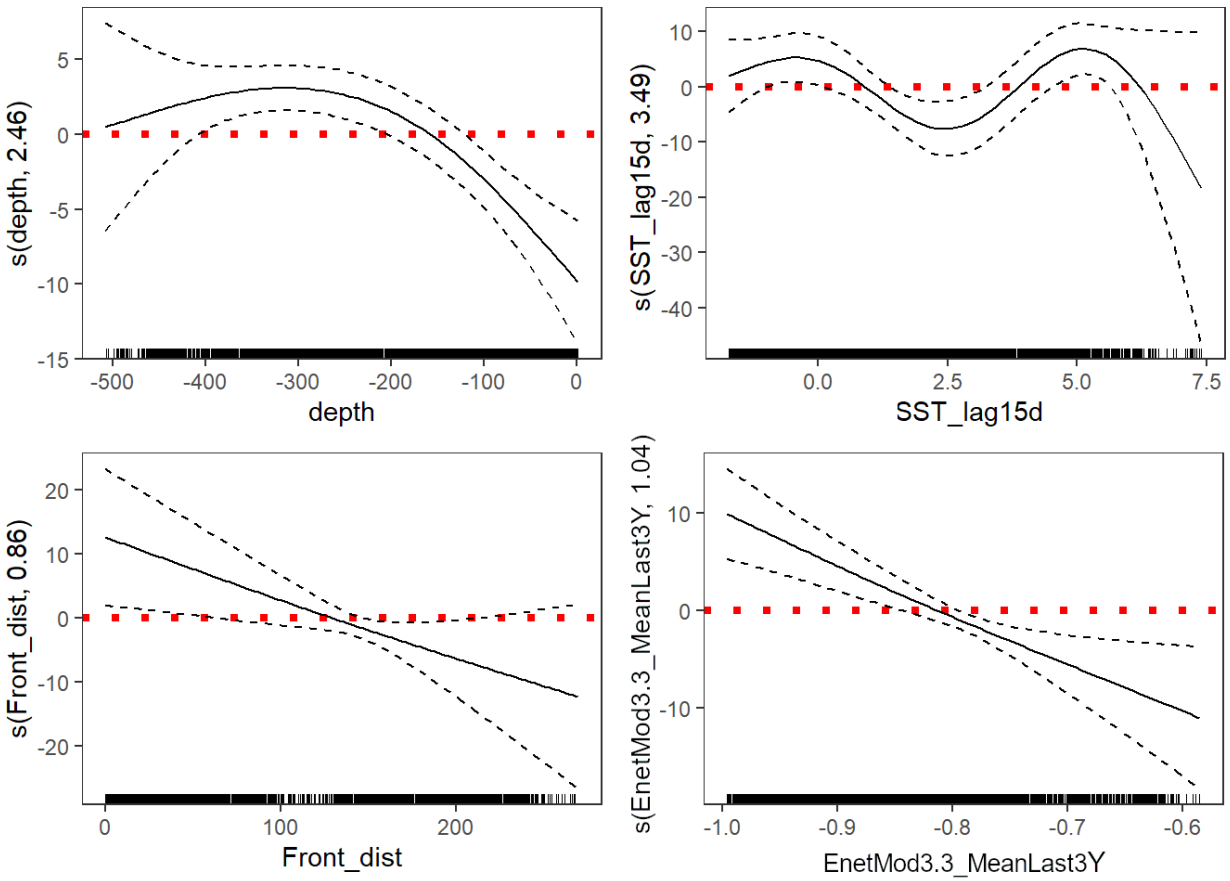

Figure C2. Estimated relationship between North Atlantic right whales, Eubalaena glacialis, occurrence in the Estuary and Gulf of St. Lawrence and explanatory variables considered in the second of two alternative best models (delta AIC <=3) for the April-May period.

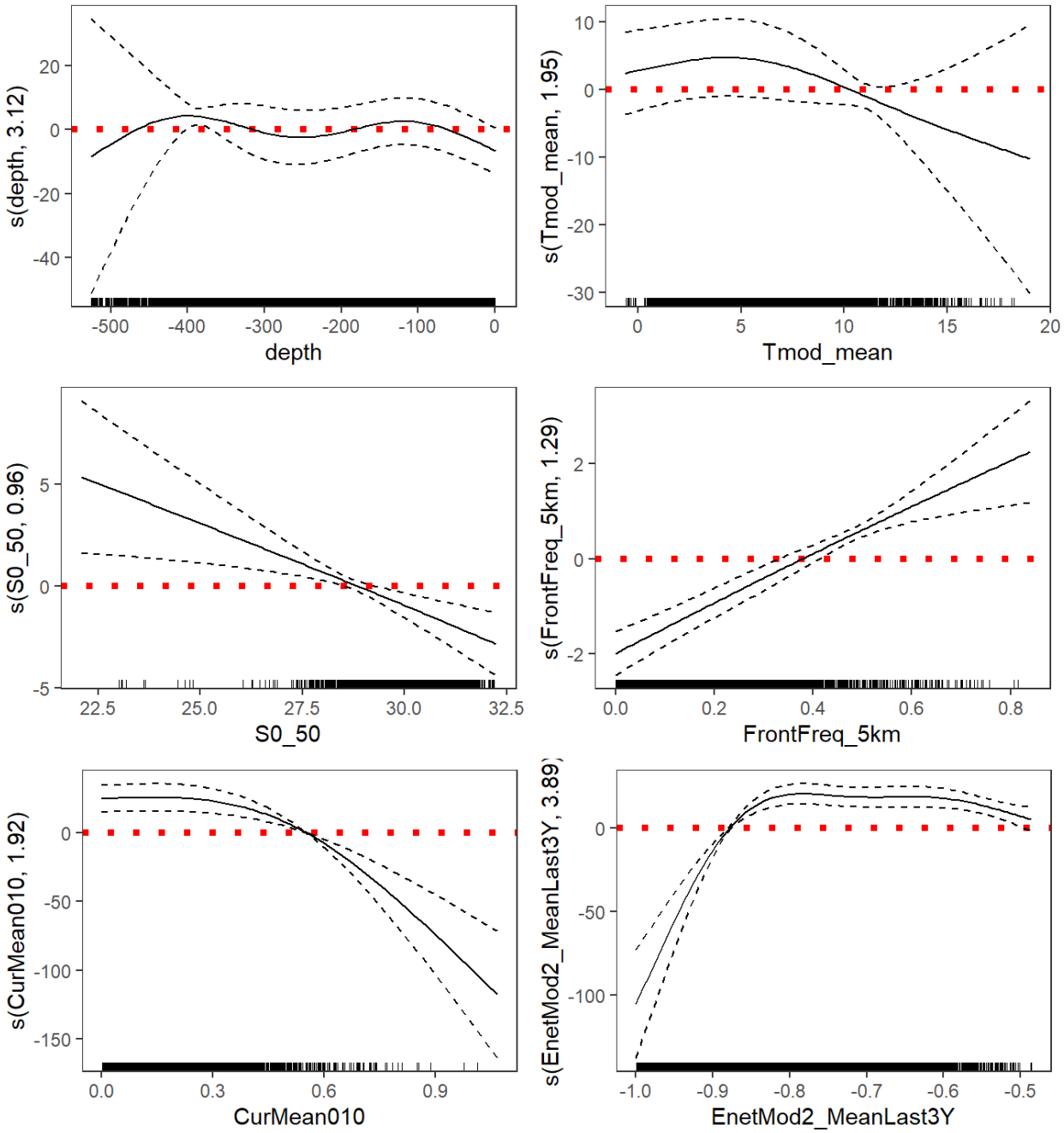

Figure C3. Estimated relationship between North Atlantic right whales, Eubalaena glacialis, occurrence in the Estuary and Gulf of St. Lawrence and explanatory variables considered in the first of two alternative best models (delta AIC <=3) for the June-July period.

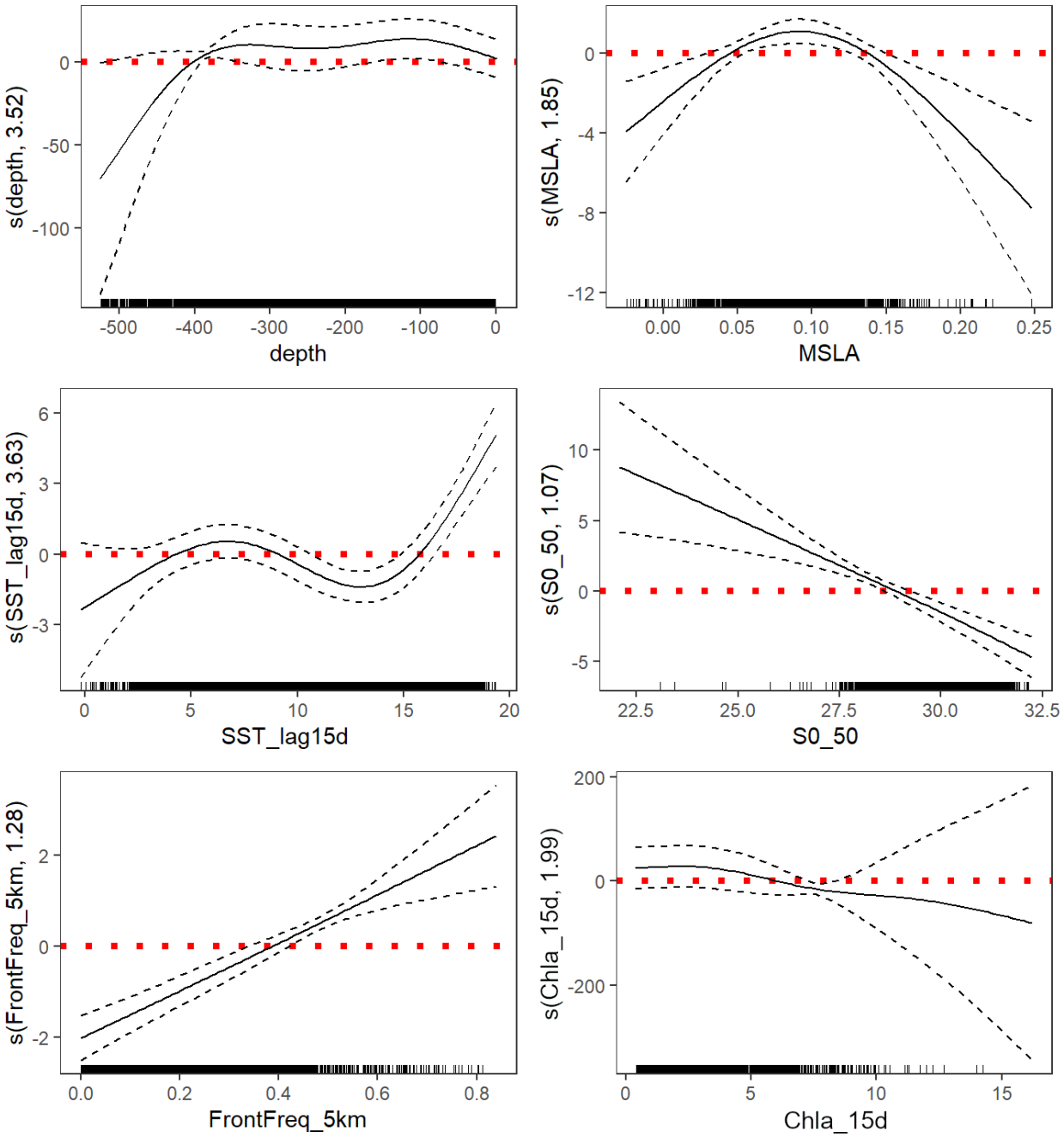

Figure C4. Estimated relationship between North Atlantic right whales, Eubalaena glacialis, occurrence in the Estuary and Gulf of St. Lawrence and explanatory variables considered in the second of two alternative best models (delta AIC <=3) for the June-July period.

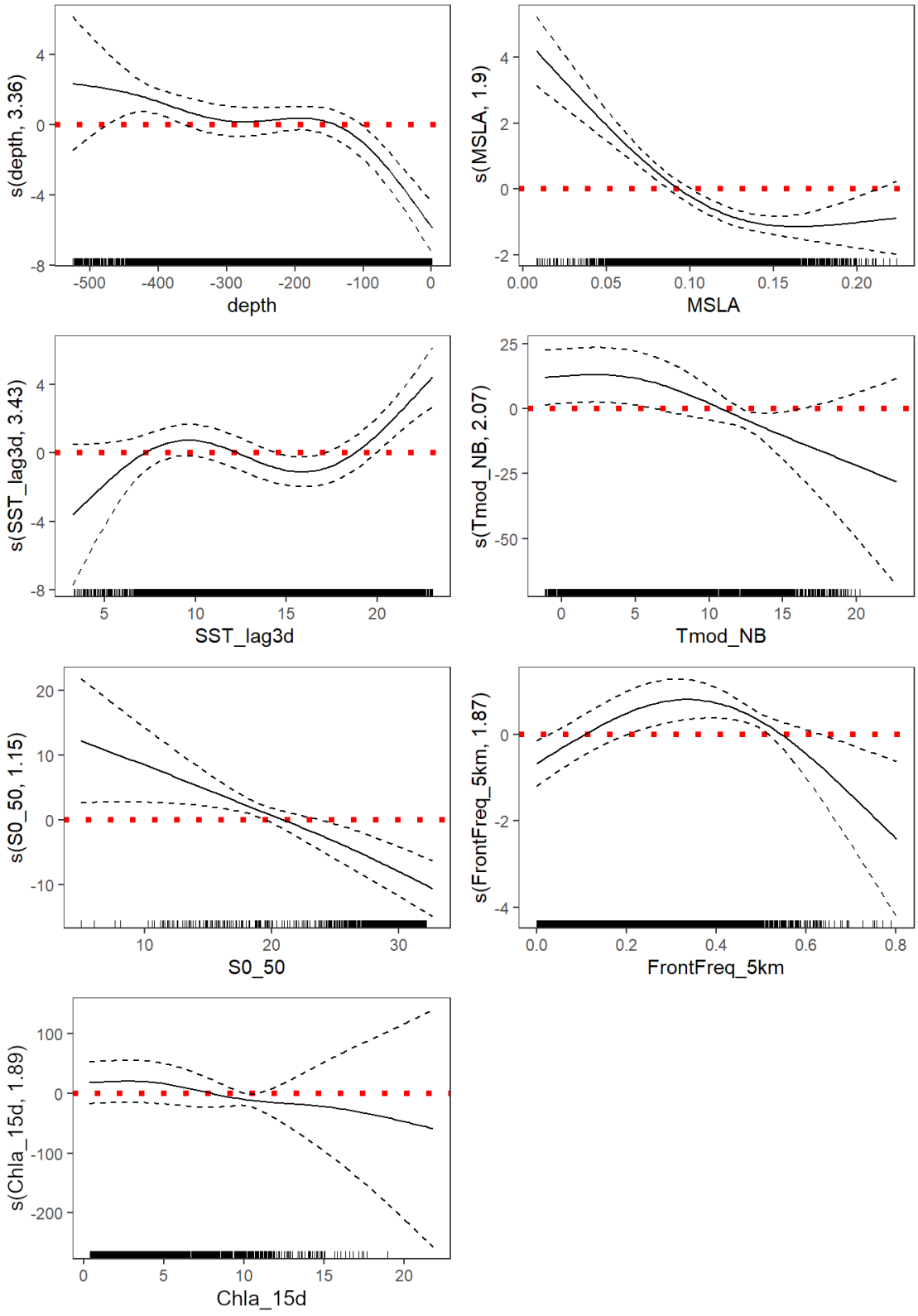

Figure C5. Estimated relationship between North Atlantic right whales, Eubalaena glacialis, occurrence in the Estuary and Gulf of St. Lawrence and explanatory variables considered in the first of three alternative best models (delta AIC <=3) for the August-September period.

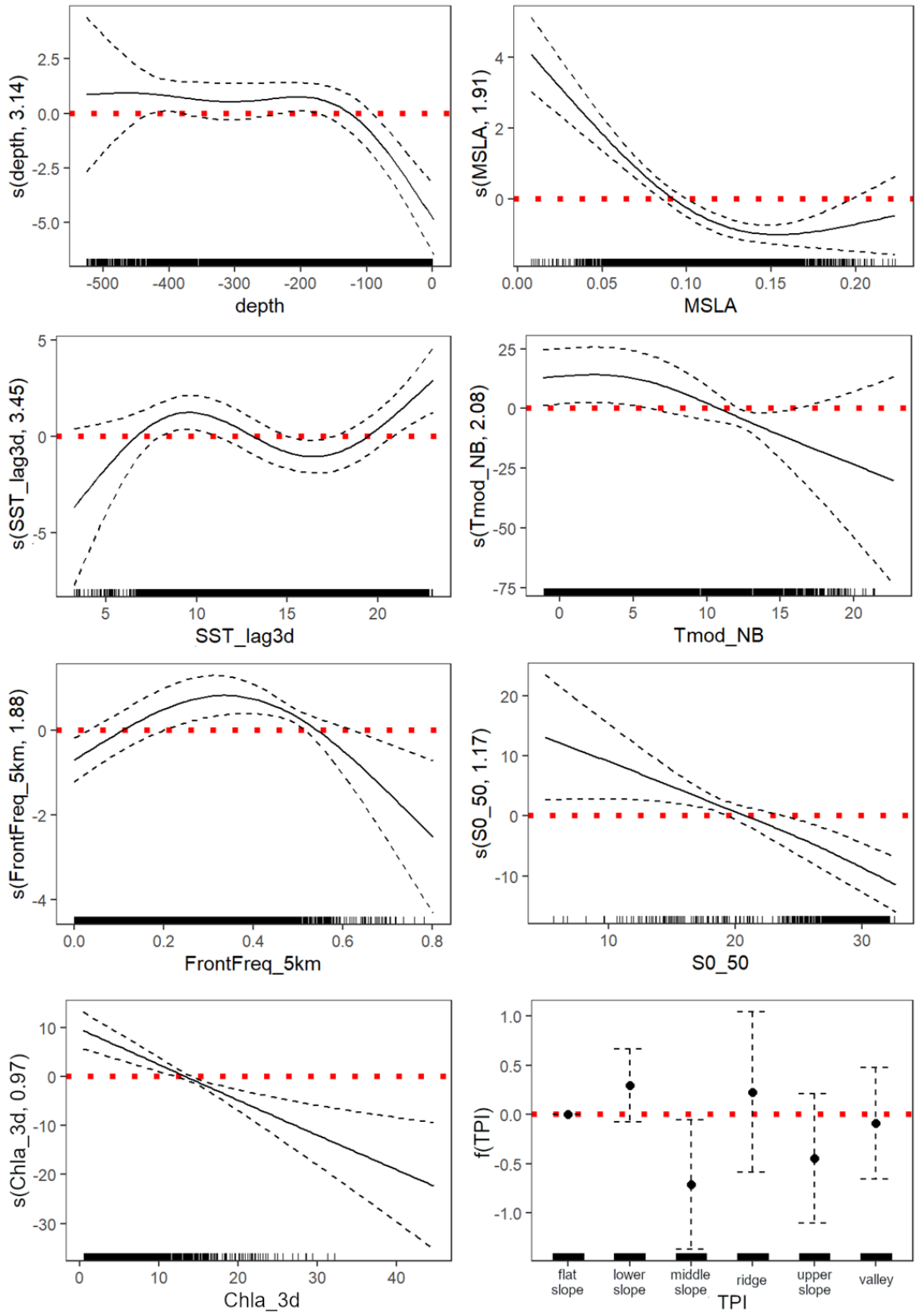

Figure C6. Estimated relationship between North Atlantic right whales, Eubalaena glacialis, occurrence in the Estuary and Gulf of St. Lawrence and explanatory variables considered in the first of two alternative best models (delta AIC <=3) for the August-September period.

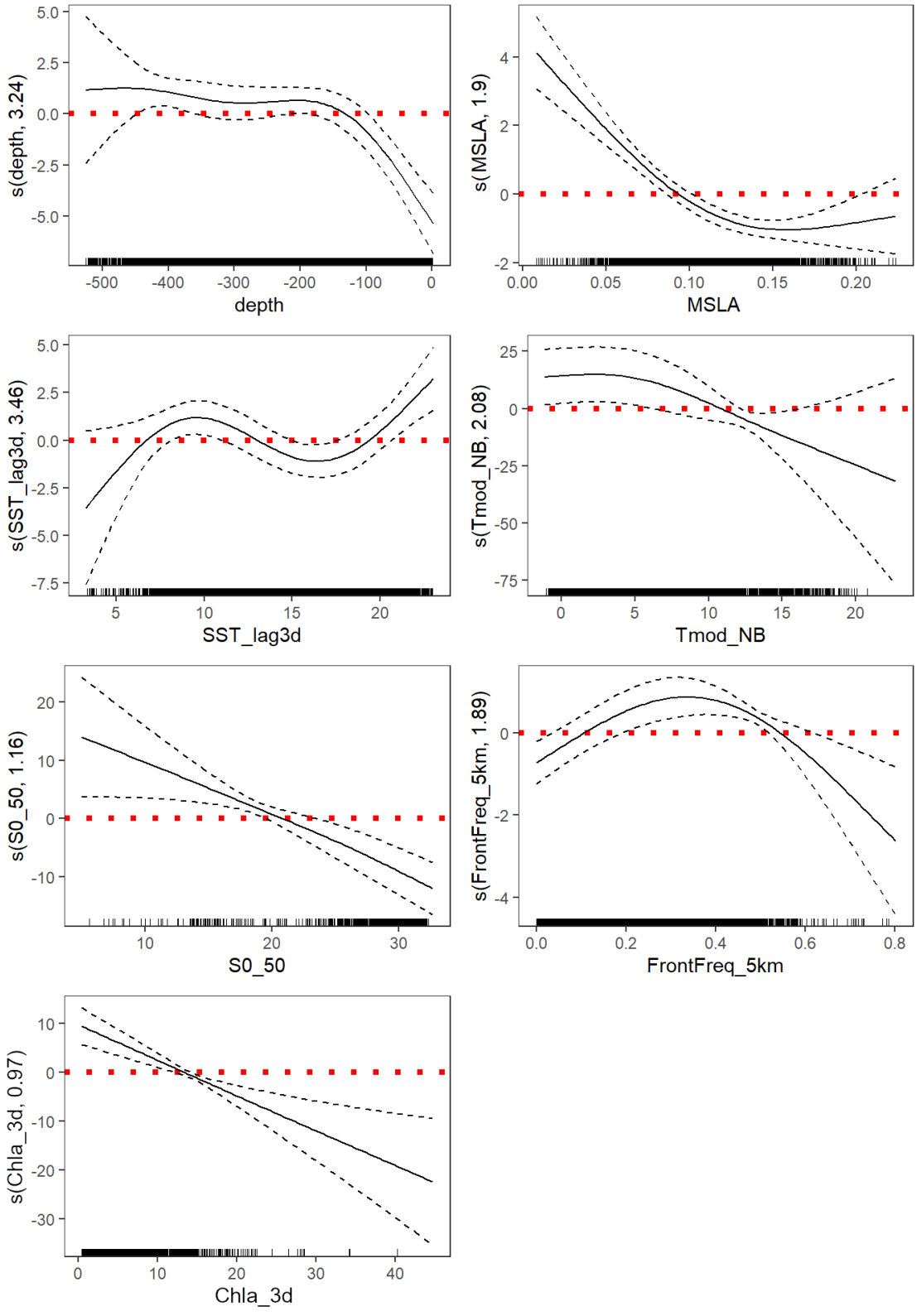

Figure C7. Estimated relationship between North Atlantic right whales, Eubalaena glacialis, occurrence in the Estuary and Gulf of St. Lawrence and explanatory variables considered in the first of two alternative best models (delta AIC <=3) for the August-September period.

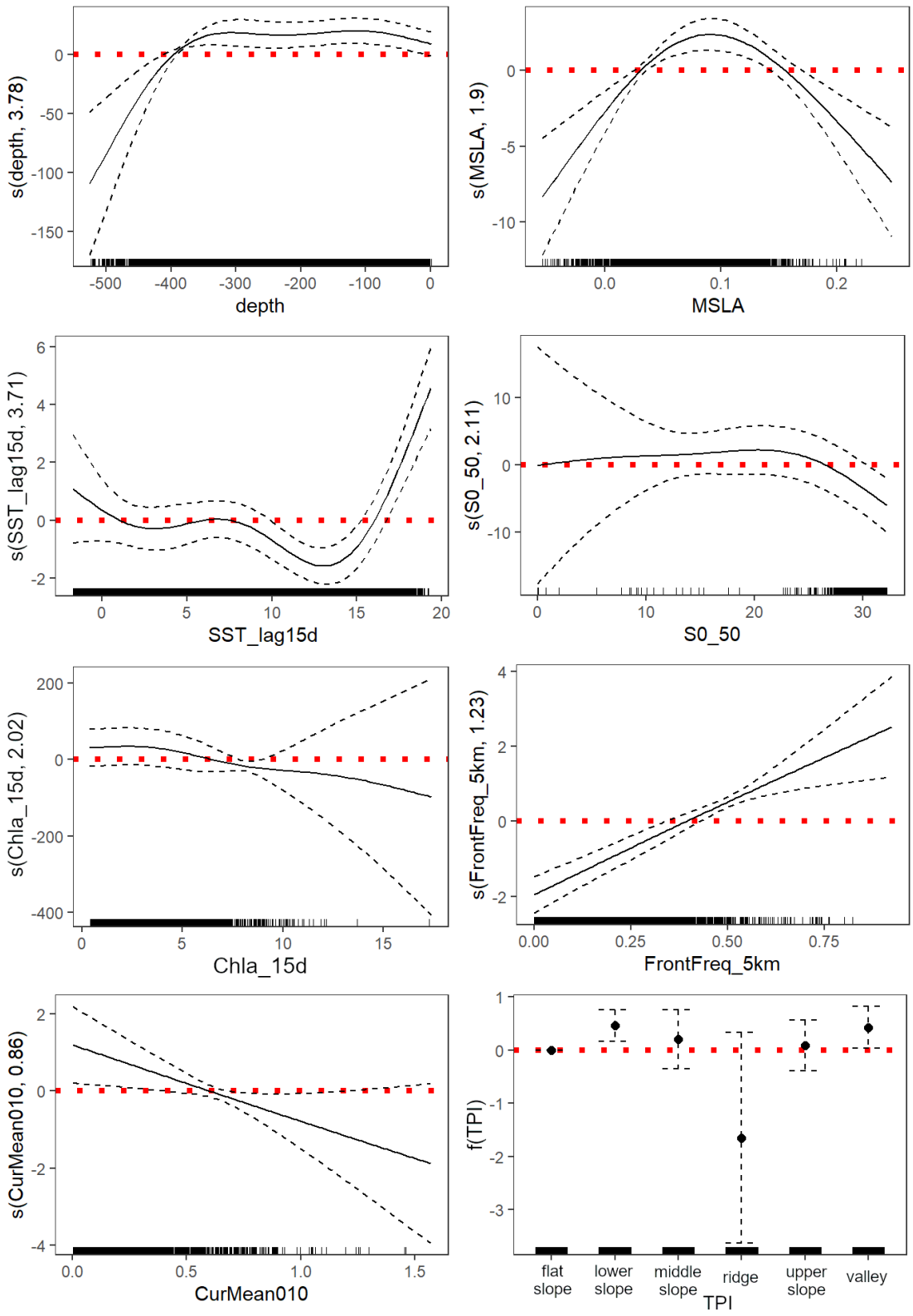

Figure C8. Estimated relationship between North Atlantic right whales, Eubalaena glacialis, occurrence in the Estuary and Gulf of St. Lawrence and explanatory variables considered in the first of two alternative best models (delta AIC <=3) for the April-July period.

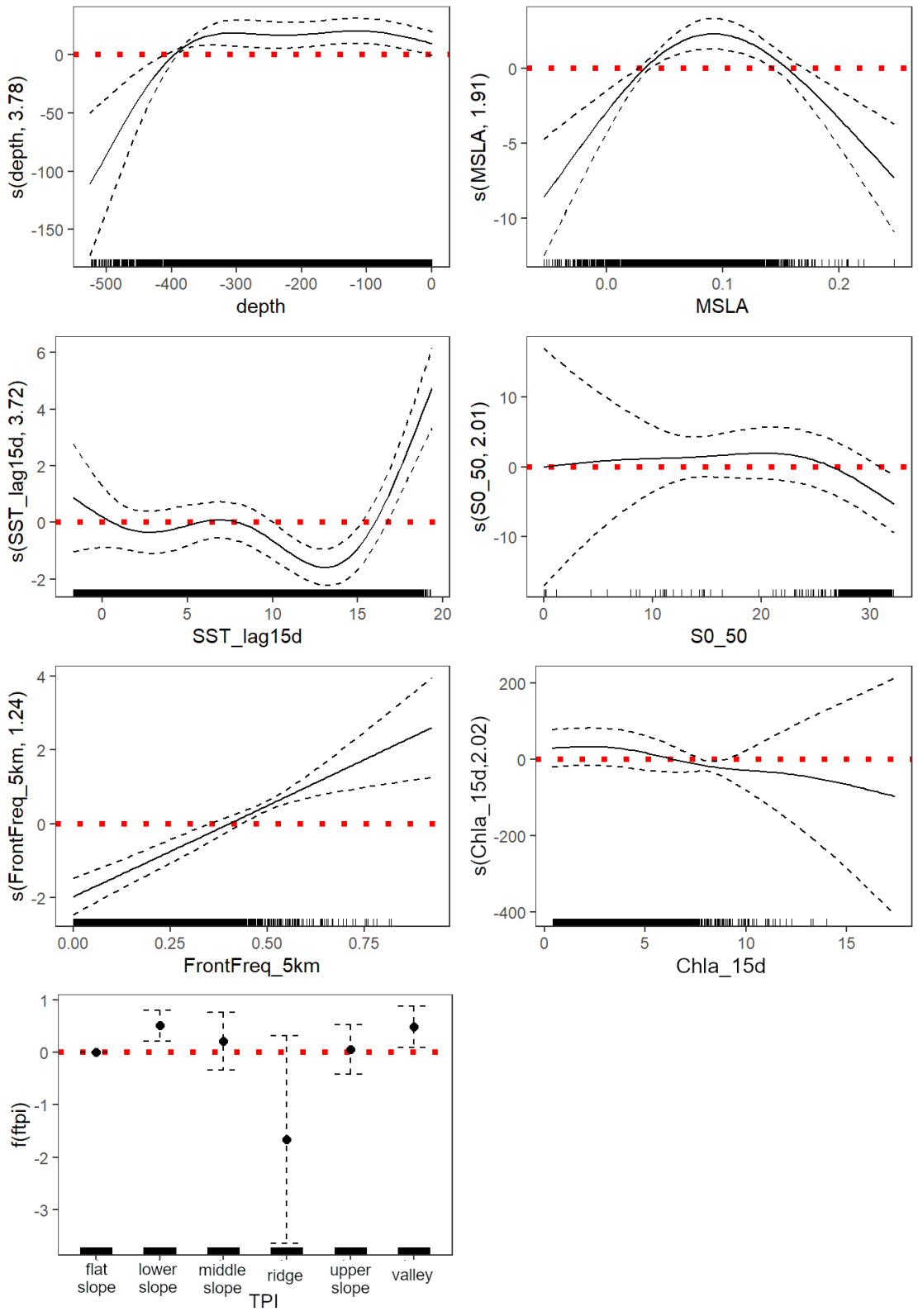

Figure C9. Estimated relationship between North Atlantic right whales, Eubalaena glacialis, occurrence in the Estuary and Gulf of St. Lawrence and explanatory variables considered in the first of two alternative best models (delta AIC <=3) for the April-July period.

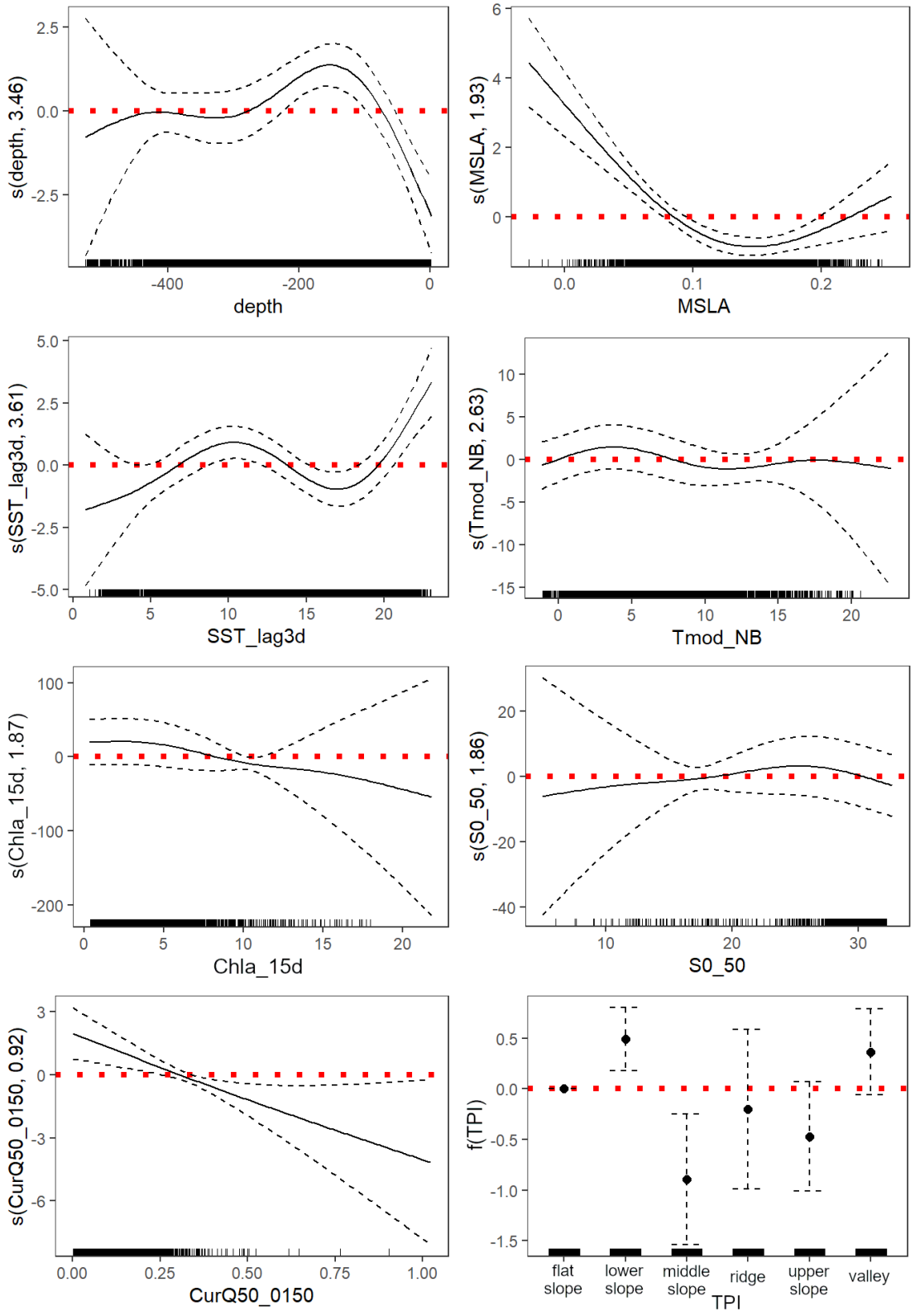

Figure C10. Estimated relationship between North Atlantic right whales, Eubalaena glacialis, occurrence in the Estuary and Gulf of St. Lawrence and explanatory variables considered in the first of two alternative best models (delta AIC <=3) for the August-November period.

APPENDIX D. RELATIONSHIP BETWEEN NARW OCCURRENCE AND EXPLANATORY VARIABLES INCLUDED IN THE BEST GLOBAL MODEL

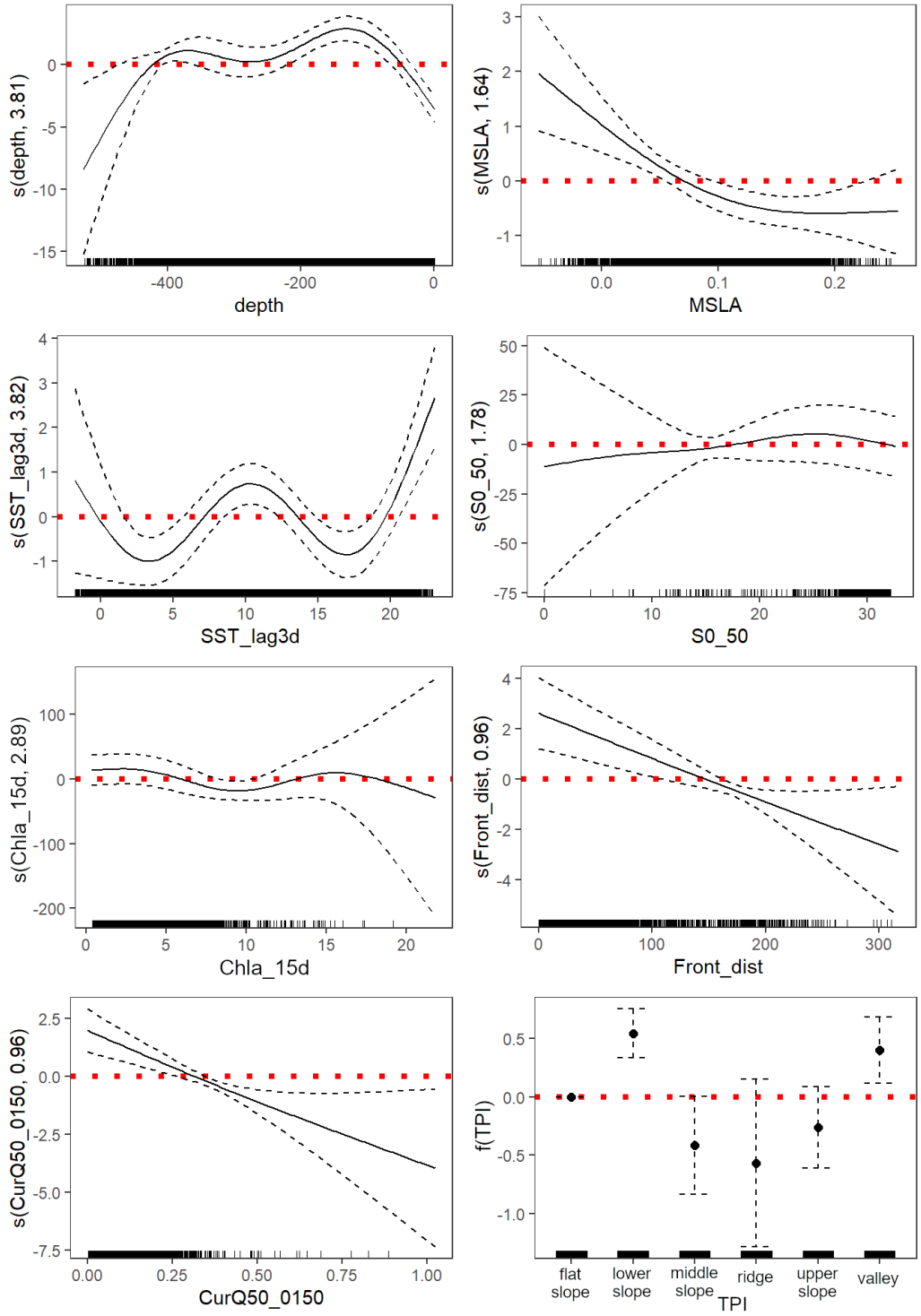

Figure D1. Estimated relationship between North Atlantic right whales, Eubalaena glacialis, occurrence in the Estuary and Gulf of St. Lawrence and explanatory variables considered in the best global model (April-November).

APPENDIX E. EXAMPLE OF MODEL PREDICTIONS VERSUS OBSERVATIONS

Examples of model predictions of the relative probability of North Atlantic right whale occurrence compared with actual observations (represented by red dots) recorded on the same day or within the same month.

For each month, we first present the monthly average predictions from the Global model, which was found to perform best overall when compared to independent data collected during the 2021-2022 survey seasons.

Following this, we show daily predictions from the same Global model for a specific day of this month when NARW were observed, alongside predictions from other models tested (Global, Half-Season and Two-Months models).

While models that included the variable representing the *Calanus spp.* energy (Enet; see material and methods) were generally outperformed by those not including it – except for the Apr-May and Oct-Nov models - we provide predictions from both types of models for comparison.

The same color scale (see below) was used for all maps, so that they can be compared directly.

May – Monthly Mean predictions – Global Model

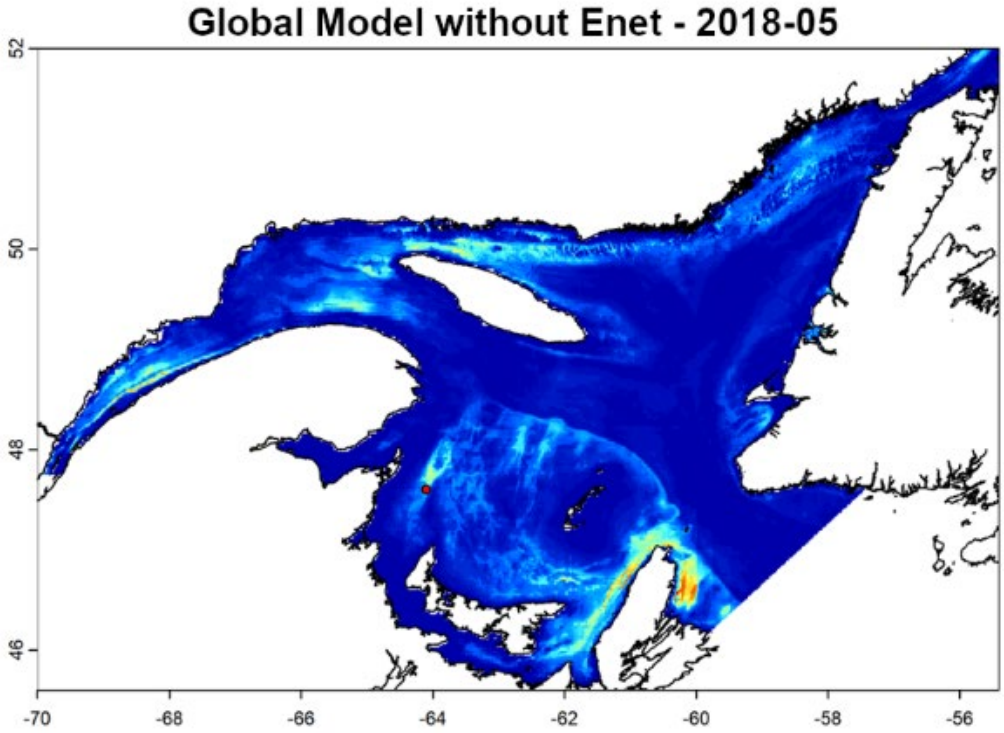

May – Daily predictions – Global models

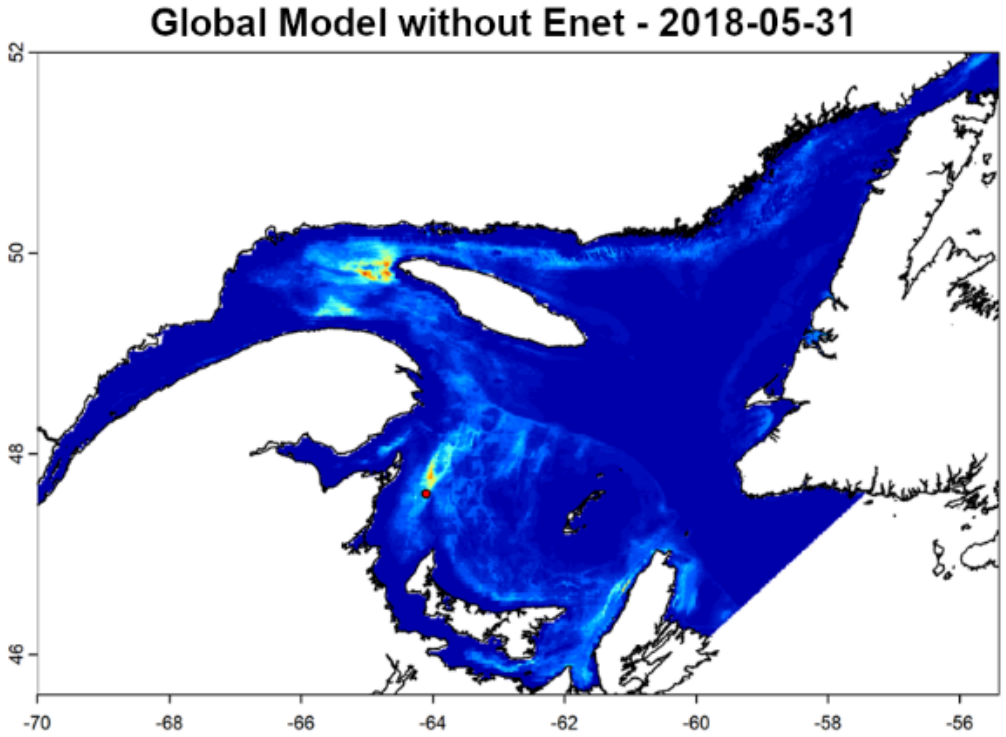

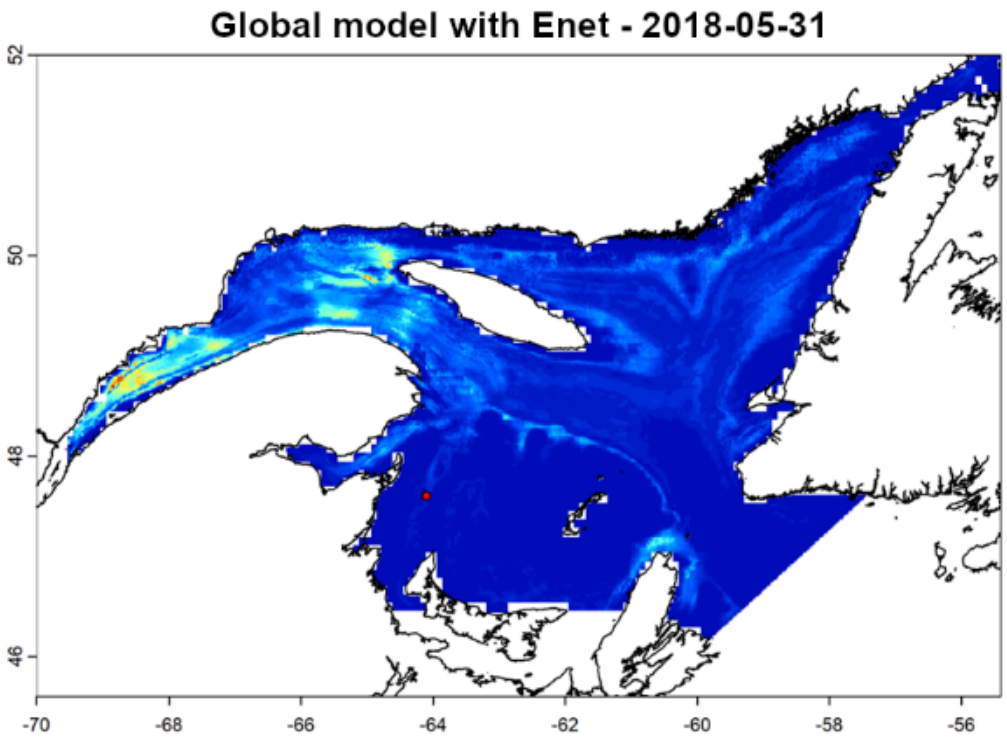

May – Daily predictions – Half-Season Models

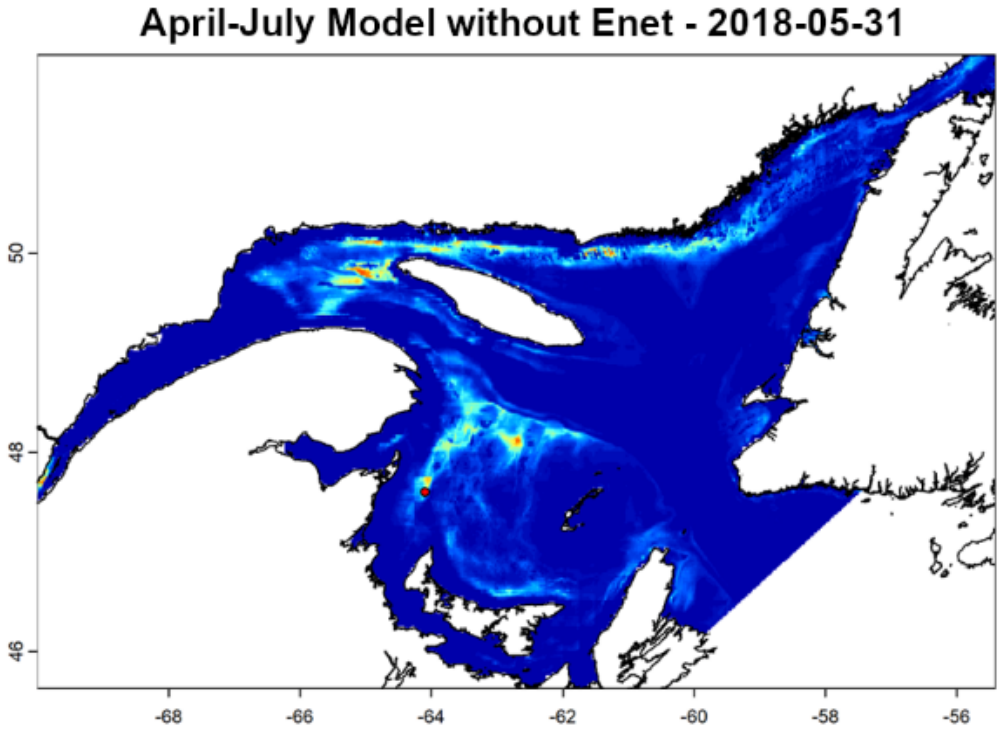

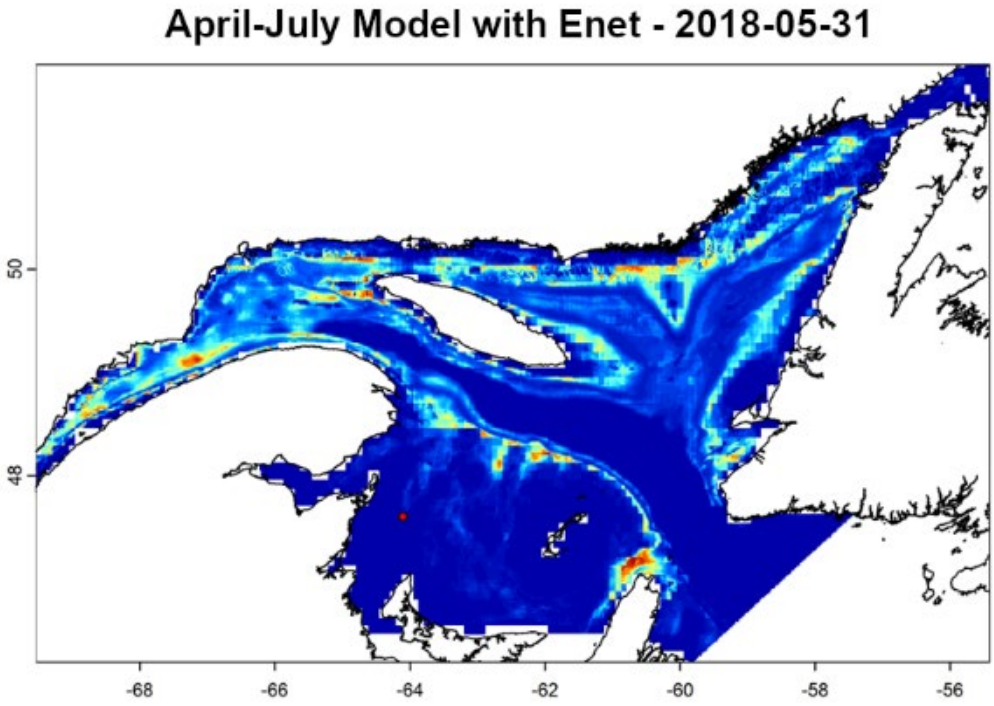

May – Daily predictions - Two-months Models

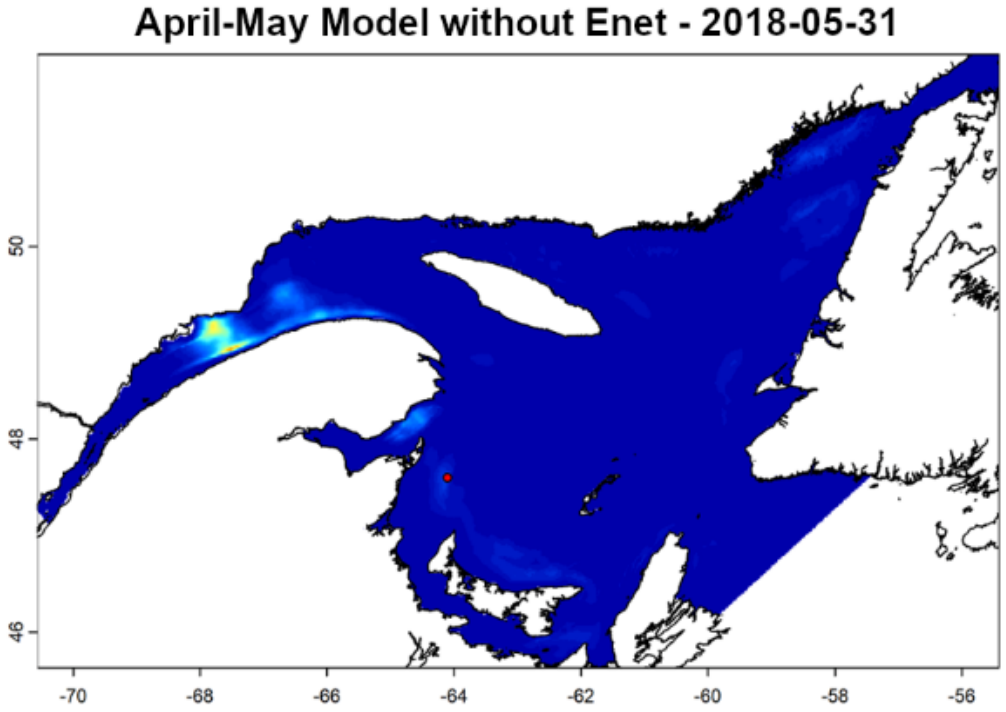

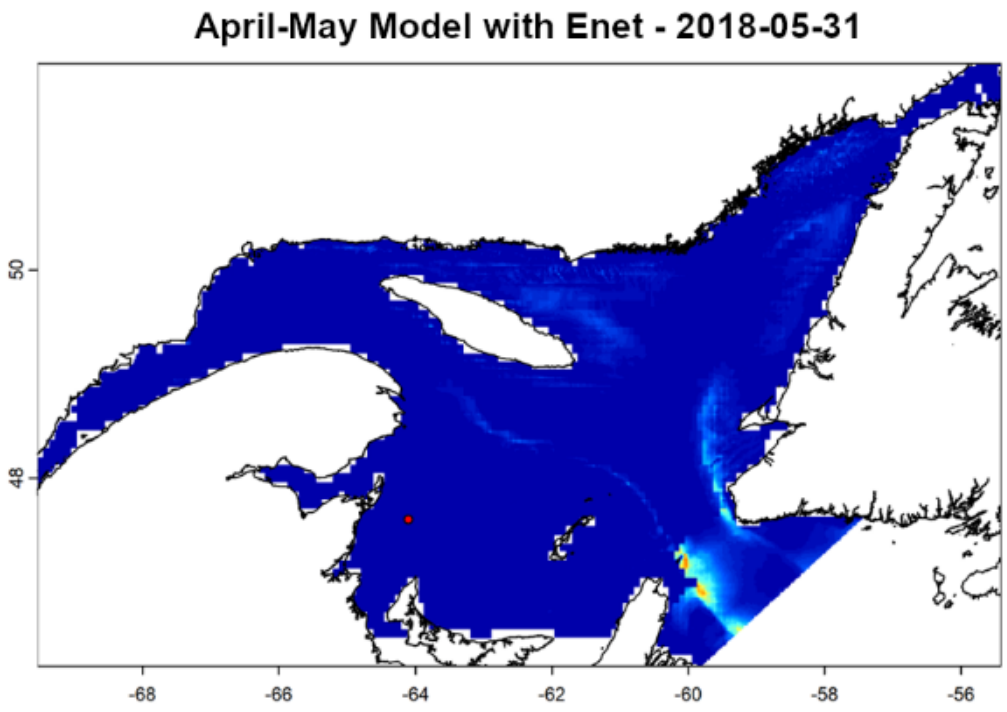

June – Monthly predictions – Global Model

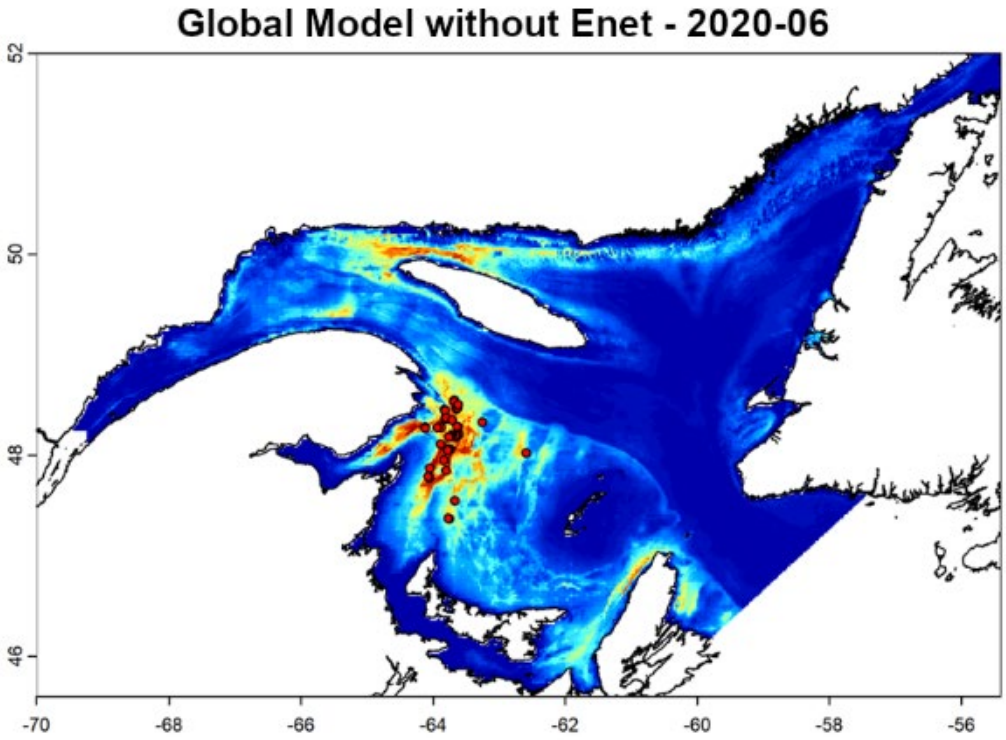

June – Daily predictions – Global models

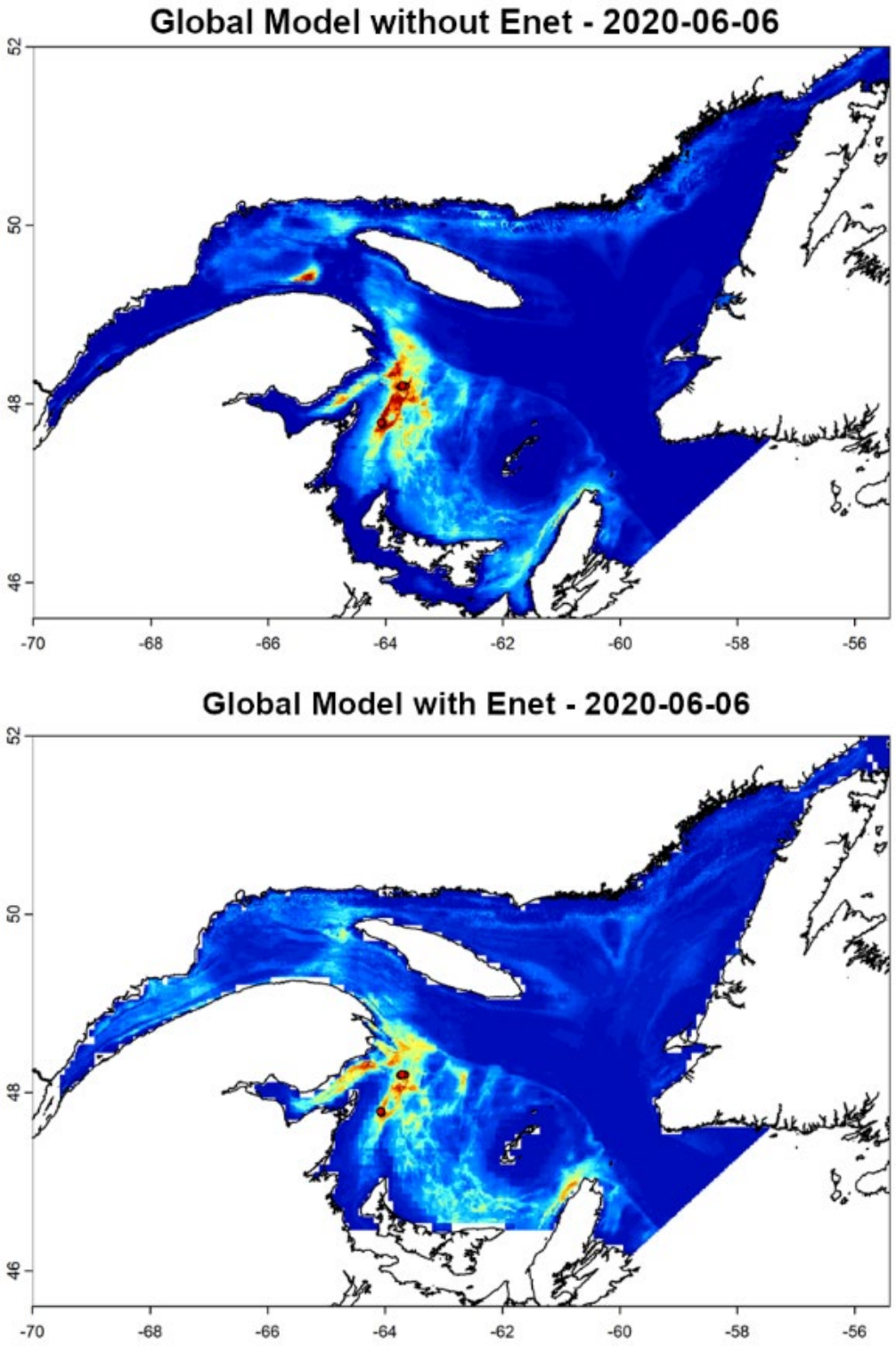

June – Daily predictions – Half-Season Models

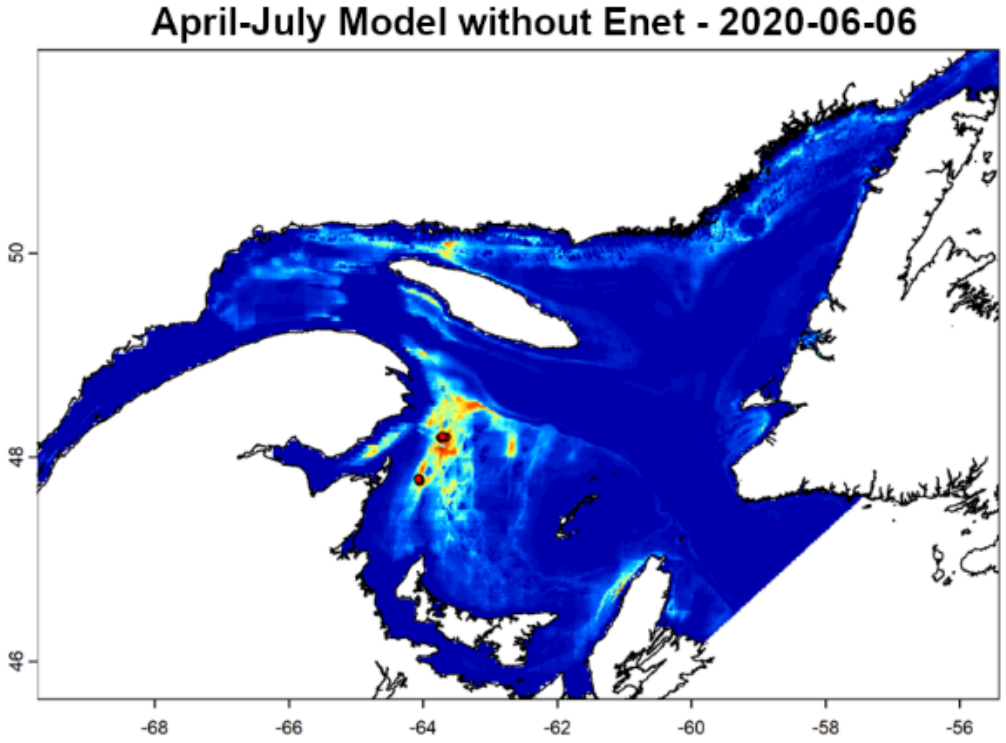

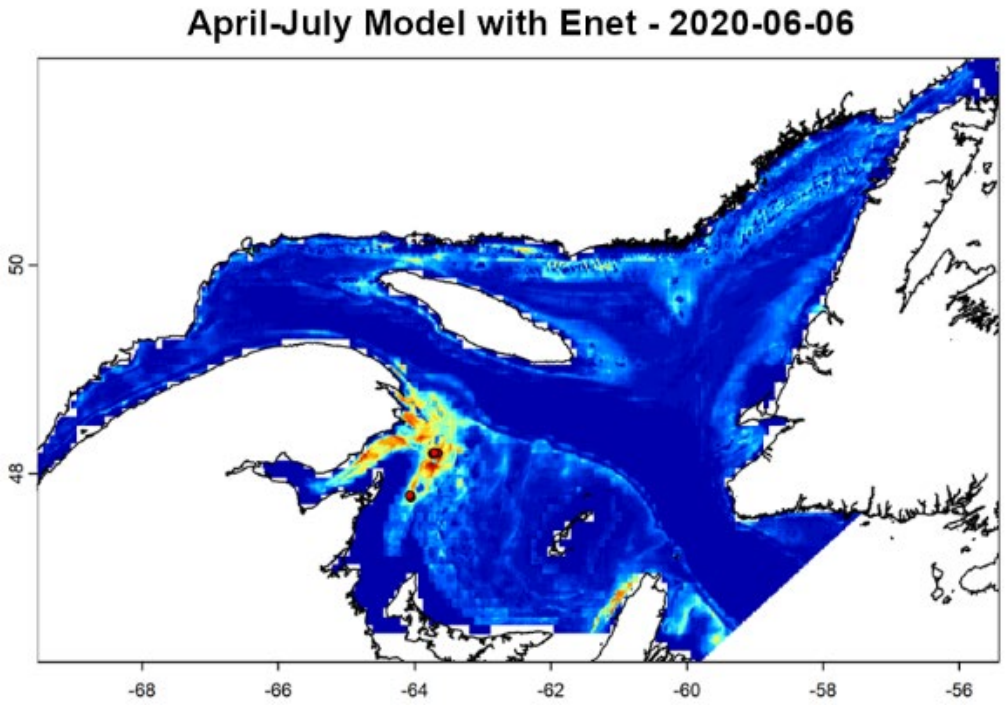

June – Daily predictions - Two-months Models

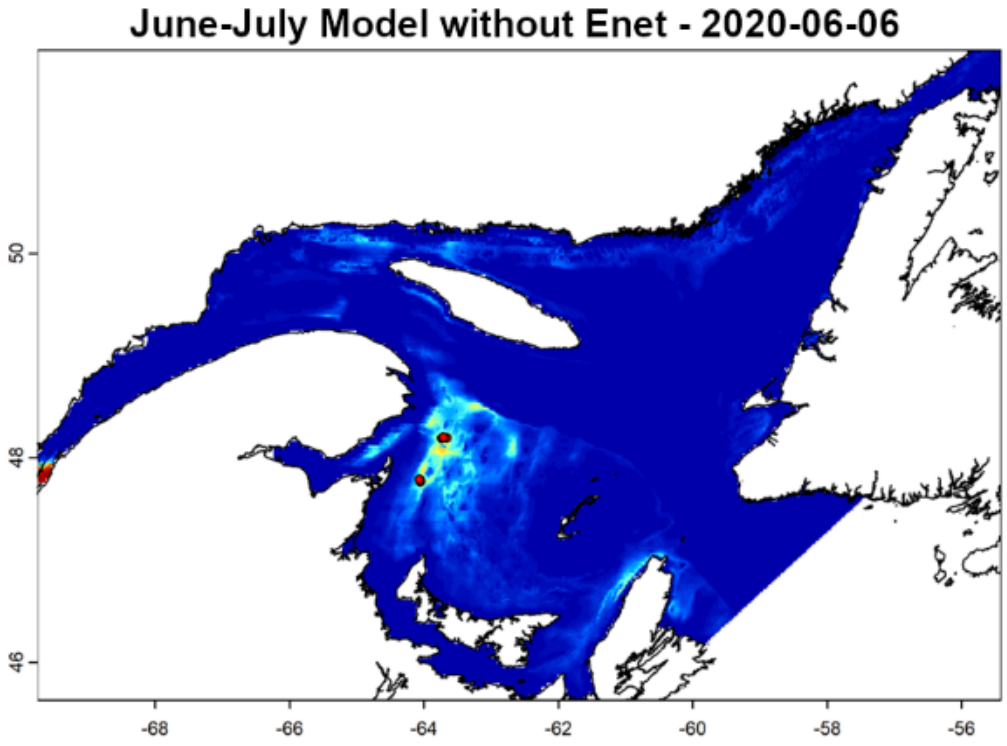

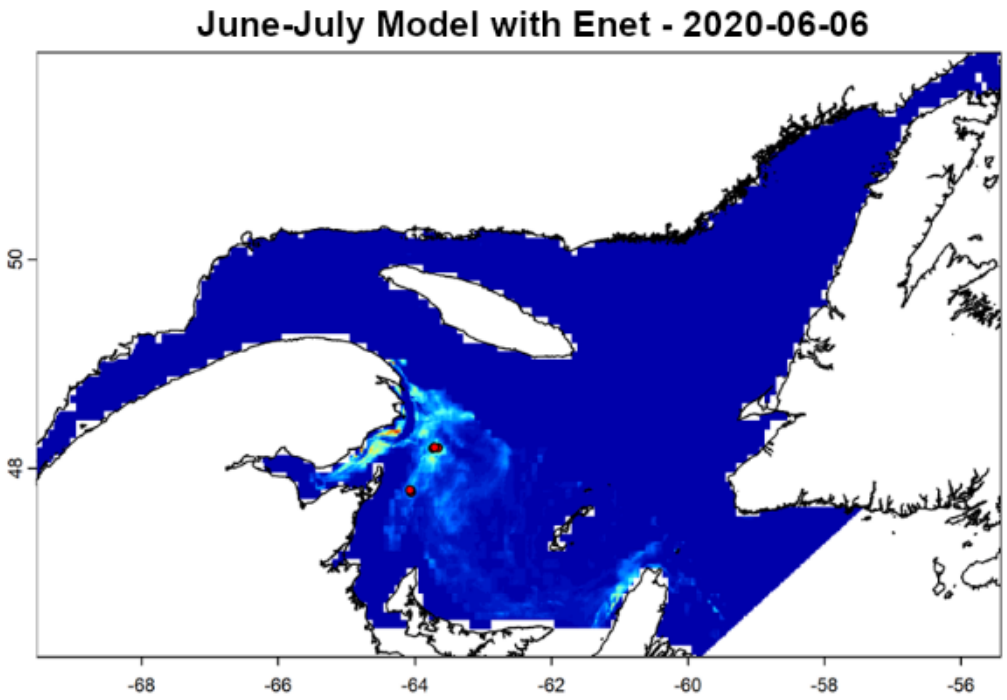

July – Monthly predictions – Global Model

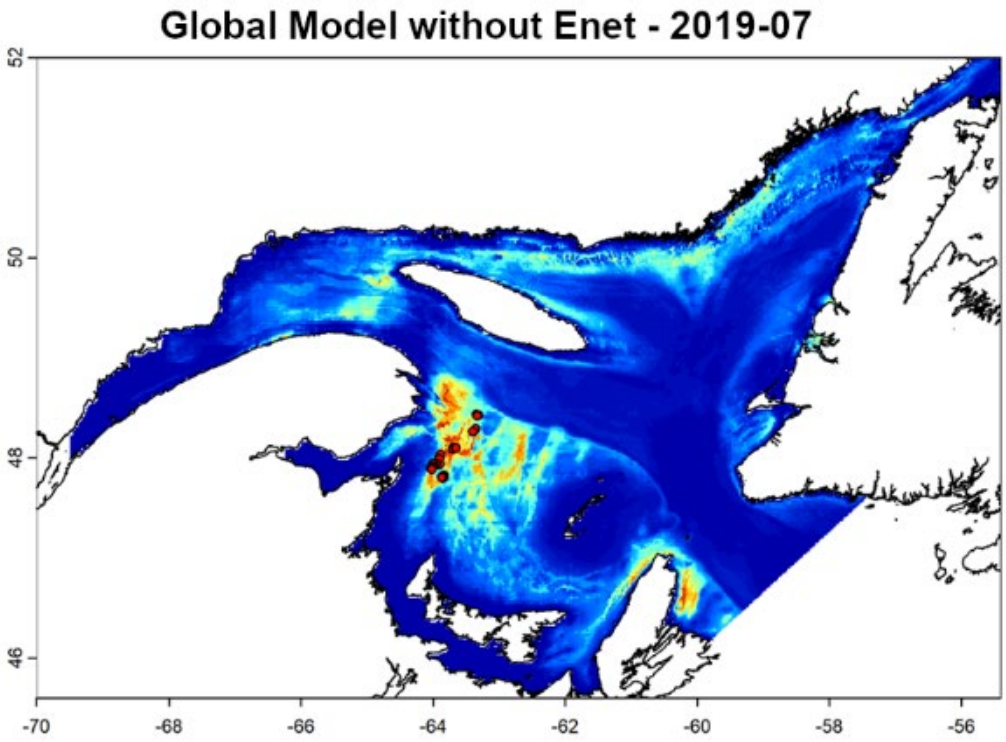

July – Daily predictions – Global models

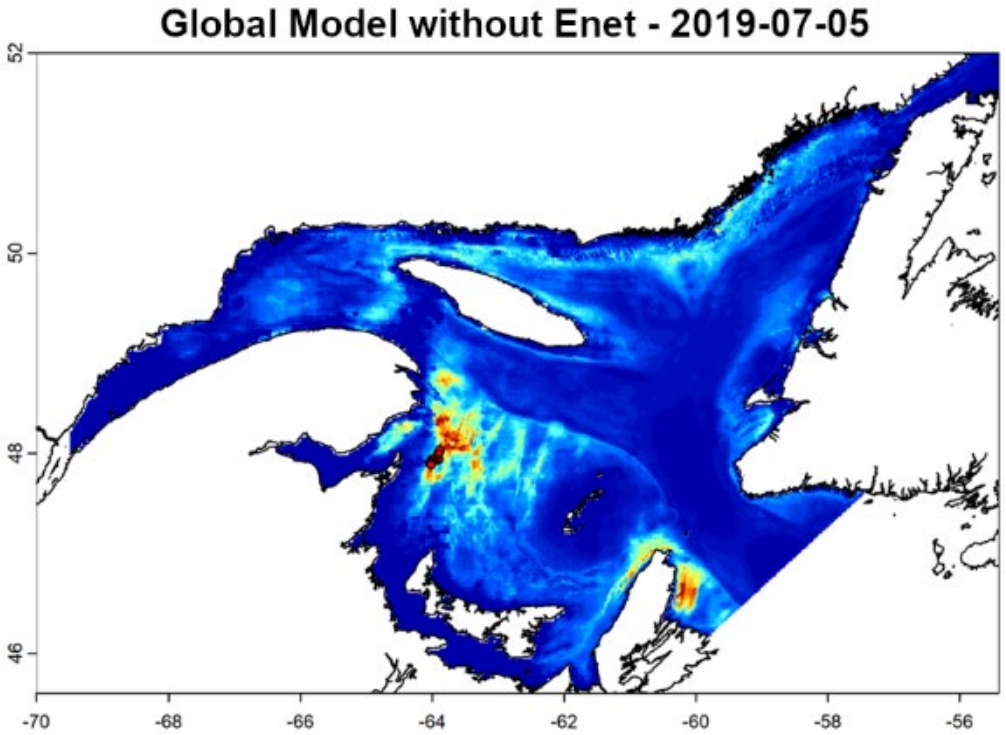

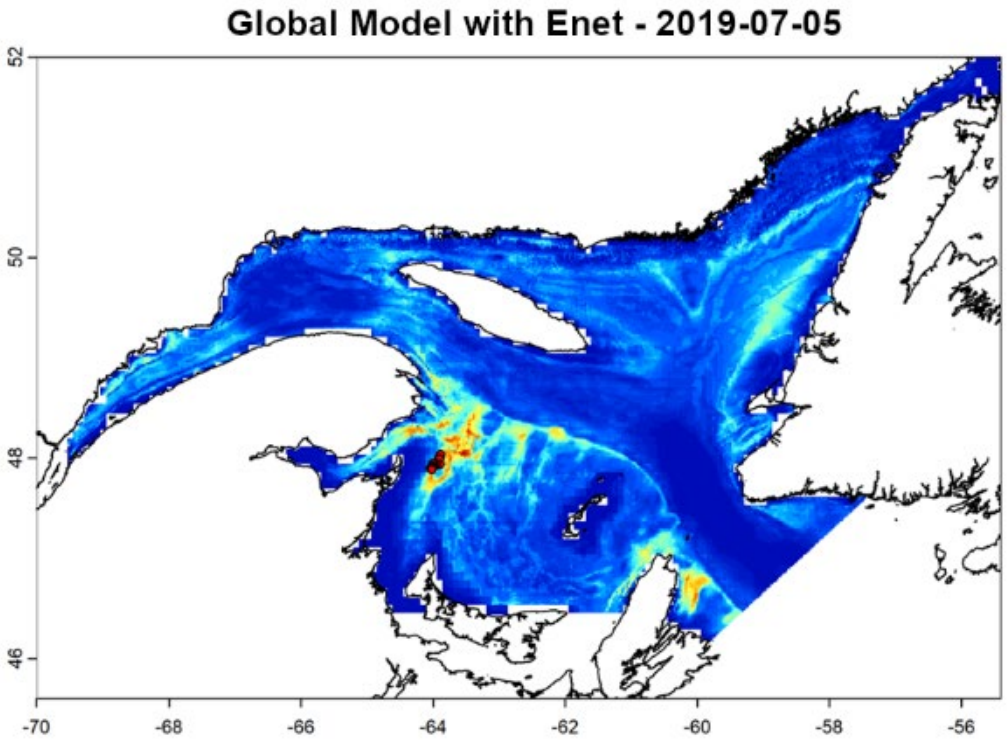

July – Daily predictions – Half-Season Models

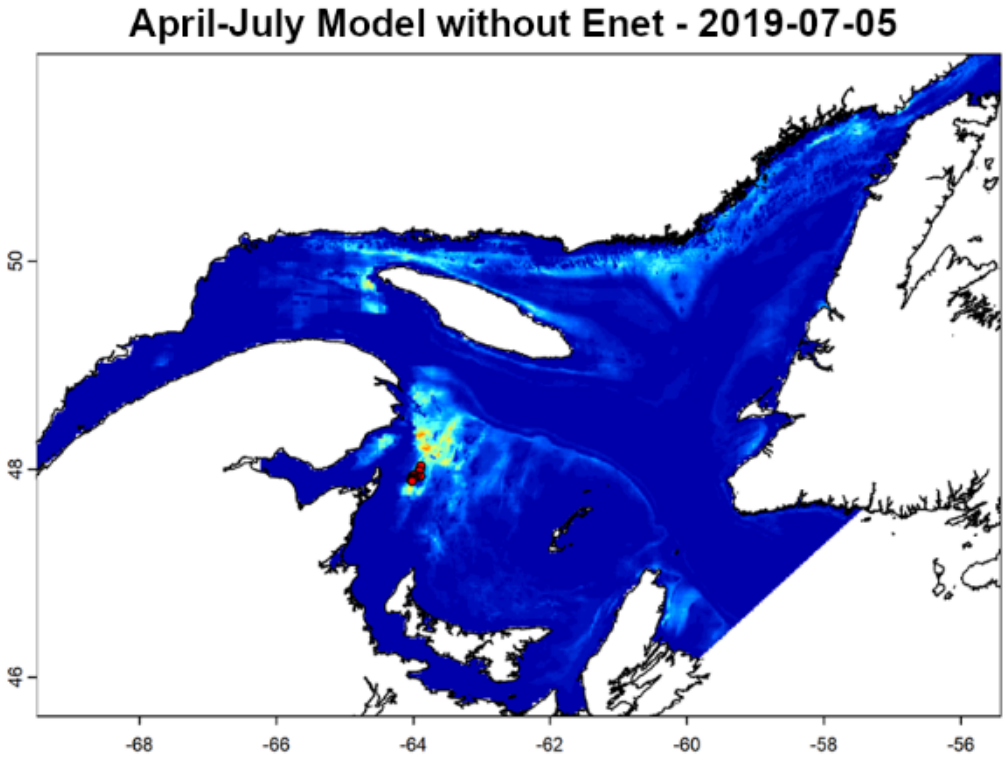

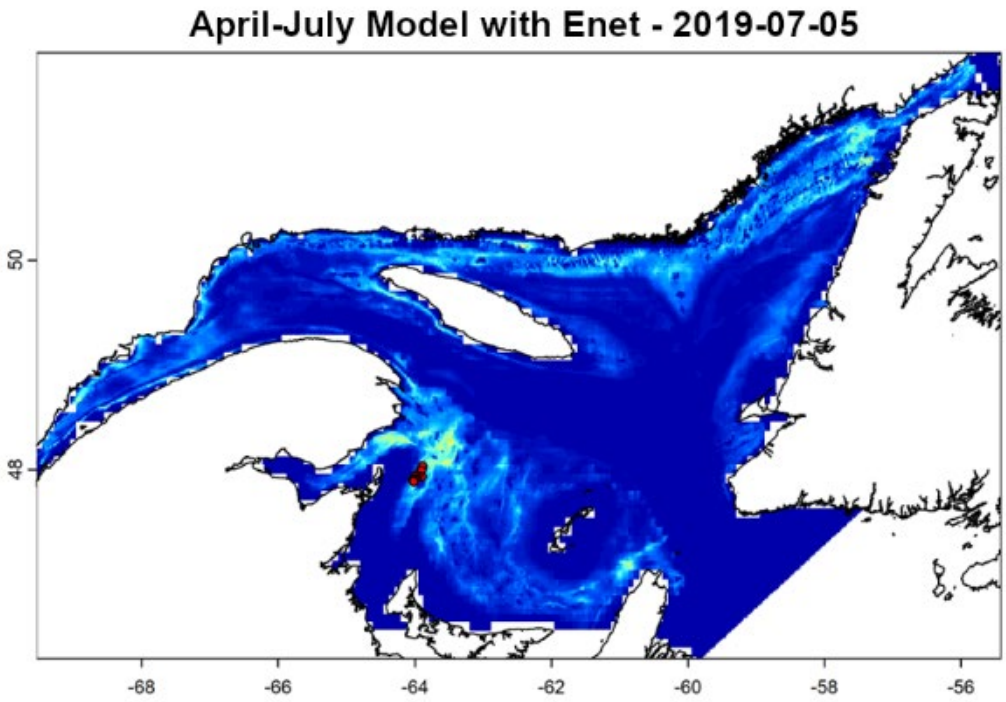

July – Daily predictions - Two-months Models

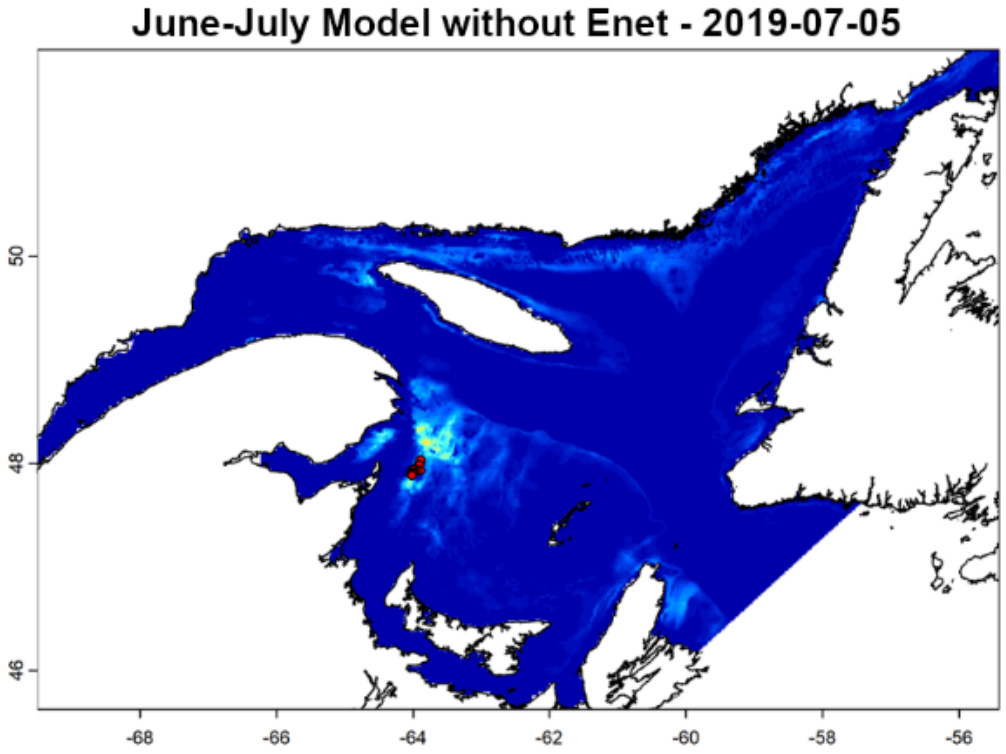

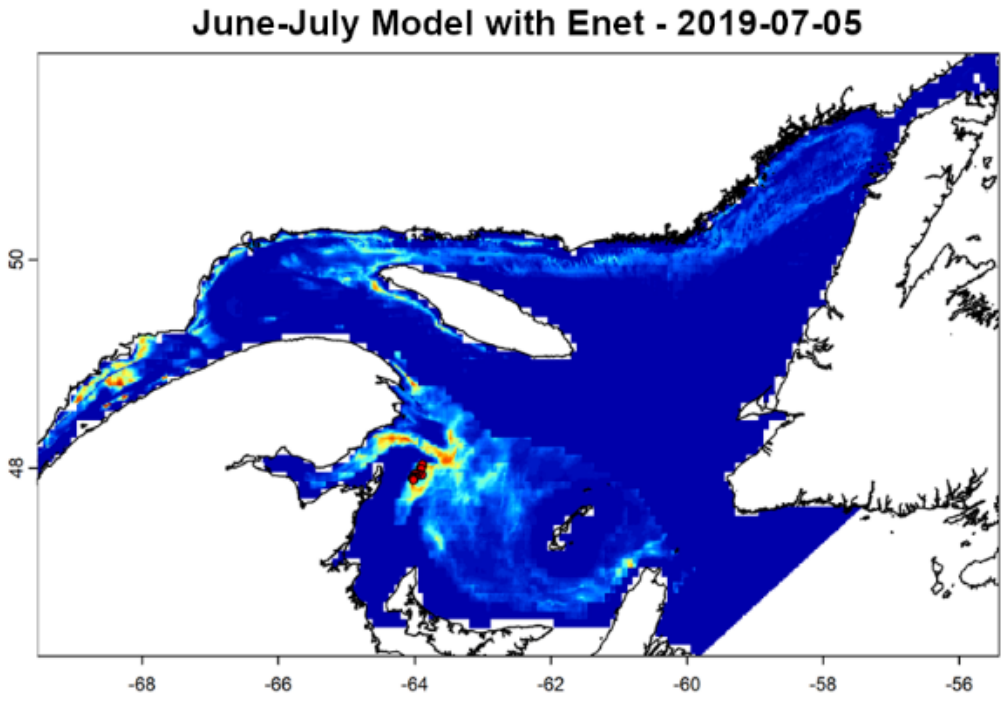

August – Monthly predictions – Global Model

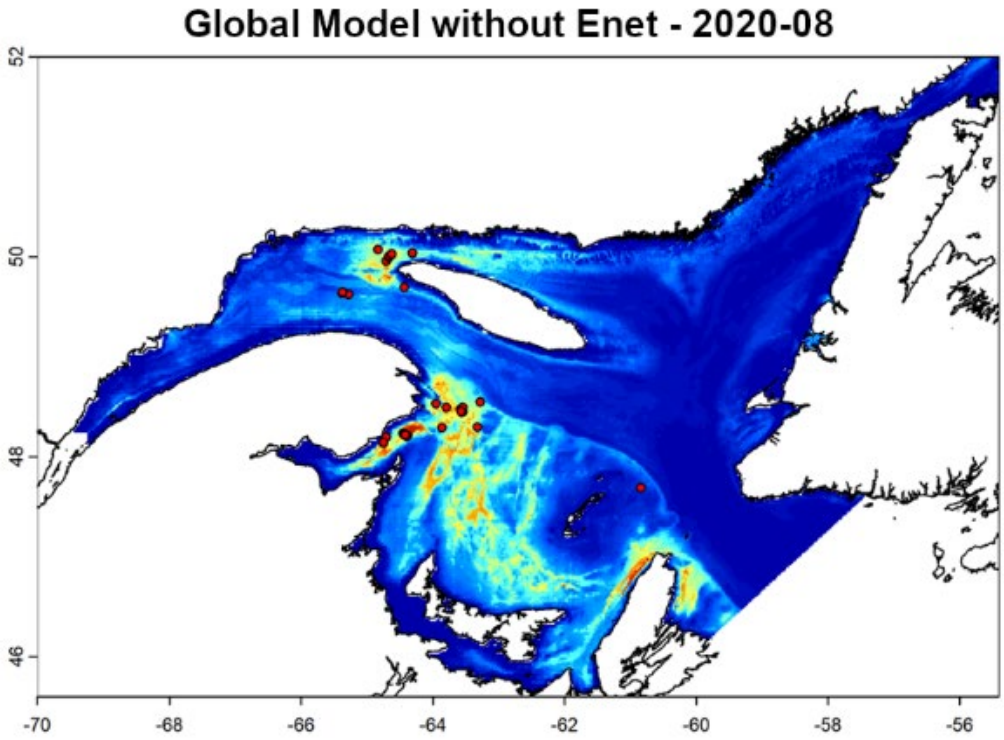

August – Daily predictions – Global models

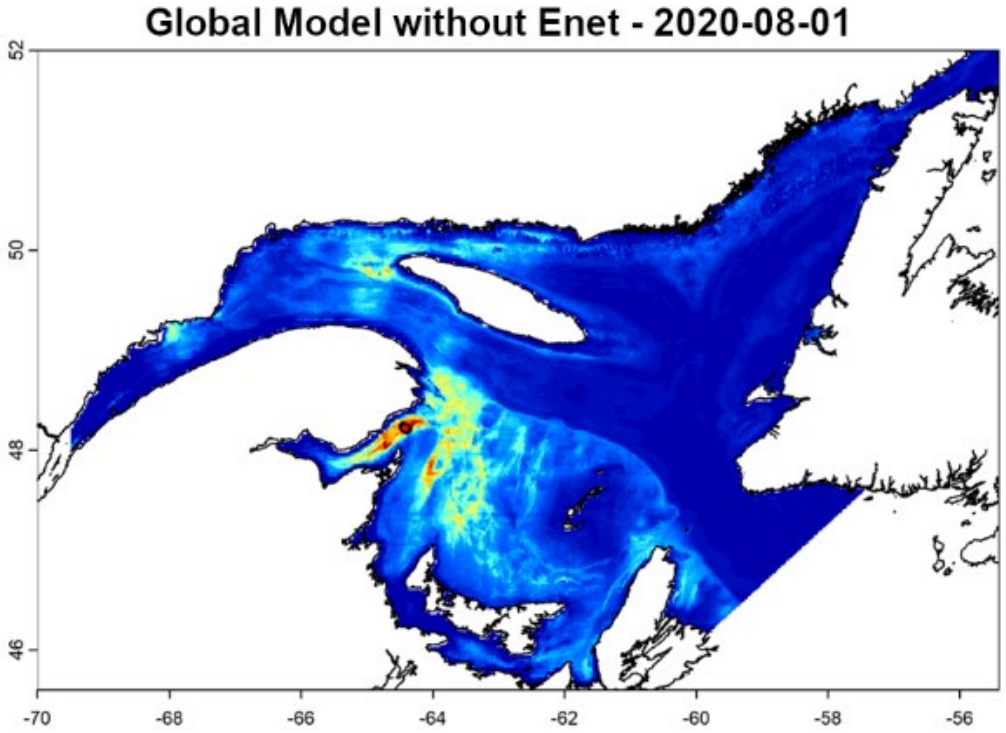

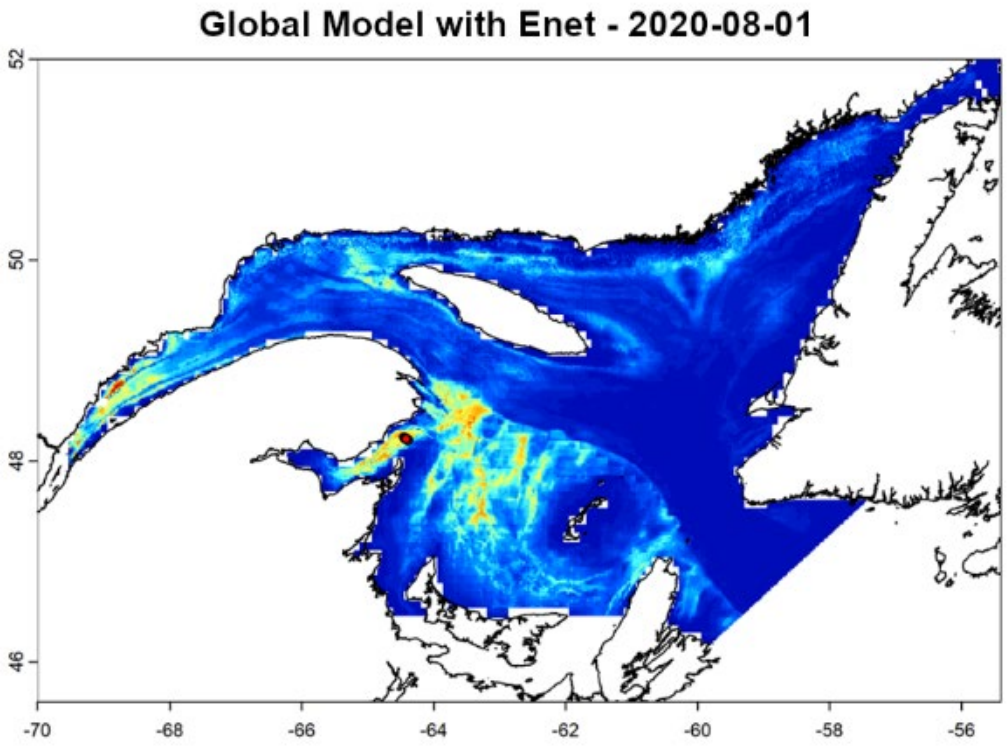

August – Daily predictions – Half-Season Models

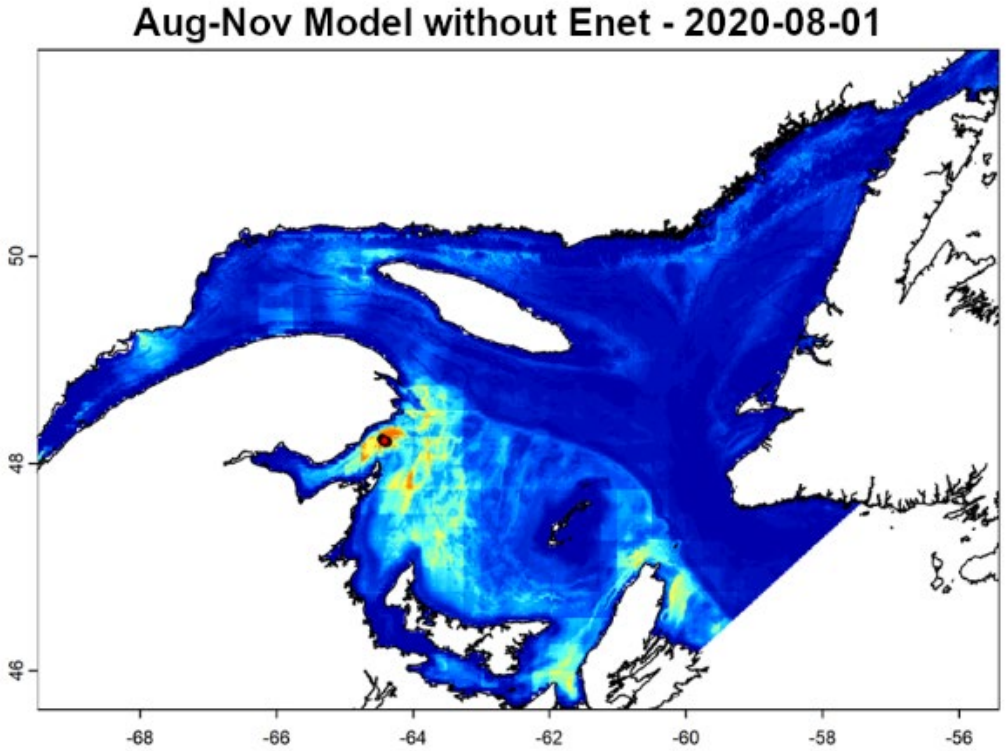

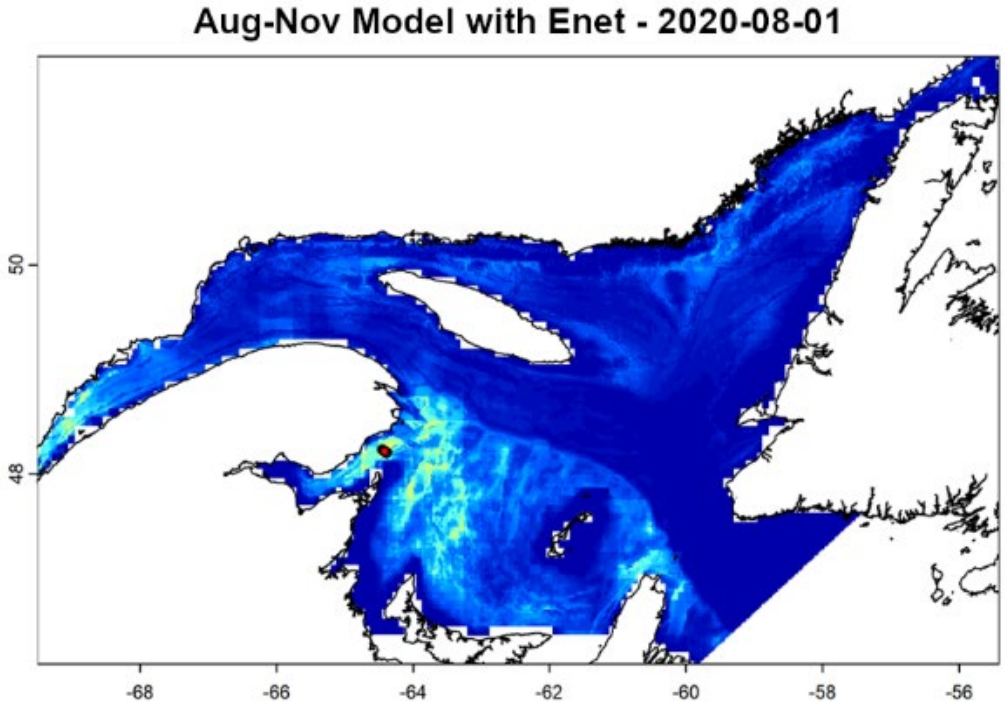

August – Daily predictions - Two-months Models

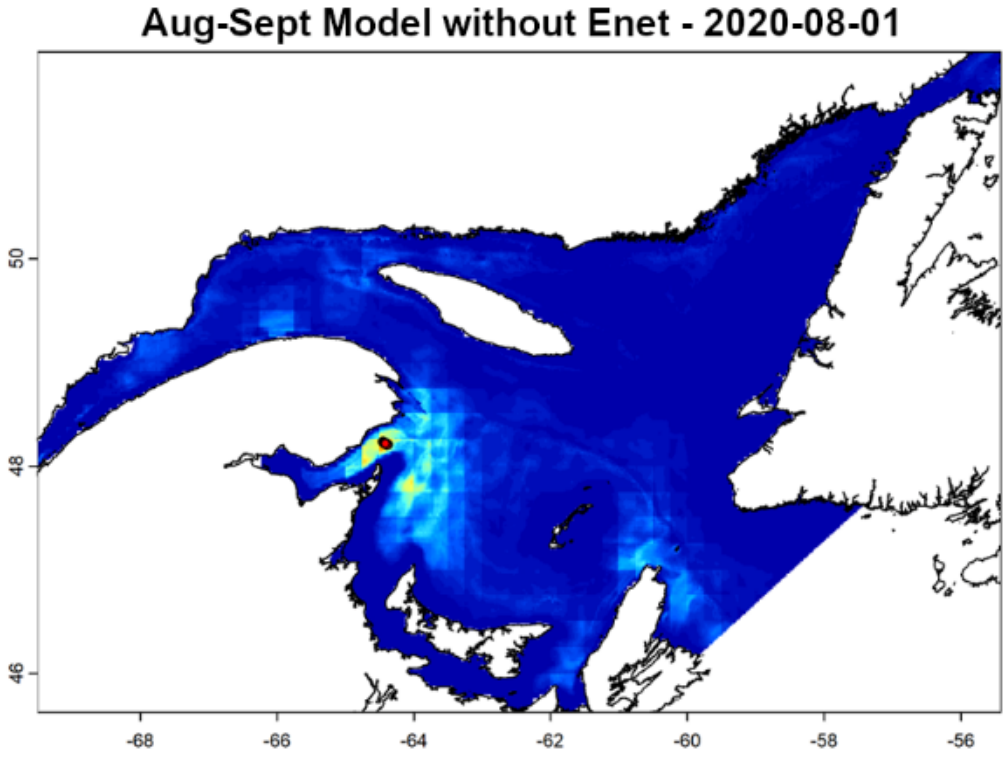

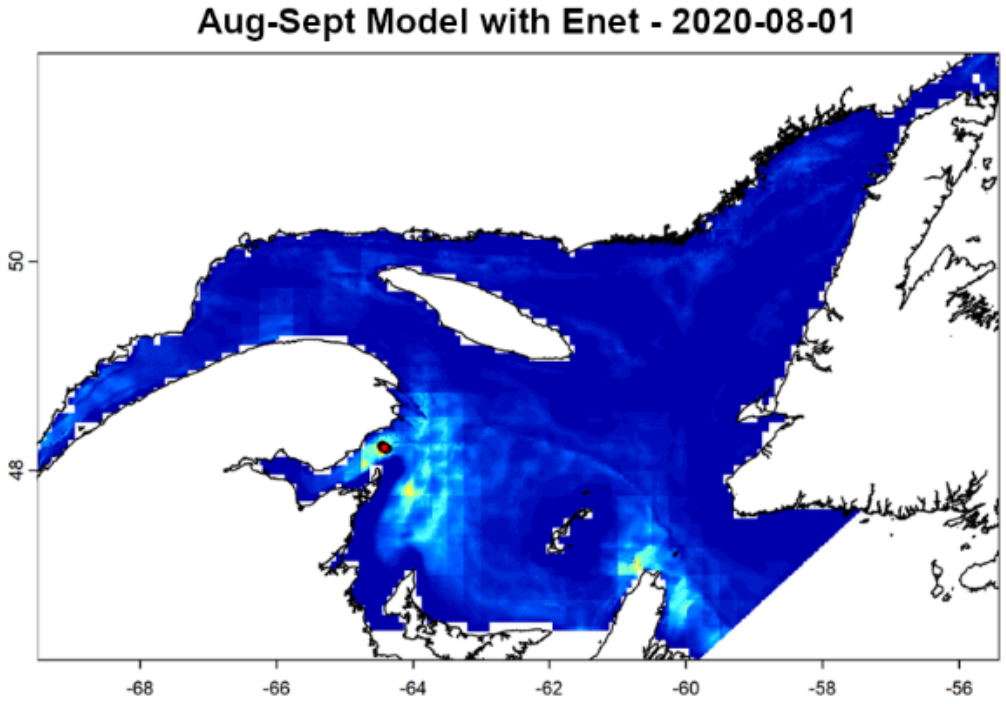

September – Monthly predictions – Global Model

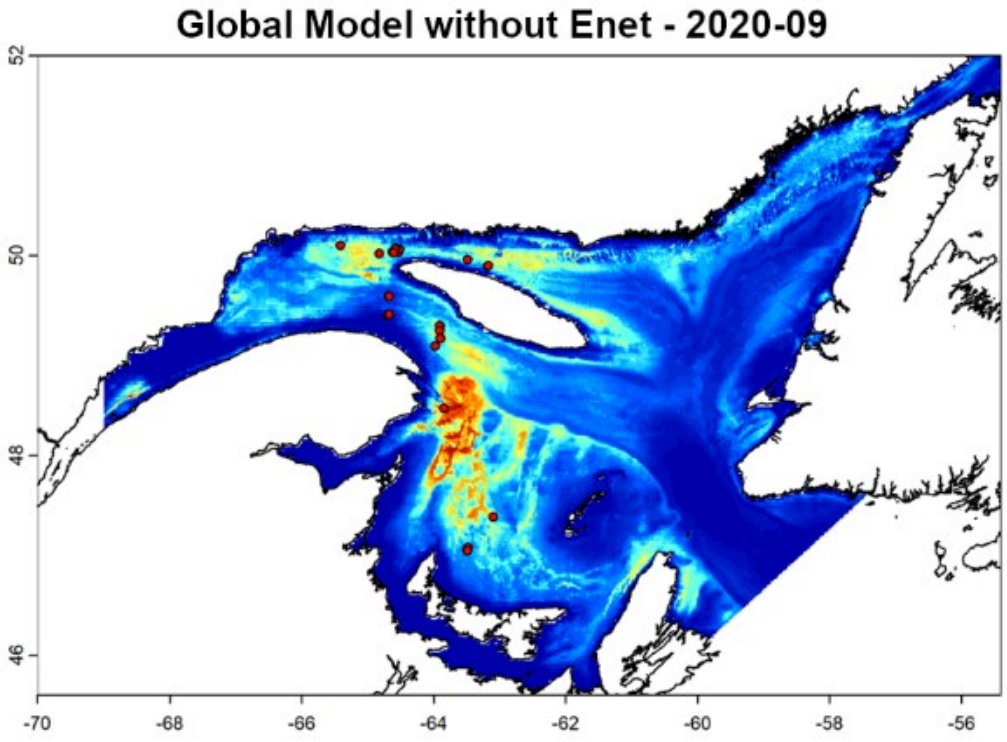

September – Daily predictions – Global models

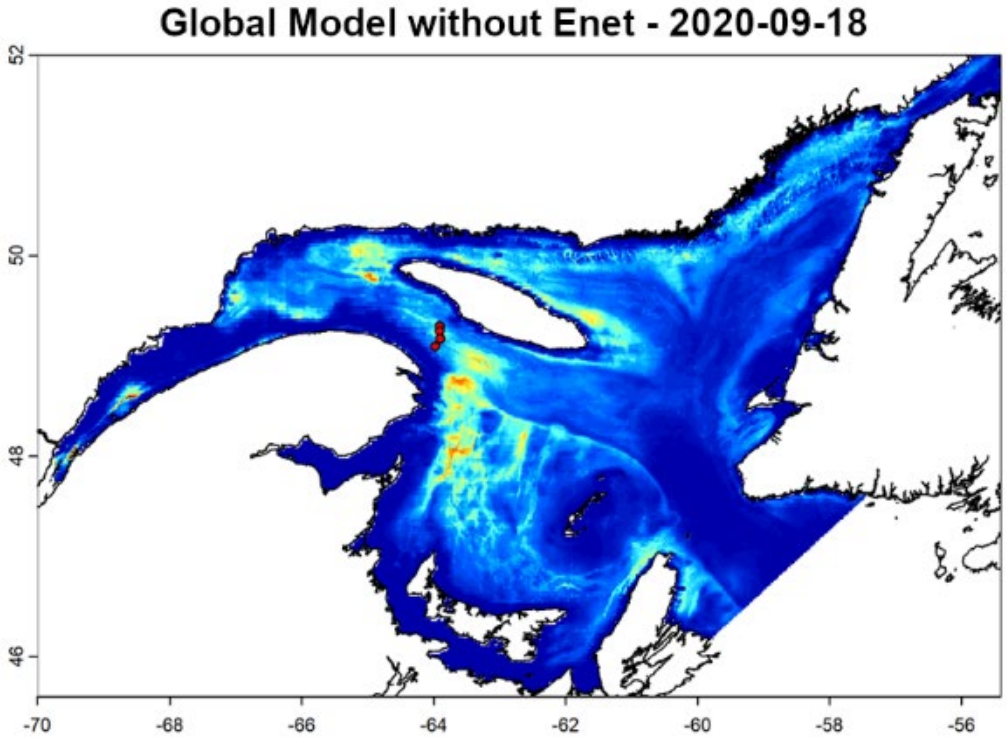

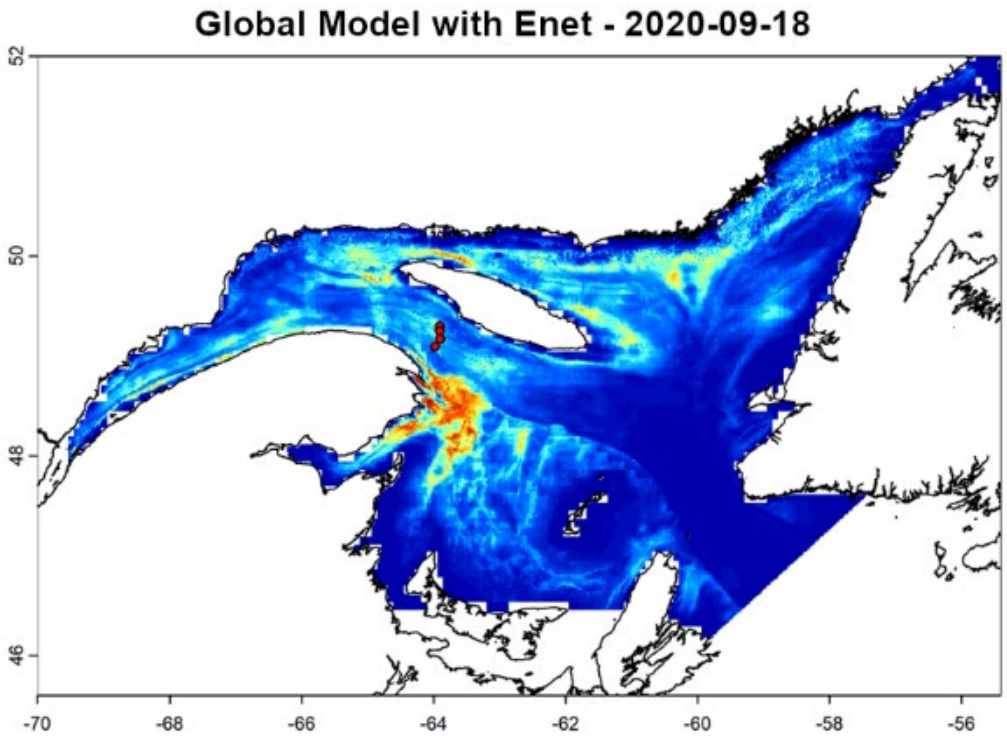

September – Daily predictions – Half-Season Models

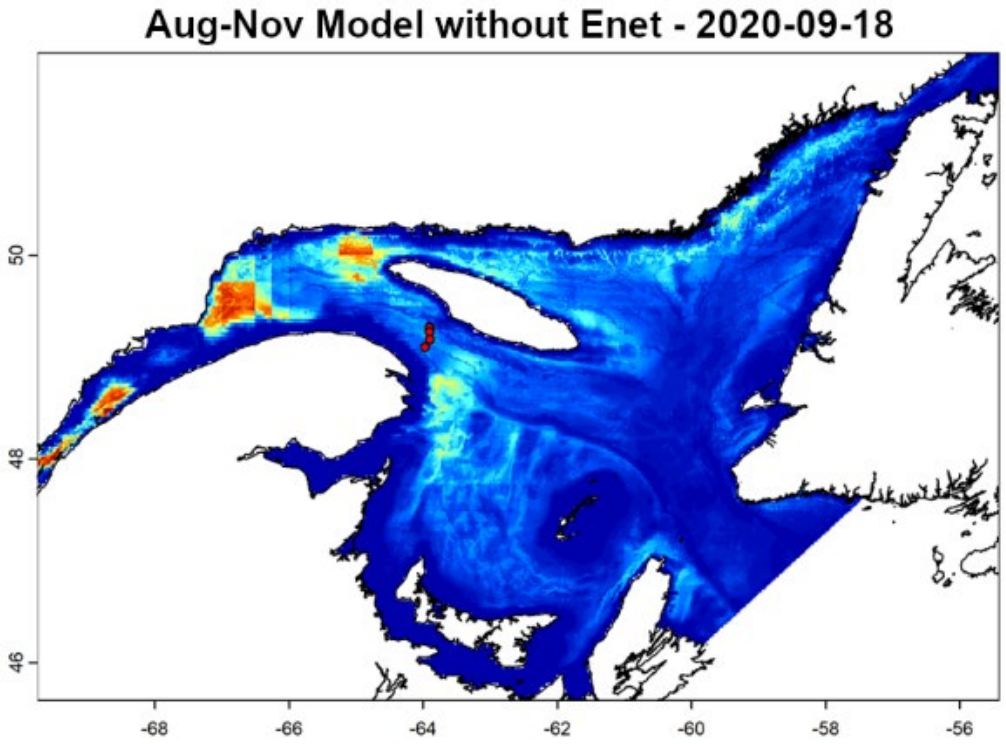

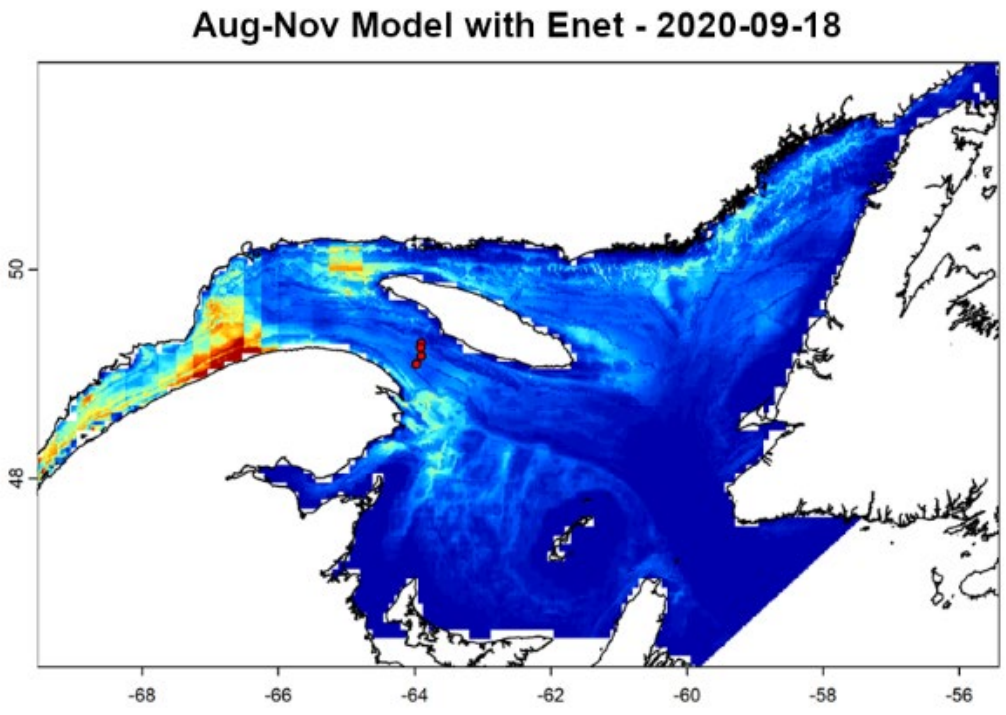

September – Daily predictions - Two-months Models

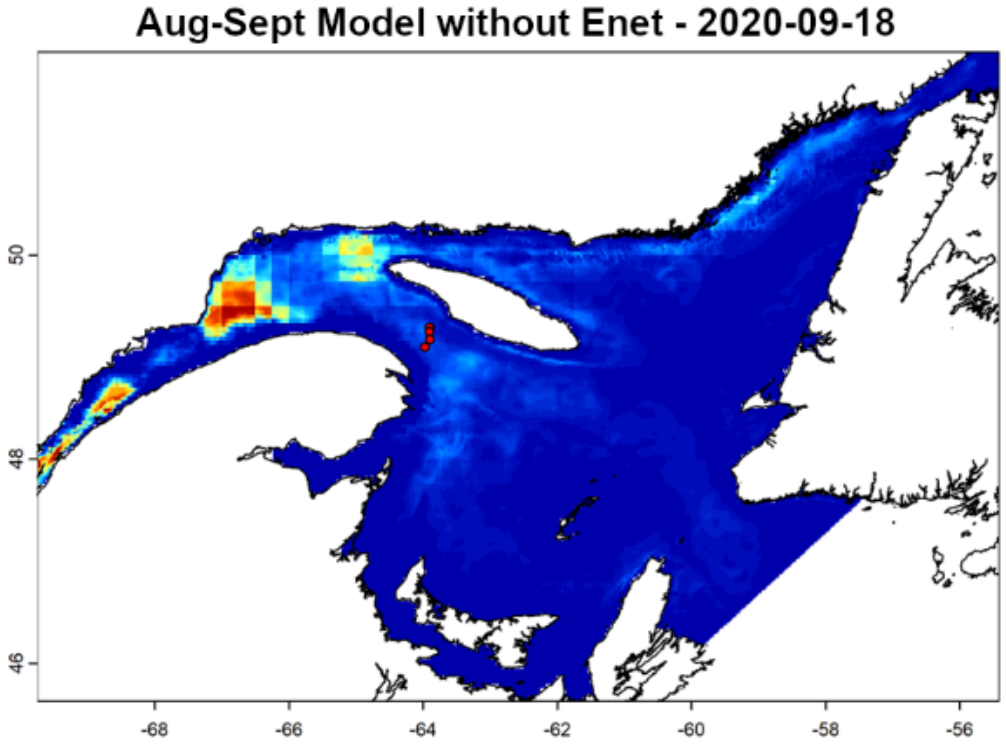

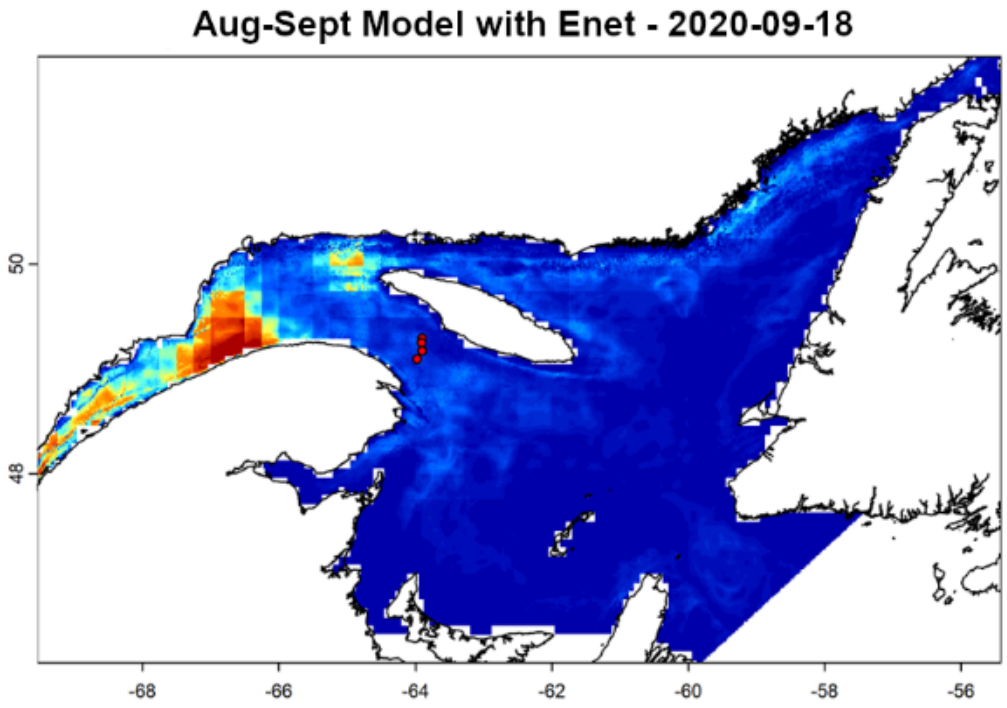

October – Monthly predictions – Global Model

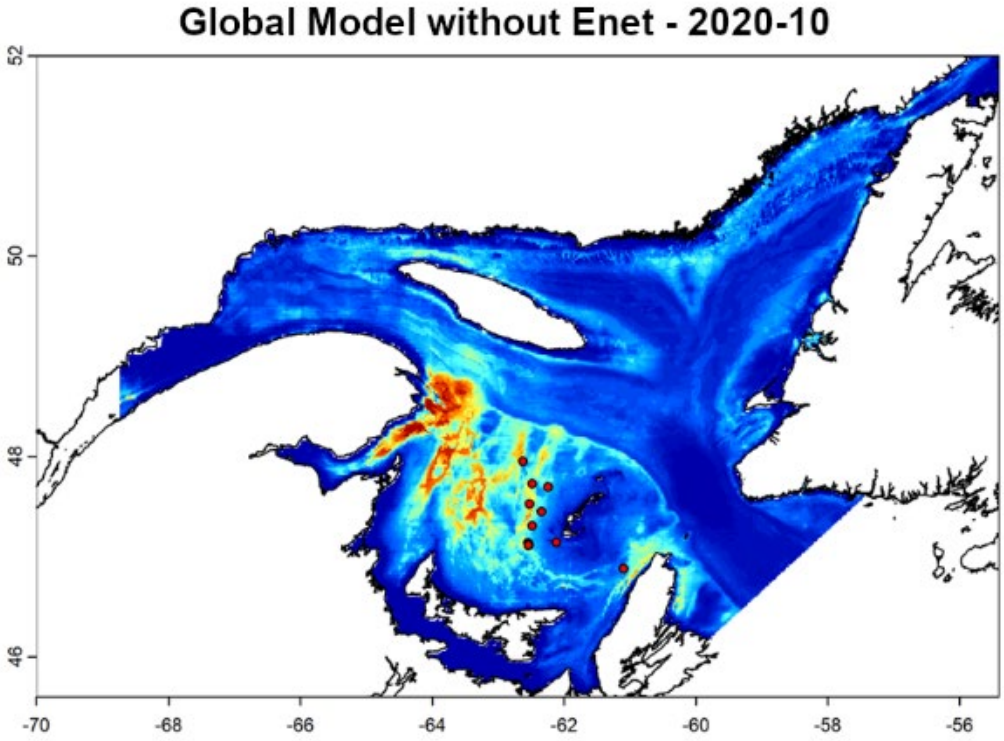

October – Daily predictions – Global models

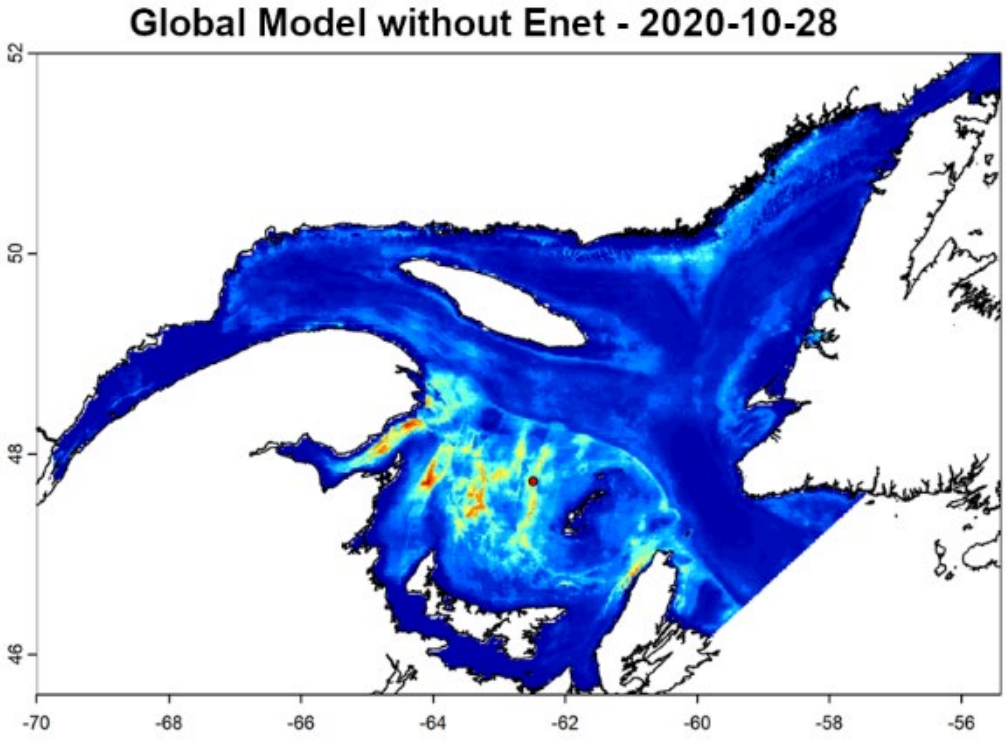

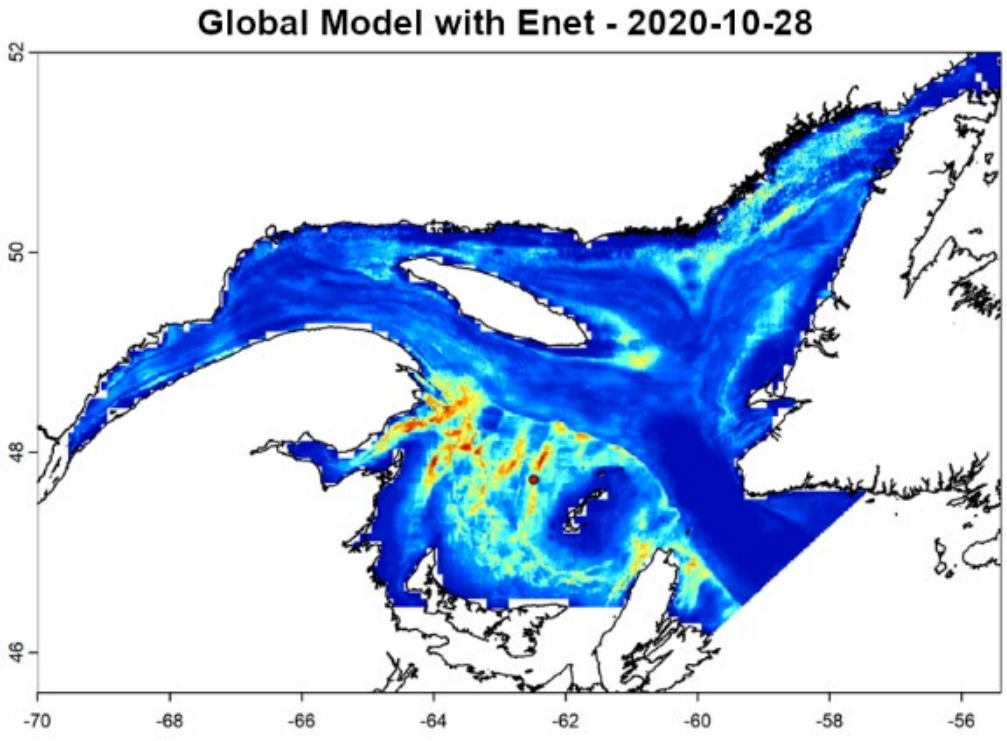

October – Daily predictions – Half-Season Models

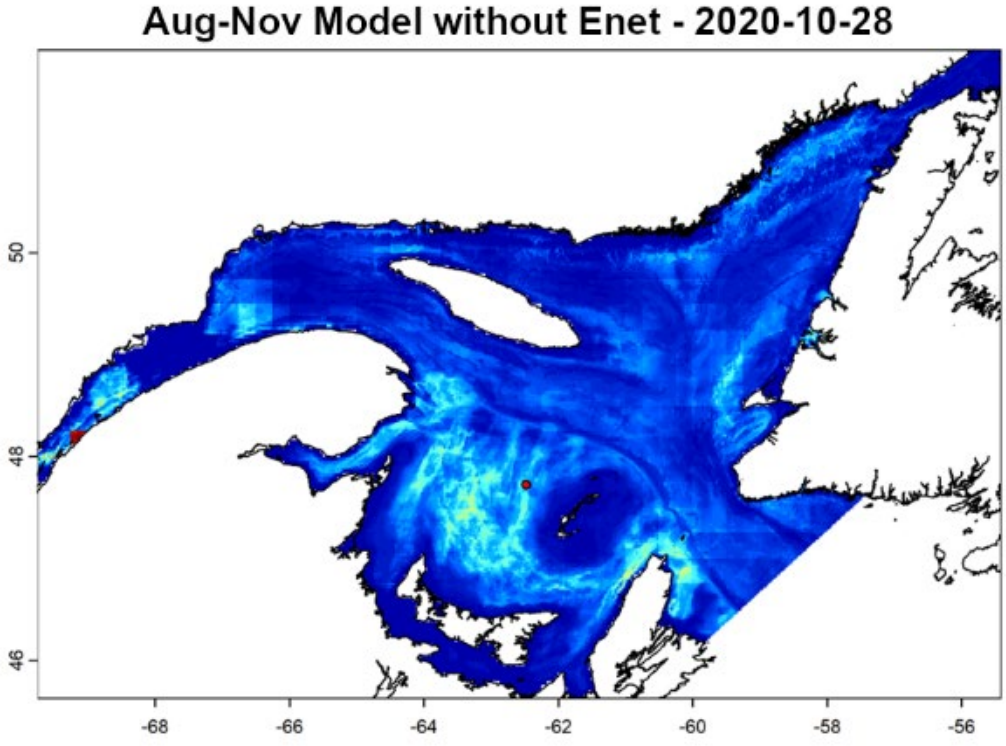

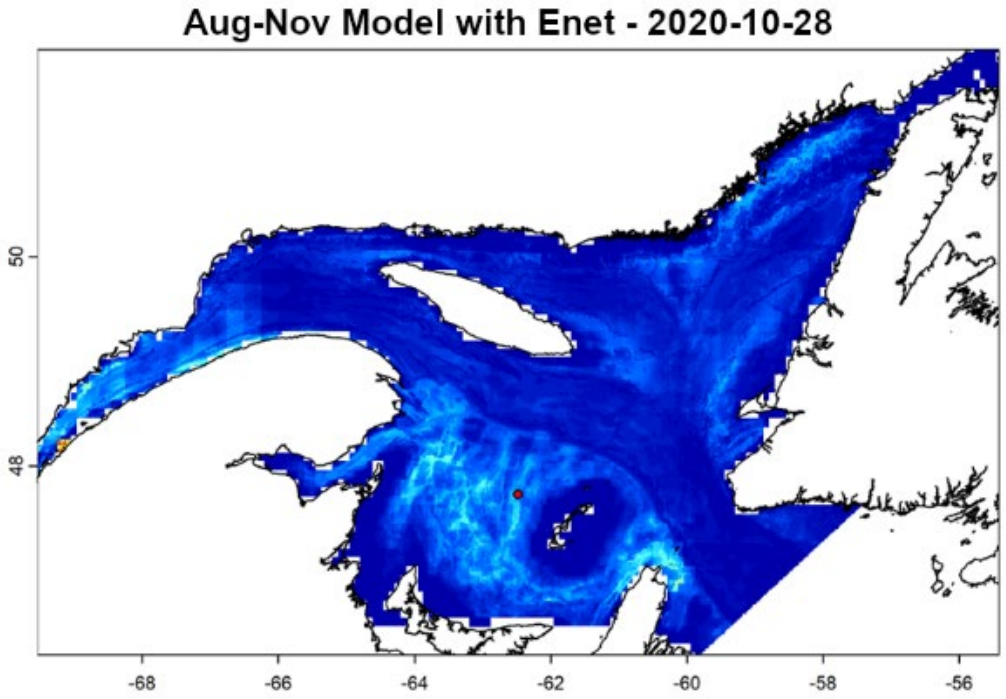

October – Daily predictions - Two-months Models

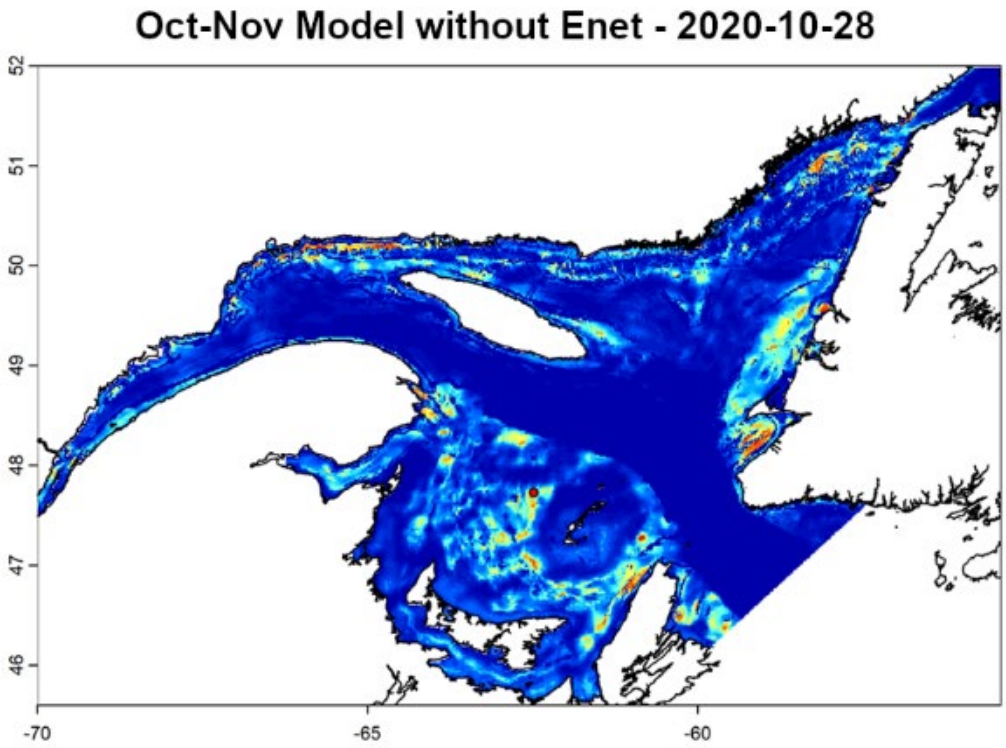

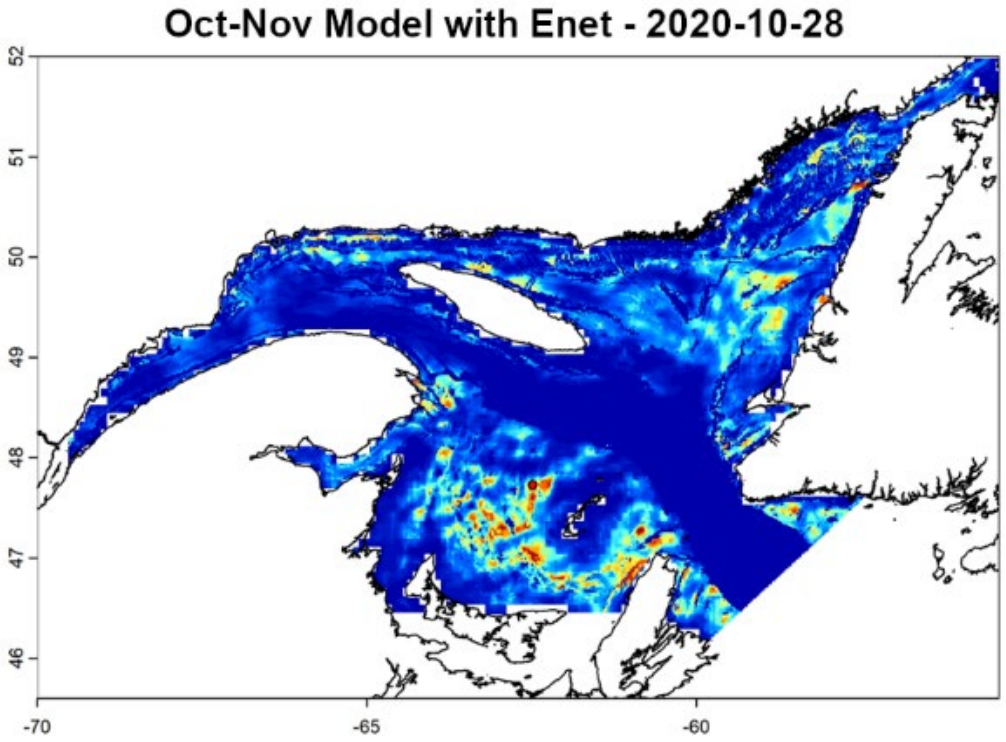

November

No sightings in 2017-2020

APPENDIX F. COMPARISON BETWEEN MODEL PREDICTIONS AND RAW DATA

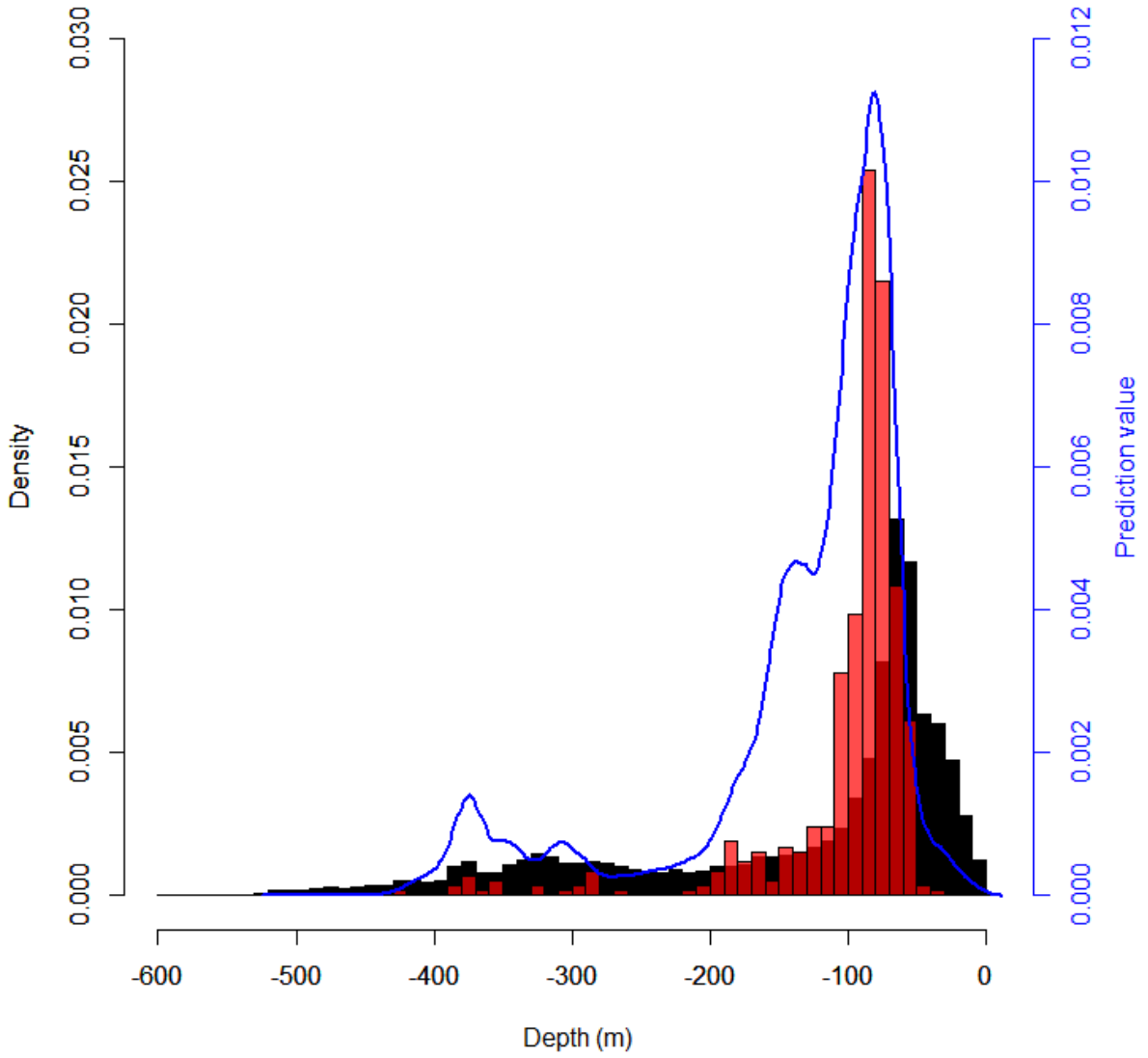

Figure F1. Comparison of the depth distribution in the Estuary and Gulf of St. Lawrence (black bars), the depth distribution at locations North Atlantic Right Whale (NARW) were observed (red bars), and the smoothed curve (blue line) representing the average value of the relative probability of North Atlantic Right whales (Eubalaena glacialis) occurrence estimated at these depths in the Gulf and the Estuary of St. Lawrence between 2017 and 2022.

APPENDIX G. MEAN SEA LEVEL ANOMALIES OVER SEASONS FOR 2017-2020

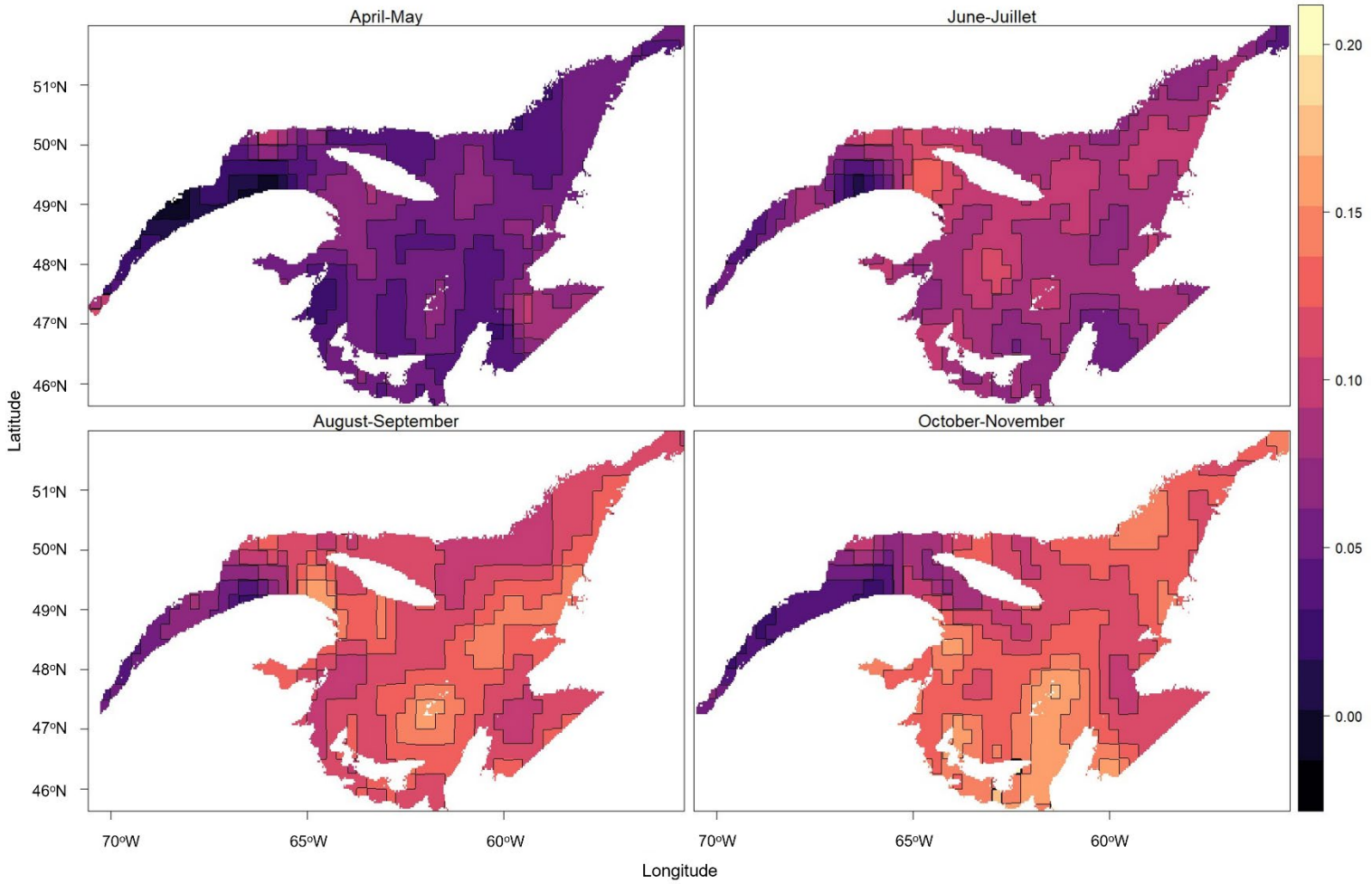

Figure G1. Average measures of sea level anomalies observed in the Gulf and the Esturay of St. Lawrence in April-May, June-July, August-September, and October-November between 2017 and 2020.

APPENDIX H. MODEL PREDICTION ERRORS

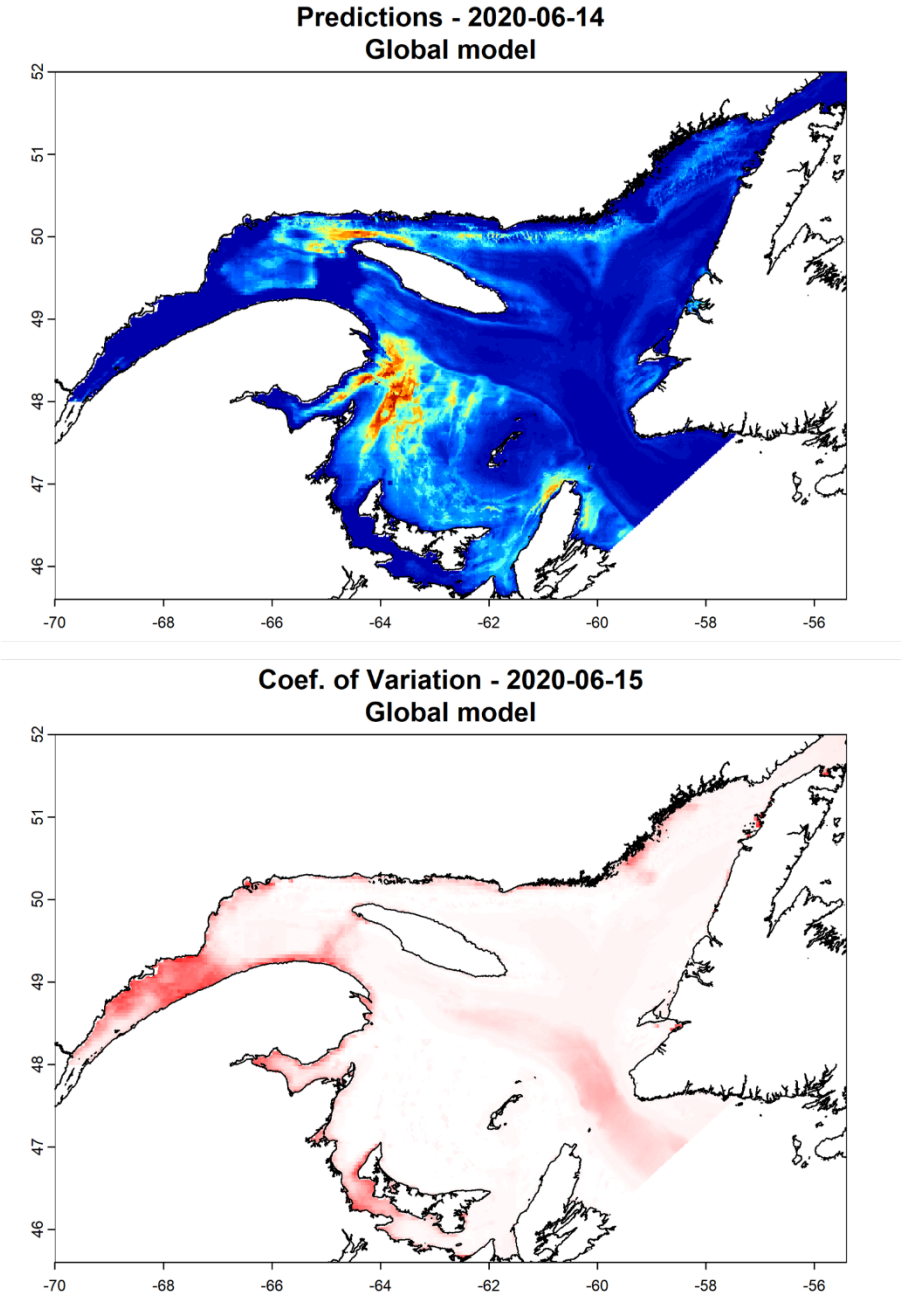

Figure H1. Example of model predictions and its associated map of error (here the coefficient of variation).